Advances in Geological Science

Yasuto Itoh
Keiji Takemura

Three-Dimensional Architecture and Paleoenvironments of Osaka Bay

An Integrated Seismic Study on the Evolutionary Processes of a Tectonic Basin

Springer

Advances in Geological Science

Studies in the twentieth century uncovered groundbreaking facts in geophysics and produced a radically new picture of the Earth's history. However, in some respects it also created more puzzles for the research community of the twenty-first century to tackle. This book series aims to present the state of the art of contemporary geological studies and offers the opportunity to discuss major open problems in geosciences and their phenomena. The main focus is on physical geological features such as geomorphology, petrology, sedimentology, geotectonics, volcanology, seismology, glaciology, and their environmental impacts. The monographs in the series, including multi-authored volumes, will examine prominent features of past events up to their current status, and possibly forecast some aspects of the foreseeable future. The guiding principle is that understanding the fundamentals and applied methodology of overlapping fields will be key to paving the way for the next generation.

More information about this series at http://www.springer.com/series/11723

Yasuto Itoh · Keiji Takemura

Three-Dimensional Architecture and Paleoenvironments of Osaka Bay

An Integrated Seismic Study on the Evolutionary Processes of a Tectonic Basin

Springer

Yasuto Itoh
Graduate School of Science
Osaka Prefecture University
Sakai, Osaka
Japan

Keiji Takemura
Institute for Geothermal Sciences
Kyoto University
Beppu, Oita
Japan

ISSN 2524-3829 ISSN 2524-3837 (electronic)
Advances in Geological Science
ISBN 978-981-13-0576-4 ISBN 978-981-13-0577-1 (eBook)
https://doi.org/10.1007/978-981-13-0577-1

Library of Congress Control Number: 2018941219

Printed on acid-free paper

This Springer imprint is published by the registered company Springer Nature Singapore Pte Ltd.
part of Springer Nature
The registered company address is: 152 Beach Road, #21-01/04 Gateway East, Singapore 189721, Singapore

Preface

Sedimentary basins act as reservoirs of natural resources and are often overlain by densely populated cities. They are notable not only because they are at the center of human-centered functions but also for their significance as buffers of global environmental changes and driving forces behind the Earth's material recycling system. Among various tectonic regions where basins develop, convergent plate margins show unmatched diversity in their basinal configurations and evolutionary processes, reflecting frequent and dynamic tectonic events.

In this book, the authors focus on the Osaka basin on the eastern Eurasian margin, which emerged in the late Pliocene. Its peripheral part is coincident with the Osaka metropolis and has been the subject of many geological and civil engineering studies. Our predecessors have succeeded in unraveling the mechanism behind the ongoing subsidence at a confining bend of an arc-bisecting transcurrent fault. However, a comprehensive timeline of the basin evolution has never been presented because its proximal part, Osaka Bay, was out of reach of geophysical measurement systems that can provide a three-dimensional view of the deep basinal interior.

Our seismic dataset, integrated with precise chronology on tied boreholes, provides insight into fault morphology, depocenter migration, and basin-wide deformation phases closely linked to tectonic regimes. Such insight is provincially important for the evaluation of basin-fringing seismogenic faults (e.g., Awaji–Rokko Fault System), the deep structures of which cannot be visualized from land. In a wider regional context, we consider that in-depth research on the tectonic basin provides a firm foundation for understanding the progressive deformation processes and related long-term environmental changes on the active margin, which has been under the control of the complicated motions of the oceanic plates competing for dominance in the Pacific.

Sakai, Japan — Yasuto Itoh
Beppu, Japan — Keiji Takemura

Acknowledgements

The authors are grateful to the Geological Survey of Japan, National Institute of Advanced Industrial Science and Technology (AIST); the Hydrographic and Oceanographic Department of the Japan Coast Guard (JCG); the Osaka Soil Test Laboratory of the Geo-Research Institute (GRI); Hyogo Prefecture; the Seismological Society of Japan; and Dr. Yoshinori Iwasaki for permission to publish this work.

Contents

Chapter 1
Tectonic Context of the Study Area

Abstract The tectonic setting of the study area, the Osaka sedimentary basin, is described from the viewpoint of changes in the plate motion around the northwestern Pacific that have occurred over the last one hundred million years and a sequence of epoch-making migration and deformation events along the southwestern Japan arc that has been investigated based on paleomagnetism and seismic interpretation. The ongoing active but subtle deformation of the island arc is also evaluated using high-resolution remote sensing data. The considerable diversity in geomorphological features and the uneven development of active faults point to the existence of a buffer zone of strong crustal strain in southwest Japan (i.e., the Kinki Triangle), where the Osaka basin is located. The dimensions of the sedimentary basin were assessed based on the gradient tensor analysis of gravity anomaly data, which revealed a deep-rooted basin morphology controlled by the architecture of major faults. To unravel the paradox of the Osaka basin having developed at a confining bend or the step of an arc-bisecting transcurrent fault, numerical modeling was used to replicate the pattern of uplift and subsidence. Such a simulation is useful for the detection of tectonically significant faults in the basin-forming process.

Keywords Southwest Japan · Osaka basin · Kinki Triangle · Active fault Paleogeography

The Japanese archipelago is located on the eastern Eurasian margin (Fig. 1.1), where subduction of oceanic plates has persisted for more than 100 M years. Reflecting strong tectonic stress related to plate convergence, numerous intra-arc basins have developed on this island arc. The Osaka basin, geographically called the Osaka Bay and the Osaka Plain, in southwest Japan occupies the easternmost portion of the Seto Inland Sea, which emerged as an arc-parallel basin during the Miocene spreading of the Japan Sea. To cultivate a vision that basins evolve as constituents of arc–trench systems and record the complicated tectonic processes that occur in them, the following sections review the development of the margin and then present instantaneous physical features in and around the studied sedimentary basin.

Y. Itoh and K. Takemura, *Three-Dimensional Architecture and Paleoenvironments of Osaka Bay*, Advances in Geological Science,
https://doi.org/10.1007/978-981-13-0577-1_1

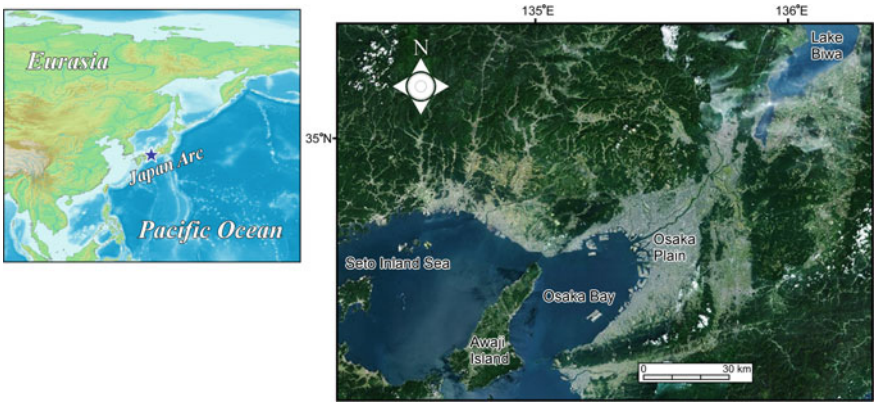

Fig. 1.1 Overview of the eastern Eurasian margin. The star indicates the Osaka basin, which is the target of the present study. Images are after Geoscience, NTT DATA, RESTEC

1.1 Plate Tectonic Framework of the Eastern Eurasian Margin

A fundamental model of plate reconstruction in the Pacific region was established by Engebretson et al. (1985), clarifying the rapid waxing and waning of the Izanagi Plate and the provoked episodic tectonic events. However, their restoration based on the relative motions of major oceanic plates did not constrain the status of the eastern Eurasian margin, which has long been facing marginal sea plates. Detailed models for southern and northern segments of the margin have been developed by Hall (2002, 2012) and Itoh et al. (2017), respectively. The latter is unique in that a lost buffer plate was introduced to reconcile the discordant time sequence of crustal collision and amalgamation episodes. As depicted in Figs. 1.2 and 1.3, this model suggests that the northeastern Eurasian margin was a site of intermittent contraction caused by the presence of landmasses on the consuming plates during the Cretaceous and the early half of the Cenozoic and has since evolved under the influence of newly formed marginal seas, namely the Philippine and Japan Seas.

1.1.1 Chronicle of Plate Motions Since 100 Ma

At the beginning of the Late Cretaceous, the present northwestern Pacific was dominated by the Izanagi Plate and characterized by rapid northward movement (Engebretson et al. 1985). This was then replaced by the westward-moving Pacific Plate. Their configuration, shown in Fig. 1.2, was interpolated using the reconstruction model by Engebretson et al. (1985) and calibrated based on their linear velocity tables.

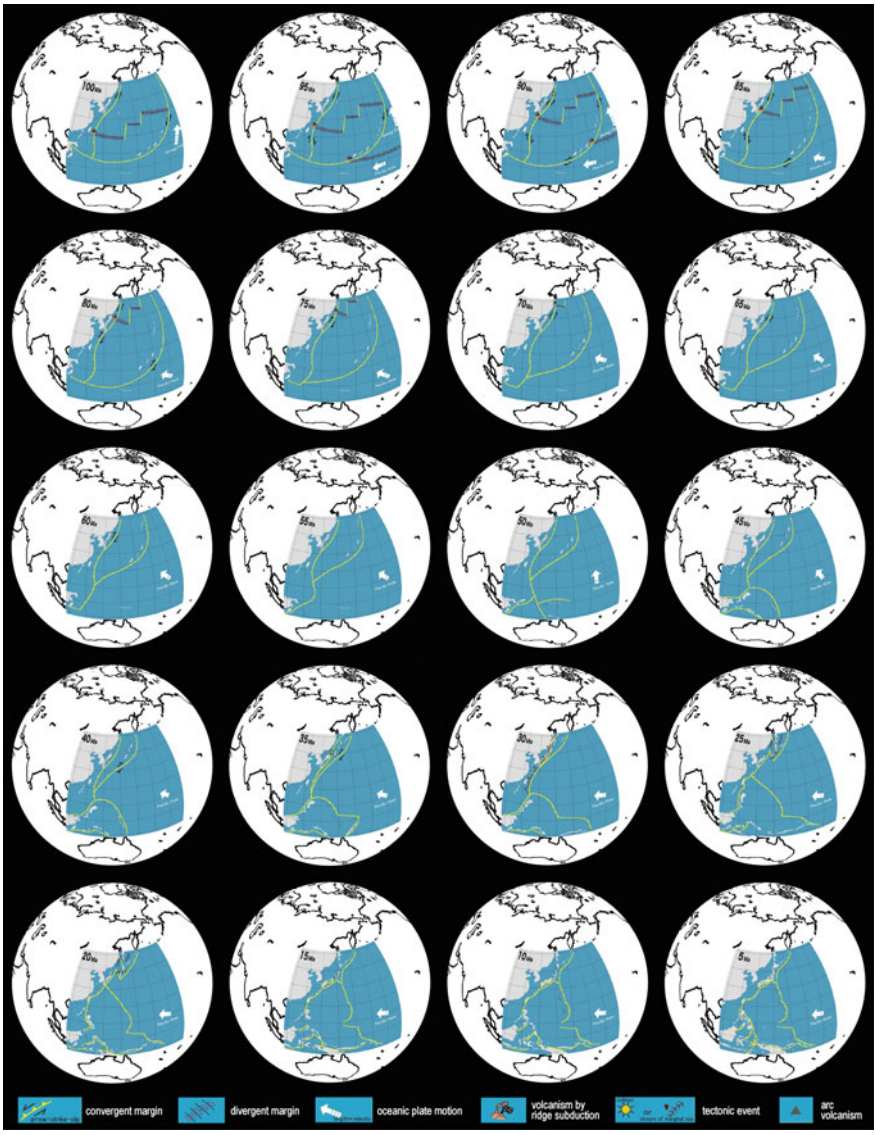

Fig. 1.2 Plate reconstruction around the eastern Eurasian margin since 100 Ma. This image was obtained from the platform of Dagik Earth (http://dagik.org/menu/land/Dagik_NWPacific_100my/e), a subproject of Dagik (https://www.dagik.net/english/) by the visualization group of the Integrated Earth Science Hub of Kyoto University

The eastern margin of Eurasia experienced intensive magma formation in the Late Cretaceous with an obvious trend toward younger activity as we move northeast. Kinoshita (1995) submitted an original hypothesis that assumed the effect of

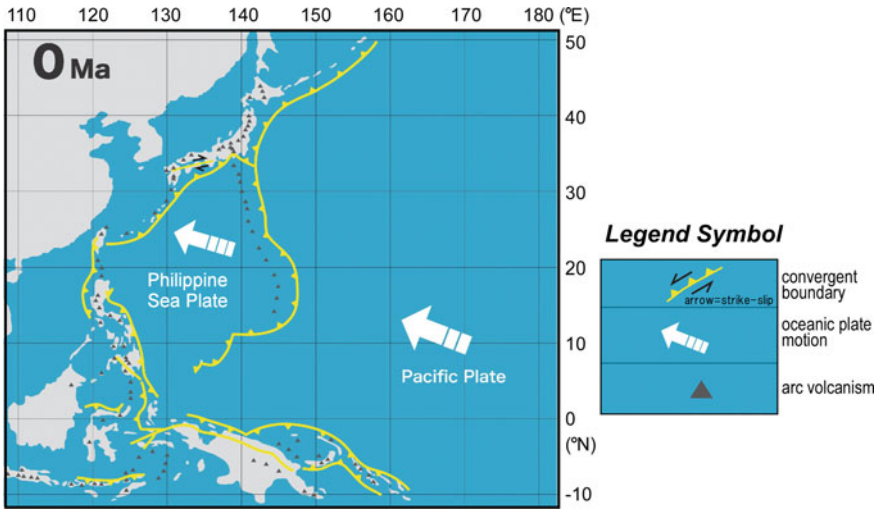

Fig. 1.3 Present-day plate configuration around the eastern Eurasian margin modified from Itoh et al. (2017)

Kula–Pacific ridge subduction on the specific magmatism. However, the pathway of the Kula–Pacific ridge that he considered does not fit with the plate reconstruction by Engebretson et al. (1985).

As an alternative, Itoh et al. (2017) hypothesized the presence of a spreading center in the newly introduced marginal sea plate (Fig. 1.2). In their model, the ridge moves at a pace consistent with the time-progressive plutonism along the continental margin. On the other hand, it is conceivable that the rapid northerly migration of the Izanagi–Pacific ridge brought about intense short-lived igneous activities in the Late Cretaceous along the eastern boundary of the marginal sea plate, which included a major portion of the present northeastern Japan forearc.

Geologic evidence compiled by Itoh et al. (2017) demonstrate that an intra-oceanic remnant arc collided against the northeastern Eurasian margin ca. 90 Ma, which provoked an intensive deformation event in the Late Cretaceous on the margin that was facing the northwestward-moving marginal sea plate. A geochemical study (Tamaki et al. 2009) clarified that the indented rim of the continent experienced a serious deformation, which is recorded as an anomalous burial rate of the forearc basin followed by a prompt exhumation.

A well-known regional unconformity, called the Cretaceous–Tertiary (K–T) Gap, developed at the end of the Mesozoic around the northwestern Pacific. However, drastic changes in plate motion and/or collision events related to this significant hiatus have not been observed. The Pacific Plate was characterized by moderate northwesterly convergence from 80 to 60 Ma. A shift in the shear direction on the Eurasian margin from sinistral to dextral has been demonstrated in the early Paleocene reconstructions, although the driving force of the transient stress modes has not been identified.

The Philippine Sea Plate began to emerge in the equatorial Pacific region 50 Ma (Hall 2002). In the southern Pacific, Australia started migrating northward ca. 45 Ma, forming embryotic convergent margins fringing around the Sundaland. The opening within the Celebes and Philippine Seas was active under a backarc setting. The famous bight between the Emperor seamount chain and the Hawaiian Islands suggests that the Pacific Plate changed its motion in the counterclockwise direction ca. 45–40 Ma. Since this episode, the Pacific Plate has continued moving steadily westward, and its linear velocity has been calibrated using data tables by Engebretson et al. (1985). The prototype of the Philippine Sea Plate continued to expand through 40 Ma (Hall 2002) with the azimuth of spreading center remaining fixed in the E–W direction. The divergence in the Celebes Sea stagnated 35 Ma. The early evolutionary phase of the Philippine Sea Plate had come to an end by ca. 30 Ma when the marginal sea was surrounded by subduction zones.

The most remarkable Paleogene tectonic episode around the northwestern Pacific margin was the formation of the regional Oligocene unconformity (Ounc; Takano et al. 2013). Reconstruction by Itoh et al. (2017) led to the interpretation of this event as an effect of strong compressive stress linked to the closure of the marginal sea plate and the subsequent collision of island arcs that occurred 30 Ma. At that point in time, all the components of the present-day arc–trench system had gathered at the margin.

The reconstruction by Hall (2002, 2012) indicates that the Philippine Sea Plate began to rotate clockwise around the beginning of the Miocene (24 Ma). However, many ambiguous points remain with regard to the kinematics of the rotation event. Kimura et al. (2014) have argued that the Philippine Sea Plate swiftly rotated clockwise simultaneously with the clockwise motion of southwest Japan that was driven by the Miocene opening of the Japan Sea. On the other hand, Yamazaki et al. (2010) have stated that the main rotational phase of the Philippine Sea Plate took place before 25 Ma based on new paleomagnetic data from the northwestern part of the plate. Hence, we refrain from passing judgment on this subject because investigations based on reliable geochronology are necessary before a strong conclusion can be reached.

The prevailing compressive regime during the formation of the regional Oligocene unconformity lingered into the Neogene. Through numerical modeling around central Hokkaido, Kusumoto et al. (2013) have clarified that an E–W compression and reverse fault motion must be combined with a longstanding dextral motion on an arc-bisecting fault zone to restore the geomorphological feature of the elongated middle Miocene basin, which may be linked to the incipient stage of the collision between the Kurile and northeastern Japan arcs.

As is fully described in Sect. 1.2.1, paleomagnetic studies spanning more than three decades have indicated that the rifting and backarc opening process of the Japan Sea occurred in a relatively short period no more recent than 15 Ma. The spatiotemporal distribution of marine sediments along the backarc coast supports this working hypothesis. Another notable finding of paleomagnetic studies is an arc bending just after the Japan Sea opening. A paleoreconstruction of the terrane arrangement in the eastern part of southwest Japan (Itoh 1988) clarified that the collision of the proto-Izu arc had precipitated the middle Miocene bending, which is a significant constraint on the coeval position of the eastern margin of the Philippine Sea Plate. Namely, the eastern margin seems to have been pinned in front of the easternmost part of southwest Japan since 15 Ma.

An overwhelming compressive stress seems to have been characteristic during the early Pliocene of Japan, resulting in E–W and N–S contraction features in the northeastern and southwestern Japan arcs, respectively. Though the driving force of such a tectonic episode has not yet been fully elucidated, some argue that subduction of the oceanic plates (Pacific and Philippine Sea Plates) is responsible for the regional arc deformation. If this is the case, the timeline of the oceanic plate movements should be reexamined in the light of deformation trends along the convergent margin.

This section represents a brief overview of the 100-M-year-long chronicle of the northwest Pacific and the Japanese Islands. Detailed investigations of existing geologic evidence have been presented by Itoh et al. (2017). As for the full set of figures like that shown in Fig. 1.2, a live video is available on the three-dimensional digital globe platform Dagik Earth, which is operated by the visualization group of the Integrated Earth Science Hub of Kyoto University (http://earth.dagik.org). Anyone can view our plate model on the Web (http://dagik.org/menu/land/Dagik_NWPacific_100my/e) in the form of animated cartoons.

1.1.2 Present-Day Configuration

As depicted in Fig. 1.3, the present-day Japanese Islands are under the influence of westward-moving Pacific and Philippine Sea Plates. The normal subduction of the Pacific Plate under the northeast Japan and Izu–Bonin arcs is responsible for the vigorous arc volcanism and frequent earthquakes on the plate interface as well as the active crustal deformation and faulting of the plates. In contrast, the Philippine Sea Plate is normally and obliquely subducting under the Ryukyu and southwestern Japan arcs, respectively, and is clearly responsible for the volcanism and seismic activity of the former and the wrench deformation of the latter.

The southwestern Japan arc also suffers from ongoing collision against the northeastern Japan arc, which results in active mountain building in its easternmost part. Some consider that this implies the commitment of the Pacific Plate, which may be a cause of prevailing E–W compression on the island arc. Thus, southwest Japan is a specific convergent margin related to multiple tectonic settings, and the Osaka sedimentary basin considered in the present study is located in the midst of a vigorous tectonic region.

1.2 Tectonic Epochs of Southwest Japan—Previous Studies

The Japan Sea formed as a result of early Miocene backarc rifting on the continental margin. Its fan-shaped opening mode inevitably caused the rotational motion of the rifted blocks, the process of which has been described in detail through laborious paleomagnetic studies (e.g., Otofuji and Matsuda 1983, 1987). Paleomagnetism also contributed to the determination of post-opening intra-arc deformation events. Itoh (1988) argued that the rapidly rotating southwest Japan collided against the Izu–Bonin arc on the eastern rim of the underthrusting Philippine Sea Plate and suffered bending of the pre-Cenozoic terranes. Figure 1.4 depicts the most probable paleoreconstruction, which takes into account the consistency of the jigsaw fitting of the subsea granitic blocks in the backarc basin. Another powerful tool for the elucidation of tectonic events is seismic interpretation. For example, through careful observation of multichannel reflection profiles covering the shelves around southwest Japan, Itoh and Nagasaki (1996) found an intensive N–S backarc contraction zone.

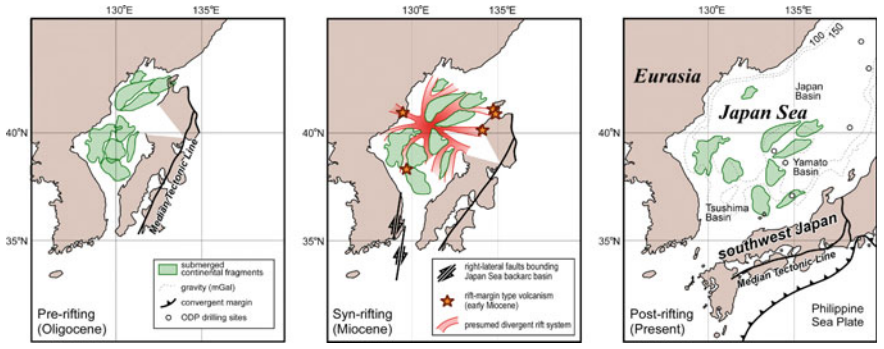

Fig. 1.4 Paleogeographic reconstruction of the opening process of the Japan Sea compiled after Itoh (2018)

1.2.1 Paleomagnetism

According to the temporal changes in declination, southwest Japan is regarded as a continental sliver that separated during the opening of the Japan Sea and rotated clockwise as much as 50° during the early Miocene (Otofuji et al. 1985, 1991). As delineated in Fig. 1.4, the Japan Sea is accompanied by abundant topographic highs with gravitational anomalies suggestive of a continental crust origin. Assuming that the topographic highs are granitic fragments submerged during or after the formation of the Japan Sea backarc basin, Torii et al. (1987) and Hayashida et al. (1991) determined the best-fitting arrangements of all of the continental jigsaw pieces. All the pieces can be successfully settled in the present Sino-Korean embayment without serious gap or overlap via rotation of southwest Japan by as much as 50°. As shown in Fig. 1.4 (left), the bending of the geologic zones of southwest Japan was restored, as represented by the straight trend of the Median Tectonic Line (MTL), by Itoh (1988), who determined the magnitude of the middle Miocene differential rotation in the eastern part of the rifted sliver.

Figure 1.4 (center) delineates the Eurasian margin during the early rifting stage. The numerous continental fragments within the Japan Sea point to the inevitable occurrence of a divergent crustal breakup. Hence, the hypothetical rift system was reconstructed as to surround the fragments. It is noteworthy that all of the rift-type volcanic rocks found around the Japan Sea (stars in the figure; e.g., Ishida et al. 1998) are located within the divergent zones. These subaerial volcanic rocks on the Japan Sea coast (e.g., Itoh et al. 2001) show a chemical affinity to the rift-margin volcanism (Ishida et al. 1998). By this stage, the sliver of the southwestern Japan arc had separated from the continent and undergone southward translation, which was promoted by right-lateral faulting at the western corner of the backarc basin (Itoh 2001) and coeval clockwise rotation on the eastern coast of the Korean Peninsula, as paleomagnetically detected by Lee et al. (1999).

Generally, the secular variation of the geomagnetic field results in considerable observational scatter and hinders the determination of precise rotational motions based on remanent magnetization. It is known, however, that fresh welded pyroclastic flow deposits preserve stable thermoremanent magnetization (TRM) as an instantaneous record of the geomagnetic field. Itoh et al. (2008) have executed an in-depth paleomagnetic investigation on a Quaternary pyroclastic flow deposit distributed in the easternmost part of southwest Japan and found that systematic deviations in the highly stable TRM directions of the volcaniclastic rock accord remarkably well with a rotation field around major active faults.

In an effort to comprehend the intra-arc neotectonic deformation, Itoh et al. (2011) investigated the distribution of coignimbrite ashes correlative with the source pyroclastic flow in remote areas. Previous studies (e.g., Hayashida et al. 1996) have shown that the directions of the detrital remanent magnetization (DRM) of such

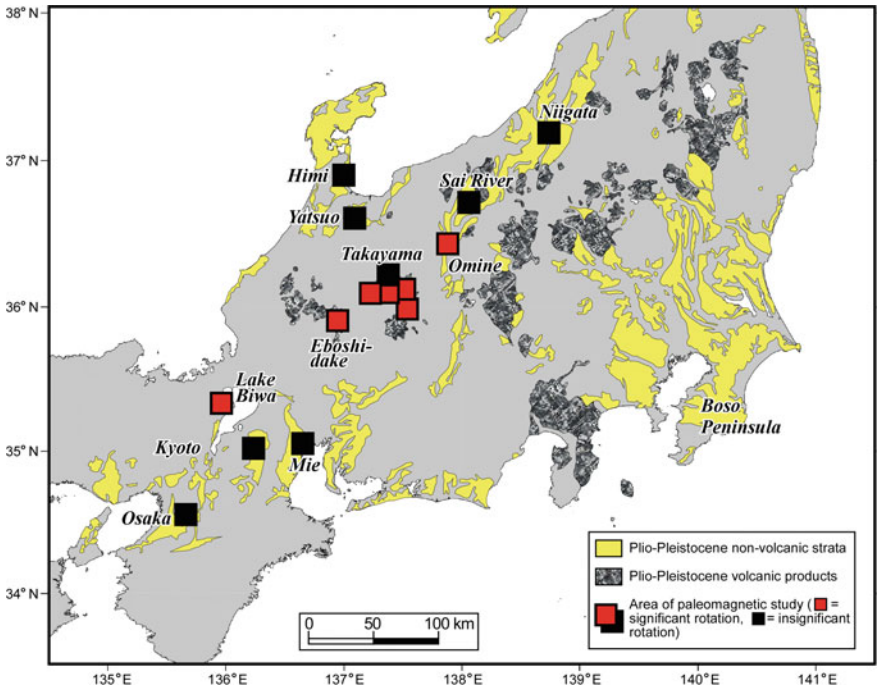

Fig. 1.5 Neotectonic clockwise rotation of the central part of Honshu Island, Japan, modified from Itoh et al. (2011)

ashes are identical with those of the TRM of the source volcanics. Figure 1.5 shows the results of a decade-long series of paleomagnetic expeditions conducted by Itoh and his coworkers. In this figure, a NE–SW zone of significant clockwise rotation is observable within the eastern part of southwest Japan.

1.2.2 Reflection Seismic Survey

The three-dimensional architectures of the shelves around the Japanese Islands have been visualized by means of detailed reflection seismic data, for the sake of natural resource exploration, and their development processes are described with reference to stratigraphic data on deep boreholes tied with seismic lines. Figure 1.6 shows an arc-parallel intensive contraction zone on the backarc shelf of southwest Japan. Itoh and Nagasaki (1996) have described the episode of the crustal shortening of southwest Japan that occurred during a short period in the latest Miocene, which is expressed as

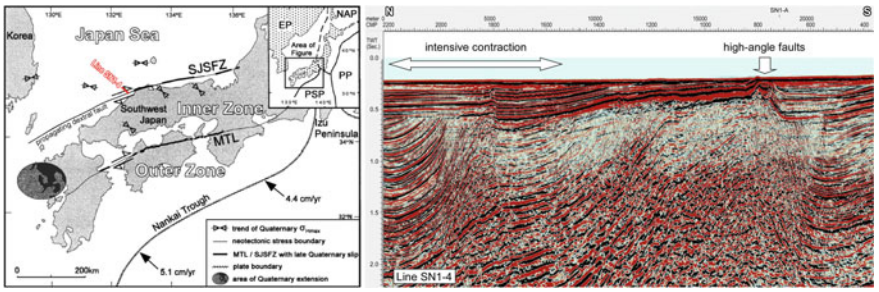

Fig. 1.6 Tectonic deformation of southwest Japan revealed by seismic reflection surveys modified from Itoh (2018). The seismic section (time migration; SN1-4) delineates a region of intensive contraction around the end of the Miocene and younger high-angle faults along the trace of the Southern Japan Sea Fault Zone (SJSFZ). EP, NAP, PP, and PSP in the regional inset represent the Eurasian, North American, Pacific, and Philippine Sea Plates, respectively

a remarkable unconformity. They attributed the extensive uplift/exhumation of the island arc to the resumed convergence of the Philippine Sea Plate. Although the fold amplitudes tend to diminish toward the intra-arc (Itoh and Nagasaki 1996), gentle undulation parallel to the arc elongation was widespread along the late Miocene convergent margin. Based on the spatiotemporal positions of tectonic events related to contraction and extension, Itoh et al. (2014) have argued that a compressive regime propagated progressively westward through the Plio-Pleistocene and have regarded the change in the stress–strain state as an effect of the shift of the Euler pole of the subducting Philippine Sea Plate.

Itoh et al. (2002) combined high-resolution single-channel data and detected a young right-lateral strike-slip deformation trend on the backarc called the Southern Japan Sea Fault Zone (SJSFZ in Fig. 1.6). High-angle faults cutting the Japan Sea floor shown in the profile of Fig. 1.6 constitute part of the embryotic rupture. This latest deformation phase is driven by the oblique convergence of the Philippine Sea Plate, which is related to the counterclockwise change in converging direction that occurred from ca. 2 to 1 Ma (Nakamura et al. 1987).

1.3 Recent Crustal Movements Revealed by Geodetic Observation

Around the beginning of this century, analytical geodetic methods substantially progressed as a result of the introduction of remote sensing data. From the long-term deviation observed in a GPS satellite network dataset, Sagiya et al. (2000) and Toya and Kasahara (2005) found a zone of exceptionally high strain rate connecting Niigata on the backarc of central Japan and Kobe on the northwestern coast of Osaka Bay. The Niigata–Kobe Tectonic Zone (NKTZ) is accompanied by numerous active faults (Fig. 1.7) and studded with many epicenters of disastrous earthquakes. It is note-

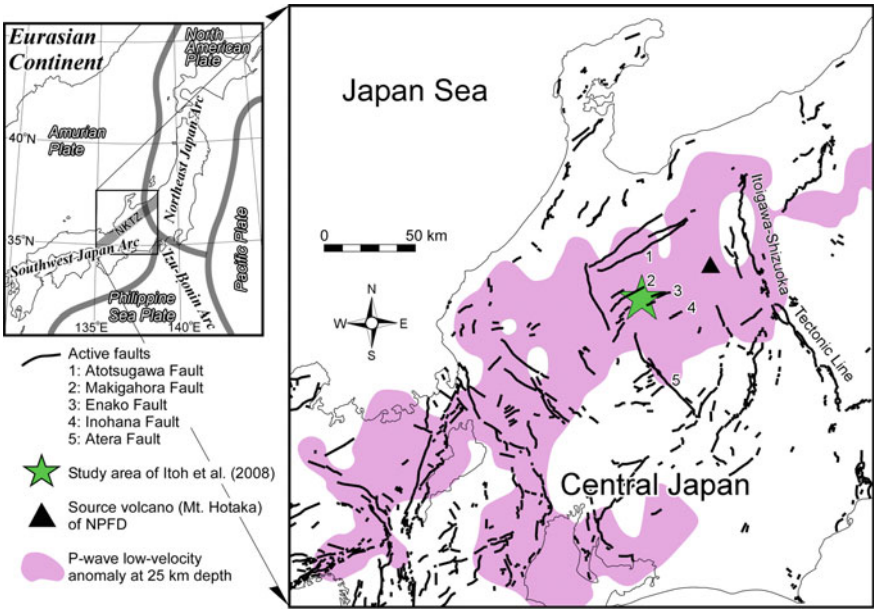

Fig. 1.7 Location of the Niigata–Kobe Tectonic Zone (NKTZ in inset map) and other neotectonic information modified from Itoh et al. (2011). The distribution of active faults is shown after the Working Group for Compilation of 1:2,000,000 Active Faults Map of Japan (2000). The P wave low-velocity anomaly is after Nakajima and Hasegawa (2007). The star denotes the paleomagnetic study area of Itoh et al. (2008)

worthy that the NKTZ coincides with the region of clockwise rotation detected in paleomagnetic studies conducted by Itoh et al. (2008, 2011). Thus, the geodetically observed deformation zone is not only an instantaneous feature but also a weak portion throughout the late Quaternary. Figure 1.7 suggests that a lower-crustal anomaly in the seismic wave velocity is present at the root of the NKTZ. This thermophysical belt runs along the north of the Osaka sedimentary basin and likely affects its evolutionary processes.

1.4 Spatiotemporal Overview of the Osaka Sedimentary Basin

Our review has shown that the Osaka basin evolved in a longstanding deformation zone and its stratigraphic and structural features are a valuable record of transient tectonic regimes. The first subsection here explores the geographic evolution of the basin over several million years (Fig. 1.8), which reflects a balance between the development of the basin accommodation and the uplift/exhumation rate of mountainous

ranges. Around the study area, temporal changes in active landforms have been governed by the mode of convergence of the Philippine Sea Plate. The subduction of the young and buoyant plate provoked strong tectonic stress and resultant ubiquitous fracturing in the brittle upper crust of the island arc. The following subsection is devoted to describing a conspicuous tectonic region, the Kinki Triangle (Fig. 1.9), which is characterized by numerous active faults. It is, in a sense, a buffer zone of complex structural building on the plate margin where the raising and lowering of fault-bounded blocks compensate for the high crustal strain rate. In the final subsection, the deep interior around Osaka Bay is assessed based on gravitational analysis. Although the analytical methods discussed in this chapter are less sensitive than the seismic methods that will be fully presented in Chap. 3, it has been demonstrated that the latest technique utilizing the gravity gradient tensor can successfully reveal the intra-basin architecture, and volumetric analysis assuming simple density contrast has yielded an order estimation of the basinal dimension. Finally, a numerical model of the crustal deformation provides some insight into the reason enormous sags develop at contractional bends of arc-bisecting active strike-slip faults.

1.4.1 Paleogeography

Paleogeographic maps for five time slices since 5–4 Ma in the Kinki district are shown in Fig. 1.8. Correlation among the sediments from the three sedimentary basins (Tokai, Lake Biwa, and Osaka from east to west) is based on tephrochronology, radiometric dating, paleomagnetism, and biostratigraphy, and the paleogeographic assessment refers to maps by Yokoyama (1969), Takemura (1985), Sugiyama (1992), and Takemura et al. (2013). The Tokai, Lake Biwa, and Osaka basins are filled by the Tokai, Kobiwako, and Osaka Groups, respectively. This paleogeographic map suggests the tectonic development in this district progressed as described in the following synopsis.

From their tectono-sedimentary facies, a comparison of the basinal transition about the Tokai, Paleo-Lake Biwa, and Osaka basins indicates that the evolutionary history of the central Kinki district can be divided into stages with transitions ca. 3.0 Ma and 1.5–1.2 Ma, which suggests the occurrence of simultaneous changes in the stress state of this province at these transition times. According to Yokoyama (1969, 1984), the history of Paleo-Lake Biwa has four stages: the Older I, Older II, Actual I, and Actual II. These roughly correspond to 5–4 Ma, 3–2 Ma, 1 Ma, and 0.5 Ma, respectively, in the chronological order of Fig. 1.8. In the early stages, the Tokai and Paleo-Lake Biwa basins emerged in the southern area and translated gradually to the north during the Older I. Subsequently, the sedimentary basin migrated northwestward around the Older II. The formation of the Osaka sedimentary basin initiated at this stage and migrated gradually to the north and west. The situations of each of these neotectonic stages are now considered one by one.

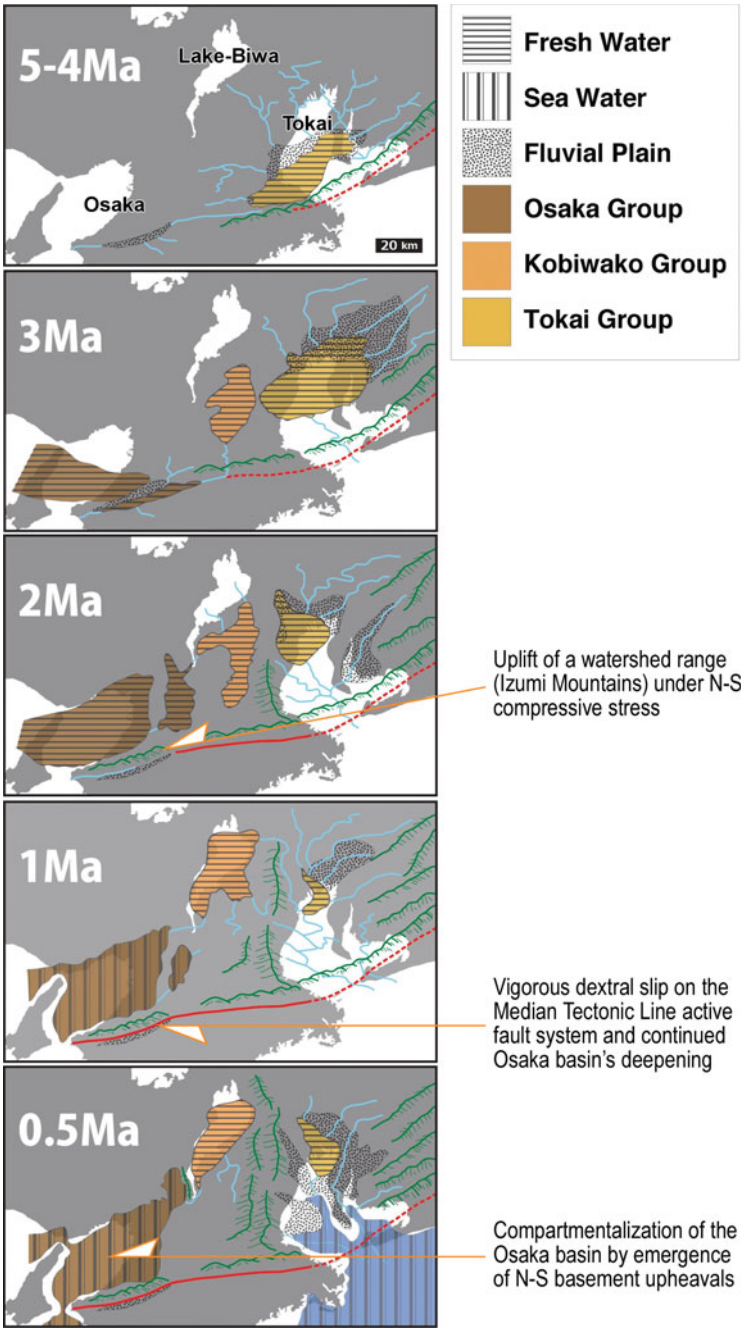

Fig. 1.8 Paleogeographic reconstruction of the Osaka basin and surrounding areas since 5 Ma after Itoh and Takemura (2016)

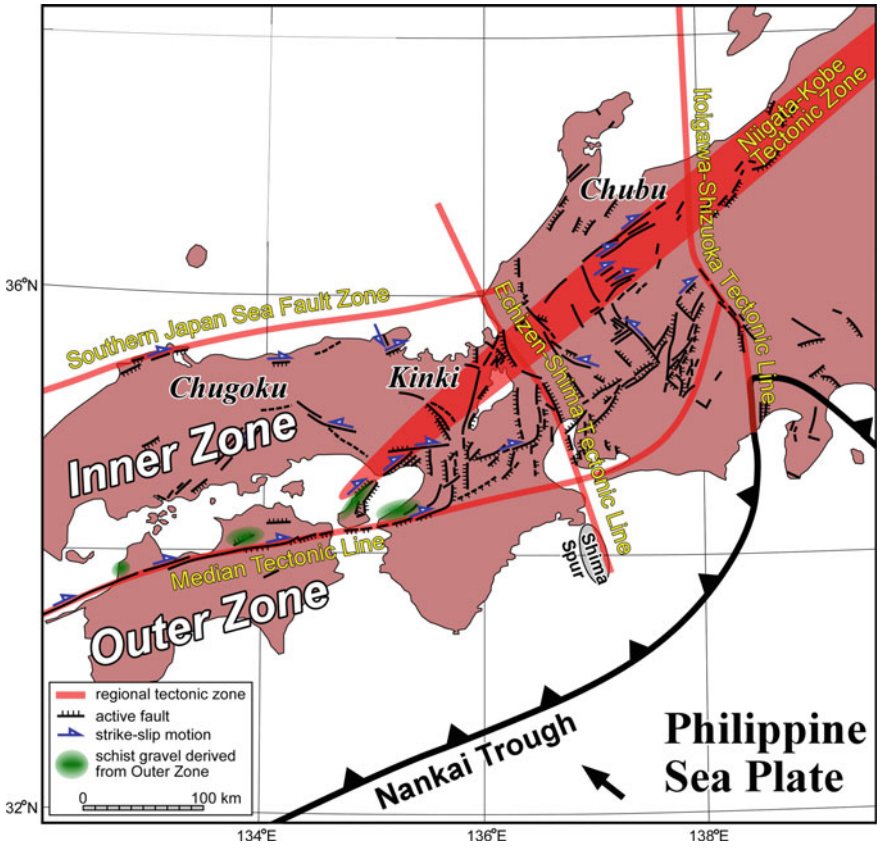

Fig. 1.9 Active fault distribution around the Kinki district and the Kinki Triangle after Huzita (1976), compiled after Itoh et al. (2013a)

The paleogeographic map for 5–4 Ma shows the basin distributions in the southern part of Lake Tokai. Although not at a mappable scale, a precursor existed around the southern part of the Paleo-Lake Biwa basin. Clay-dominant sediments were deposited in the lacustrine water in this region. These two basins may have been connected in the earlier stages of the Older I. It should be noted that the shape of the sedimentary basin is elongated in the E–W direction. The pathway formation and basin morphology indicated here may be attributable to the upheaval of the southern area under tectonic stress in N–S direction.

The paleogeographic map for 3 Ma delineates the northward shift of the Tokai basin, which was connected with the Paleo-Lake Biwa basin. The initiation of the Osaka basin is also observable in this map. The basin center in the Tokai area shifted from south to north, forming a stable accommodation filled with massive clay deposits. The northward migration of the Lake Tokai and Paleo-Lake Biwa

basins developed throughout the Plio-Pleistocene, forming a sharp contrast to the Osaka basin, which was pinned around the present depocenter at that time.

The paleogeographic map for 2 Ma shows the distribution of sediments in the northern part of the Tokai basin and an elongated basin shape with a N–S orientation in the Paleo-Lake Biwa basin area. The distribution of freshwater sediments in the Osaka basin is clearly identifiable in this map. The N–S elongation of these basins may imply a stress state with an E–W trend. However, the coeval uplift of an east-trending watershed of the Izumi Mountains on the southern margin of the Osaka basin (Fig. 1.8; Oka 1978) reveals the great complexity of the evolutionary plot of the Kinki district. More precise age control of tectonic events is needed to determine the actual course of events and establish a causal relationship between spatiotemporal stress changes and the basin development processes.

The paleogeographic map for 1 Ma represents the earlier stage of the Actual I. From the Older II to the Actual I, the center of the sedimentary basin migrated northwestward. Abundant gravels are characteristic in the uppermost sediments of the Older II. Around the transition from the Older II to the Actual I, the Tokai sedimentary basin was diminished. The sedimentary basin of the Actual I in the Lake Biwa region shifted gradually to the west, accompanied by the upheaval of the eastern N–S mountains. In the Osaka sedimentary basin, marine transgressions have occurred since 1.3 Ma, as recorded in offshore sequences around the Kansai International Airport (KIX18-1 Editorial Committee 2011). The marine environment invaded the eastern intermontane basin at that time (Fig. 1.8). This rearrangement of the basins may be related to accelerated right-lateral slips on the Median Tectonic Line (MTL) and a driving regional shear stress provoked by a highly oblique subduction of the Philippine Sea Plate.

The paleogeographic map for 0.5 Ma shows the situation of the ongoing Actual II stage. Topographic contrast between the present Lake Biwa basin and the west-adjoining mountainous areas can be distinguished. Repeated marine transgressions related to global sea level changes reached the Kyoto basin and have been preserved as marine sediments around the ancient capital. During this stage, the basin was divided by structural movements with a N–S trend accompanied by rapid subsidence and upheaval during the Actual I and Actual II stages in the present Lake Biwa and Osaka Bay areas. This episode resulted in the conspicuous N–S alignment of the basins and mountains.

In this way, the migration patterns of the sedimentary basins in the Kinki district seem to have a common explanation regarding the interaction between the upheaval of southern areas and the tilting of eastern areas. We propose that the ongoing deposition in the central part of the Kinki region since the Pliocene is the result of two juxtaposed tectonic stress states. Huzita (1969) stated that the change in tectonic stress states took place in the inner zone of southwest Japan during the Plio-Pleistocene. This transition from a N–S to an E–W compressional state has been regarded as conspicuous. The present review encompassing the latest event chronology basically supports his model of the ongoing tectono-sedimentary turnover process since the Pliocene.

1.4.2 Active Faults on Land

1.4.2.1 Geomorphological achievements

As depicted in Fig. 1.9, the Chubu and Kinki districts in the eastern portion of the southwestern Japan arc are scarred by countless active faults. Through their thorough geomorphological examination, the Research Group for Active Faults (1991) has made a substantial contribution to the present understanding of the ongoing deformation mode of the island arc. They found that north- and east-trending faults show unexceptionally reversed and dextral slips, respectively. Another provocative finding is that NE–SW and NW–SE faults have systematic right- and left-lateral motion senses, respectively. The insight gained from this is that the fracture pattern works to reconcile E–W regional tectonic stress likely related to the westward-moving Pacific Plate (e.g., Huzita 1980). Dextral activities dominant upon the trench (Nankai Trough; Fig. 1.9)-parallel intra-arc faults, such as the MTL and Arima—Takatsuki Tectonic Line, may be linked with the counterclockwise shift of motion of the Philippine Sea Plate during the late Quaternary, which is discussed in this book.

1.4.2.2 Tectonic significance of the "Kinki Triangle"

Huzita (1976) noted that a triangular portion within the central Kinki district, which he named the "Kinki Triangle," is characterized by intensive deformation and basin formation. The southern base of this triangle is coincident with the MTL, and its northwestern side roughly corresponds to the NKTZ, the features of which are documented in Sect. 1.3. However, the tectonic context of the northeastern side was not initially clearly defined.

Itoh et al. (2013a) attempted to redefine this significant tectonic boundary from the perspective of consistency in the deformation trends on both the forearc and backarc regions. Formerly, Itoh et al. (2006) had described the geologic structures of the southwestern Japan backarc and found an inversion trend nearly normal to the elongation of the arc. Based on seismic profiles, they suggested that the inversion had developed during the Plio-Pleistocene. On the opposite side of the arc, the Shima Spur built up in the early Quaternary (see Fig. 1.9; Takano et al. 2009). These structural trends are bridged linearly by onshore active faults and constitute a regional contraction zone. This evidence directed Itoh et al. (2013a) to the notion that the zone is a significant neotectonic boundary, which was newly named the Echizen-Shima Tectonic Line (ESTL). Although the origin of the ESTL is not yet fully understood, it may have a close connection with the middle Miocene bending event in eastern southwest Japan caused by the collision of the Izu–Bonin arc (see Sect. 1.2) because paleomagnetic studies (e.g., Itoh and Ito 1989) have demonstrated that the hinge line of the collision-driven intensive arc deformation was located around the ESTL.

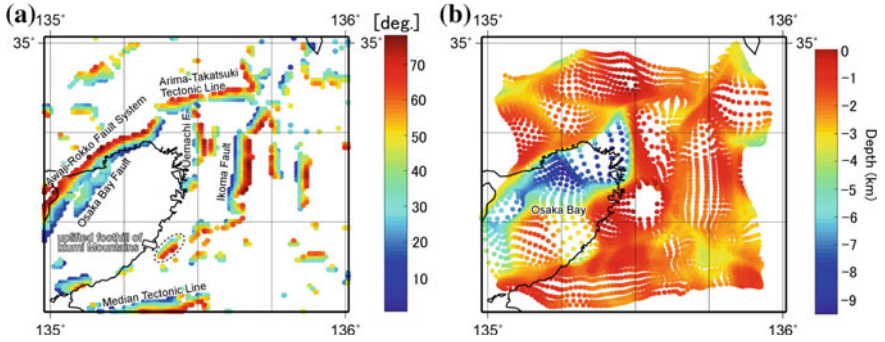

Fig. 1.10 Gravity gradient tensor analysis results. **a** Distribution of estimated dip angles of faults and/or structural boundaries around the Osaka basin, which was first preliminarily characterized by Itoh et al. (2015) and then refined by Kusumoto (2016). The dip angle estimation was conducted in the areas with a dimensionality index *I* of less than 0.5 and a horizontal gravity gradient *HG* of 20 E (2 mGal/km) or greater. **b** Solution clouds obtained by tensor Euler deconvolution. Refer to Kusumoto (2016) for the calculation parameters

1.4.3 Geophysical Studies

1.4.3.1 Gravity anomaly and gravity gradient tensor

Beiki (2013) suggested that the dip angle of the causative body of a gravity anomaly can be estimated from the three Cartesian components of the maximum eigenvector of the gradient tensor of the potential field. In the present study area, Itoh et al. (2015) and Kusumoto (2016) have applied this technique to estimate the dip angles of faults and/or structural boundaries and obtained an angle distribution compatible with the results from other geophysical studies, such as reflection seismic surveys. Figure 1.10a depicts their analytical results. Most of the faults in this region are characterized by dip angles exceeding 55°. For example, the dip angles of the Uemachi Fault and Arima–Takatsuki Tectonic Line range from 55° to 65°, and those of the Ikoma Fault and Awaji–Rokko Fault System are even steeper, reaching or even exceeding 70°. The Ikoma Fault shows particularly high dip angles on the inland side. Because most of the active faults have both lateral and reversed slip components within the analyzed area, these estimations seem to be realistic and reasonable.

On the other hand, a notable feature of the diagram is unexpected zones of low dip angles parallel to some major faults. On the western side of the Ikoma Fault, we can see a low-angle lobe running near the N–S depocenter trend of an elongated subbasin. As described by Itoh (2016), this is a zone of concealed reverse faults that are partly responsible for the vigorous uplift of the Ikoma Mountains. It is plausible

that the terraced displacement of basement rocks cut by a number of secondary faults has been recognized as a low-angle structural boundary in the gravity analysis. Another wider low-angle structure zone lies on the basin side of the Awaji–Rokko Fault System and seems to coincide with the broad strands of the Osaka Bay Fault. The tectonic context of the low dip angles based on the gravity gradient tensor is discussed in Chaps. 3 and 4 through the interpretation of reflection seismic data.

Euler deconvolution is a semi-automated method of interpreting geophysical data on the basis of Euler's homogeneity equation and is often employed to estimate the locations and/or outlines of causative bodies. Kusumoto (2016) employed tensor Euler deconvolution (Zhang et al. 2000) to obtain information on subsurface structures. After determining suitable values for the input parameters, he found the morphological features of the Osaka sedimentary basin, as presented in Fig. 1.10b. On the assumption that the solution clouds roughly represent the basement structure in this region, they provide interesting information on the subsurface structures. These results indicate that the northern part of Osaka Bay is much deeper than its southern counterpart and that the Awaji–Rokko Fault System and the Uemachi Fault have steep dip angles toward the Osaka Bay area. In the Ikoma Fault area, the basement is deeper toward the inland side. In addition, an outline of the circular structures within the Osaka Plain has been extracted and presents a very shallow depth (0–1 km). In summary, the abovementioned dip values are supported by the results obtained by Kusumoto (2016) using tensor Euler deconvolution.

1.4.3.2 Volumetric analysis

In the Kinki district, the Arima–Takatsuki Tectonic Line (east-trending fault on the northern flank of the Osaka basin; Fig. 1.10) is a unique branch-off fault from the trunk line (eastern part of the active MTL) and has a dextral slip rate comparable to the parallel MTL during the Quaternary (Research Group for Active Faults 1991). Although this left-stepping fault alignment should result in a confining bend, the area is featured by a recent vigorous basin formation centered around Osaka Bay.

Itoh et al. (2013b) have presented a simple dimensional model at this termination of the MTL, in which the mass deficiency was estimated from the gravity anomaly data of the Osaka basin represented on a mesh with a 5 km interval (Fig. 1.11) using Gauss's theorem (e.g., Wangen 2010). The first approximation of the sedimentary basin volume was 9.1×10^2 km^3 under the assumption of a density contrast of 400 kg/m^3 between sediment and basement rock. Their calculation clarified that the total volume of the sedimentary basin at the eastern end of the MTL is approximately one-tenth of that at the western end around central Kyushu. This difference may be attributable to a difference in the basin-forming mechanism between the releasing and confining steps of a transcurrent fault.

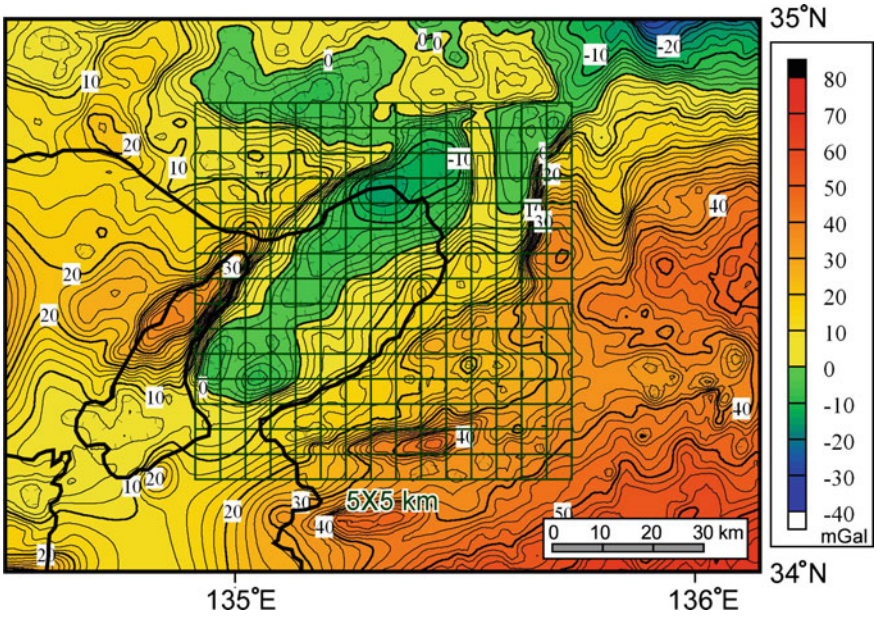

Fig. 1.11 Bouguer gravity anomaly map (Geological Survey of Japan 2004) around the Osaka basin (Bouguer density of 2670 kg/m^3). The grid shows data points for the volumetric analysis executed by Itoh et al. (2013b)

1.4.3.3 Numerical modeling of basin formation

Figure 1.12 depicts a schematic of the deformation at stepping parts of strike-slip faults. Generally, a depression is formed at a right-stepping part of a dextral fault (Fig. 1.12a), whereas an upheaval is formed at a left-stepping part (Fig. 1.12b). The MTL and the Arima–Takatsuki Tectonic Line (Fig. 1.12c) constitute a confining left-step of the regional dextral fault. However, geologic information clearly indicates that the Osaka region was a site of vigorous basin formation during the Quaternary. To solve this paradox, Kusumoto et al. (2001) attempted to develop a dislocation model to assess the vertical displacement at a complex termination of the strike-slip fault. They found that the actual basin morphology can be successfully restored by introducing reverse motions on the transverse secondary faults, which are delineated in Fig. 1.12c. The simulated deformation pattern predicts that a relative basement high emerged within a depression surrounded by the modeled active faults, which may correspond to the basin compartmentalization phenomenon that occurred throughout the late Pleistocene.

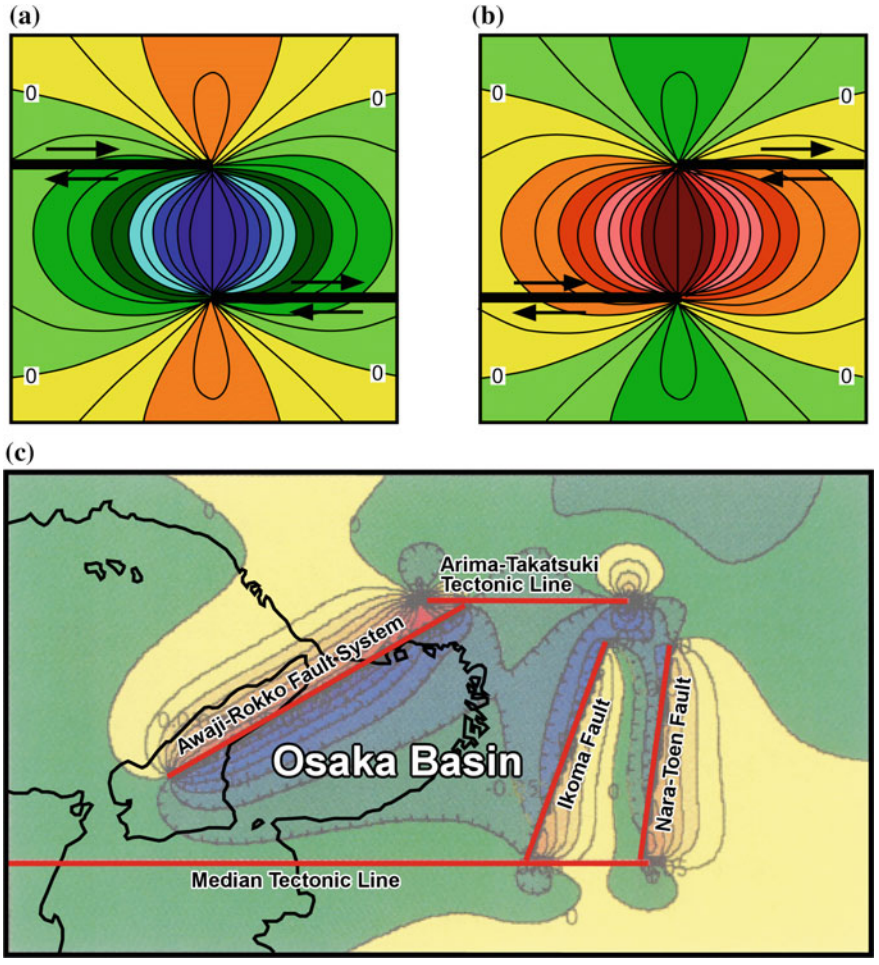

Fig. 1.12 Numerical model of basin formation after Kusumoto et al. (2001), compiled after Itoh et al. (2013b). **a** Normalized vertical displacement at a releasing bend of a strike-slip fault. **b** Normalized vertical displacement at a confining bend of a strike-slip fault. **c** Dislocation model of the Osaka basin. Red lines are major faults adopted for the model. Warm and cold color gradations indicate upheaval and subsiding areas, respectively

References

Beiki M (2013) TSVD analysis of Euler deconvolution to improve estimating magnetic source parameters: an example from the Asele area, Sweden. J Appl Geophys 90:82–91. https://doi.org/10.1016/j.jappgeo2013.01.002

Engebretson DC, Cox A, Gordon RC (1985) Relative motions between oceanic and continental plates in the Pacific Basin. Geol Soc Am Spec Paper 206:1–59

Geological Survey of Japan (2004) Gravity CD-ROM of Japan, ver 2, digital geoscience map P-2. Geological Survey of Japan AIST, Tsukuba
Hall R (2002) Cenozoic geological and plate tectonic evolution of SE Asia and the SW Pacific: computer-based reconstructions, model and animations. J Asian Earth Sci 20:353–431
Hall R (2012) Late Jurassic-Cenozoic reconstructions of the Indonesian region and the Indian Ocean. Tectonophysics 570–571:1–41
Hayashida A, Fukui T, Torii M (1991) Paleomagnetism of the Early Miocene Kani Group in southwest Japan and its implication for the opening of the Japan Sea. Geophys Res Lett 18:1095–1098
Hayashida A, Kamata H, Danhara T (1996) Correlation of widespread tephra deposits based on paleomagnetic directions: link between a volcanic field and sedimentary sequences in Japan. Quat Int 34–36:89–98
Huzita K (1969) Tectonic development of southwest Japan in the Quaternary period. J Geosci Osaka City Univ 12:53–70
Huzita K (1976) The Quaternary tectonic stress states of southwest Japan. J Geosci Osaka City Univ 20:93–103
Huzita K (1980) Role of the Median Tectonic Line in the Quaternary tectonics of the Japanese islands. Mem Geol Soc Jpn 18:129–153
Ishida H, Ishiwatari A, Kagami H (1998) The Mt. Wasso moonstone rhyolitic welded tuff in the Neogene Hokuriku Group, central Japan. J Geol Soc Jpn 104:281–295
Itoh Y (1988) Differential rotation of the eastern part of southwest Japan inferred from paleomagnetism of Cretaceous and Neogene rocks. J Geophys Res 93:3401–3411
Itoh Y (2001) A Miocene pull-apart deformation zone at the western margin of the Japan Sea back-arc basin: implications for the back-arc opening mode. Tectonophysics 334:235–244
Itoh Y (2016) Subsurface structure of Osaka sedimentary basin and its tectonic evolution. In: Itoh Y (ed) Research frontiers of sedimentary basin interiors—a case study and methodological review on an oblique convergent margin. Nova Science Publishers Inc., NY, pp 27–70
Itoh Y (2018) Post-opening deformation history of the Japan Sea backarc basin: tectonic processes on an active margin governed by the mode of plate convergence. In: Sharkov EV (ed) Tectonics. InTech, Croatia (in press)
Itoh Y, Ito Y (1989) Confined ductile deformation in the Japan arc inferred from paleomagnetic studies. Tectonophysics 167:57–73
Itoh Y, Nagasaki Y (1996) Crustal shortening of southwest Japan in the Late Miocene. The Island Arc 5:337–353
Itoh Y, Takemura K (2016) Subsurface structure of the Osaka Plain—its perspective based on geophysical data and future problems. News Osaka Micropaleontol 17:1–74
Itoh Y, Doshida S, Kitada K, Danhara T (2001) Paleomagnetism and fission-track ages of the Mt. Wasso moonstone rhyolitic welded tuff in the Ishikawa Prefecture, Central Japan. Bull Geol Surv Jpn 52:573–579
Itoh Y, Tsutsumi H, Yamamoto H, Arato H (2002) Active right-lateral strike-slip fault zone along the southern margin of the Japan Sea. Tectonophysics 351:301–314
Itoh Y, Uno K, Arato H (2006) Seismic evidence of divergent rifting and subsequent deformation in the southern Japan Sea, and a Cenozoic tectonic synthesis of the eastern Eurasian margin. J Asian Earth Sci 27:933–942
Itoh Y, Kusumoto S, Furubayashi T (2008) Quantitative evaluation of Quaternary crustal deformation around the Takayama Basin, Central Japan: a paleomagnetic and numerical modeling approach. Earth Planet Sci Lett 267:517–532
Itoh Y, Kusumoto S, Miyamoto K, Inui Y (2011) Short-/long-term deformation of upper crust: integrated and quantitative approach for neotectonics. In: Sharkov EV (ed) New frontiers in tectonic research—general problems, sedimentary basins and island arcs. InTech, Croatia, pp 283–308
Itoh Y, Takemura K, Kusumoto S (2013a) Neotectonic intra-arc basins within southwest Japan—-conspicuous basin-forming process related to differential motion of crustal blocks. In: Itoh Y (ed)

Mechanism of sedimentary basin formation—multidisciplinary approach on active plate margins. InTech, Croatia, pp 191–207. http://dx.doi.org/10.5772/56588
Itoh Y, Kusumoto S, Takemura K (2013b) Characteristic basin formation at terminations of a large transcurrent fault—basin configuration based on gravity and geomagnetic data. In: Itoh Y (ed) Mechanism of sedimentary basin formation—multidisciplinary approach on active plate margins. InTech, Croatia, pp 255–272. http://dx.doi.org/10.5772/56702
Itoh Y, Kusumoto S, Takemura K (2014) Evolutionary process of Beppu Bay in central Kyushu, Japan: a quantitative study of the basin-forming process controlled by plate convergence modes. Earth Planet Space 66:74. https://doi.org/10.1186/1880-5981-66-74
Itoh Y, Kusumoto S, Takemura K (2015) Tectonically controlled asymmetric basin formation and evolution: an example from an active plate margin. In: Veress B, Szigethy J (eds) Horizons in Earth science research, vol 14. Nova Science Publishers Inc., NY, pp 123–141
Itoh Y, Takano O, Takashima R (2017) Tectonic synthesis: a plate reconstruction model of the NW Pacific region since 100 Ma. In: Itoh Y (ed) Dynamics of arc migration and amalgamation—architectural examples from the NW Pacific margin. InTech, Croatia, pp 93–111. http://dx.doi.org/10.5772/67358
Kimura G, Hashimoto Y, Kitamura Y, Yamaguchi A, Koge H (2014) Middle Miocene swift migration of the TTT triple junction and rapid crustal growth in southwest Japan: a review. Tectonics 33:1219–1238. https://doi.org/10.1002/2014TC003531
Kinoshita O (1995) Migration of igneous activities related to ridge subduction in southwest Japan and the East Asian continental margin from the Mesozoic to the Paleogene. Tectonophysics 245:25–35
KIX18-1 Editorial Committee (2011) Report on KIX18-1 in Kansai International Airport. KIX18-1 Editorial Committee, Osaka
Kusumoto S (2016) Estimations of subsurface structures by gravity anomaly and gravity gradient tensor. In: Itoh Y (ed) Research frontiers of sedimentary basin interiors—a case study and methodological review on an oblique convergent margin. Nova Science Publishers Inc, NY, pp 9–26
Kusumoto S, Fukuda Y, Takemura K, Takemoto S (2001) Forming mechanism of the sedimentary basin at the termination of the right-lateral left-stepping faults and tectonics around Osaka Bay. J Geogr 110:32–43
Kusumoto S, Itoh Y, Takano O, Tamaki M (2013) Numerical modeling of sedimentary basin formation at the termination of lateral faults in a tectonic region where fault propagation has occurred. In: Itoh Y (ed) Mechanism of sedimentary basin formation—multidisciplinary approach on active plate margins. InTech, Croatia, pp 273–304. http://dx.doi.org/10.5772/56558
Lee YS, Ishikawa N, Kim WK (1999) Paleomagnetism of Tertiary rocks on the Korean Peninsula: tectonic implications for the opening of the East Sea (Sea of Japan). Tectonophysics 304:131–149
Nakajima J, Hasegawa A (2007) Deep crustal structure along the Niigata-Kobe Tectonic Zone, Japan: its origin and segmentation. Earth Planet Space 59:e5–e8
Nakamura K, Renard V, Angelier J, Azema J, Bourgois J, Deplus C, Fujioka K, Hamano Y, Huchon P, Kinoshita H, Labaume P, Ogawa Y, Seno T, Takeuchi A, Tanahashi M, Uchiyama A, Vigneresse JL (1987) Oblique and near collision subduction, Sagami and Suruga Troughs—preliminary results of the French-Japanese 1984 Kaiko cruise, Leg 2. Earth Planet Sci Lett 83:229–242
Oka Y (1978) The formation of the Izumi range and the Osaka Group. Quat Res Jpn 16:201–210
Otofuji Y, Matsuda T (1983) Paleomagnetic evidence for the clockwise rotation of southwest Japan. Earth Planet Sci Lett 62:349–359
Otofuji Y, Matsuda T (1987) Amount of clockwise rotation of southwest Japan—fan shape opening of the southwestern part of the Japan Sea. Earth Planet Sci Lett 85:289–301
Otofuji Y, Hayashida A, Torii M (1985) When was the Japan Sea opened?: paleomagnetic evidence from southwest Japan. In: Nasu N, Uyeda S, Kushiro I, Kobayashi K, Kagami H (eds) Formation of active ocean margins. Terra Publishing Co., Tokyo, pp 551–566
Otofuji Y, Itaya T, Matsuda T (1991) Rapid rotation of southwest Japan—palaeomagnetism and K-Ar ages of Miocene volcanic rocks of southwest Japan. Geophys J Int 105:397–405

Research Group for Active Faults (1991) The active faults in Japan: sheet maps and inventories, rev edn. University of Tokyo Press, Tokyo

Sagiya T, Miyazaki S, Tada T (2000) Continuous GPS array and present-day crustal deformation of Japan. Pure Appl Geophys 157:2303–2322

Sugiyama Y (1992) Neotectonics of the forarc zone and the Setouchi province in southwest Japan. Mem Geol Soc Jpn 40:219–233

Takano O, Nishimura M, Fujii T, Saeki T (2009) Sequence stratigraphic distribution analysis of methane-hydrate-bearing submarine-fan turbidite sandstones in the eastern Nankai trough area: relationship between turbidite facies distributions and BSR occurrence. J Geogr 118:776–792

Takano O, Itoh Y, Kusumoto S (2013) Variation in forearc basin configuration and basin-filling depositional systems as a function of trench slope break development and strike-slip movement: examples from the Cenozoic Ishikari–Sanriku-Oki and Tokai-Oki–Kumano-Nada forearc basins, Japan. In: Itoh Y (ed) Mechanism of sedimentary basin formation—multidisciplinary approach on active plate margins. InTech, Croatia, pp 3–25. http://dx.doi.org/10.5772/56751

Takemura K (1985) The Plio-Pleistocene Tokai Group and the tectonic development around Ise Bay of central Japan since Pliocene. Mem Fac Sci, Kyoto Univ, Ser Geol Mineral 51:21–96

Takemura K, Haraguchi T, Kusumoto S, Itoh Y (2013) Tectonic basin formation in and around Lake Biwa, central Japan. In: Itoh Y (ed) Mechanism of sedimentary basin formation—multidisciplinary approach on active plate margins. InTech, Croatia, pp 209–229. http://dx.doi.org/10.5772/56667

Tamaki M, Tsuchida K, Itoh Y (2009) Geochemical modeling of sedimentary rocks in the Central Hokkaido, Japan: episodic deformation and subsequent confined basin-formation along the eastern Eurasian margin since the Cretaceous. J Asian Earth Sci 34:198–208

Torii M, Ishikawa N, Hayashida A, Nishimura S (1987) Paleomagnetic and geochronological study on Miocene rocks around Kyushu Island and Korean Peninsula: regional tectonics at the time of back-arc opening of the Japan Sea. In: Tsuchi R (ed) Pacific Neogene events in time and space. IGCP-246 Working Group, Shizuoka, p 99–101

Toya Y, Kasahara M (2005) Robust and exploratory analysis of active mesoscale tectonic zones in Japan utilizing the nationwide GPS array. Tectonophysics 400:27–53

Wangen M (2010) Physical principles of sedimentary basin analysis. Cambridge University Press, London

Working Group for Compilation of 1:2,000,000 Active Faults Map of Japan (2000) New 1:2,000,000 active faults map of Japan. Active Fault Res 19:3–12

Yamazaki T, Takahashi M, Iryu Y, Sato T, Oda M, Takayanagi H, Chiyonobu S, Nishimura A, Nakazawa T, Ooka T (2010) Philippine Sea Plate motion since the Eocene estimated from paleomagnetism of seafloor drill cores and gravity cores. Earth Planets Space 62:495–502

Yokoyama T (1969) Tephrochronology and paleogeography of the Plio-Pleistocene in the eastern Setouchi geologic province, southwest Japan. Mem Fac Sci, Kyoto Univ, Ser Geol Mineral 36:19–85

Yokoyama T (1984) Stratigraphy of the Quaternary system around Lake Biwa and geohistory of the ancient Lake Biwa. In: Horie S (ed) Lake Biwa. Dr. W. Junk, The Hague, pp 43–128

Zhang C, Mushayandebvu MF, Reid AB, Fairhead JD, Odegrad ME (2000) Euler deconvolution of gravity tensor gradient data. Geophysics 65:512–520

Chapter 2
Basic Knowledge—Stratigraphy of the Osaka Group

Abstract This chapter briefly describes the stratigraphic basis of the Osaka Group, which has been accumulating within the Osaka sedimentary basin since ca. 3.5 Ma. Among the three Plio-Pleistocene basins in the Kinki district of southwest Japan (Tokai, Paleo-Lake Biwa, and Osaka), the Osaka basin, which has a wide aperture connecting the inlet and the open sea, shows the largest diversity in sedimentary environments (fluvial, lacustrine, tidal, and deltaic) as a result of the influence of eustatic sea-level changes and the tectonic deformation of the crust of the island arc. This chapter provides an overview of the biostratigraphy, magnetostratigraphy, and tephrochronology of the event sediments, which are then used to reconstruct a detailed paleogeographic description of the study area during recent periods. Then, the results of deep drilling surveys are described to cultivate a fundamental notion of the evolutionary processes of the basin. Finally, tectonic movements are evaluated quantitatively from the burial histories of select boreholes, which have been finely tuned based on the oxygen isotope stage boundaries. The interval subsidence rates through the late Quaternary were calculated based on subsurface datum levels in the Osaka Group. The results revealed that the differential subsidence of the basement was likely controlled by changes in the tectonic stress regime related to the transient mode of oceanic plate convergence.

Keywords Quaternary · Osaka Group · Kinki district · Paleoenvironment Stratigraphy

After a dormant period from the middle to late Miocene, the Japanese Islands became a vigorous tectonic zone around the beginning of the Pliocene. Their northern half has basically been ruled by the steady subduction of the Pacific Plate. Its westward motion is a plausible cause of the longstanding collision between the wrenched-off forearc sliver of the Kurile Islands and the northeastern Japan arc at the island of Hokkaido. Northeast Japan has also suffered E–W contraction, which has formed mountainous ranges and fault-related intermontane basins (e.g., Nakajima 2013). As we have learned, southern Japan has been under the governance of the Philippine Sea Plate, which resumed its underthrusting of southwest Japan ca. 5 Ma, bringing about an episodic strong N–S contraction. It then changed its direction of movement

Y. Itoh and K. Takemura, *Three-Dimensional Architecture and Paleoenvironments of Osaka Bay*, Advances in Geological Science,
https://doi.org/10.1007/978-981-13-0577-1_2

from north-northwestward to west-northwestward in the mid-Quaternary (Nakamura et al. 1987) and enhanced dextral slips on the Median Tectonic Line (MTL). Itoh et al. (2002) has stated that the prevalent shear stress induced the formation of another trench-parallel fault, the Southern Japan Sea Fault Zone (SJSFZ), on the backarc side, and a sliver sandwiched by two transcurrent faults of the southwestern Japan arc has been colliding with the Ryukyu arc at the island of Kyushu. The Plio-Pleistocene Osaka Group filling the Osaka sedimentary basin, which lies to the north of the MTL, has preserved a tectonic and paleoenvironmental record of the island arc extending back to 3 Ma. In this chapter, the authors outline the stratigraphy of this event sequence, which provides a geological basis for the seismic interpretation presented in the next chapter.

2.1 Overview of Sedimentary Basins

Three sedimentary basins dating to the Pliocene are aligned in the Kinki district; from east to west, they are the Tokai basin around Ise Bay, the Paleo-Lake Biwa basin around Lake Biwa, and the Osaka basin around Osaka Bay (Fig. 2.1). All of these basins contain Plio-Pleistocene deposits. The deposits in the three basins are independently named the Tokai, Kobiwako, and Osaka Groups, respectively.

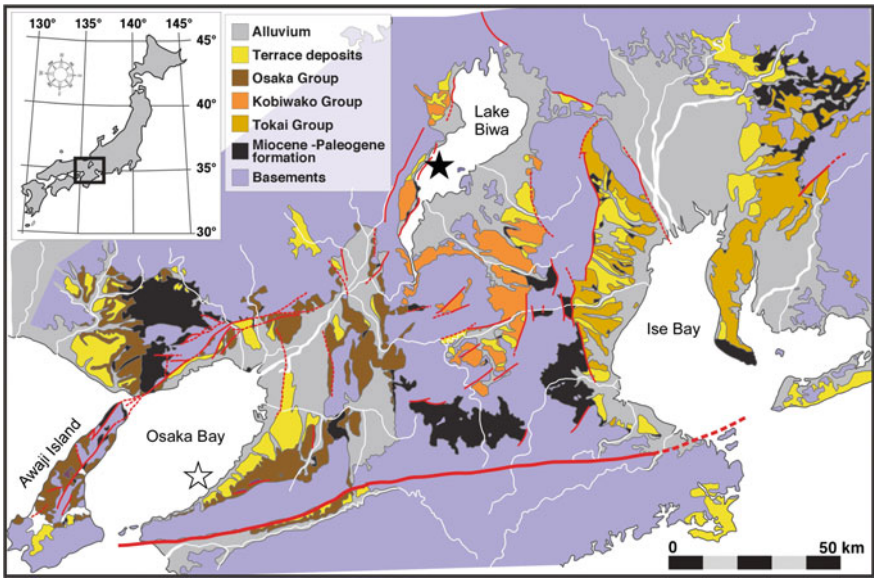

Fig. 2.1 Distribution of the Plio-Pleistocene sedimentary sequence in the Kinki district modified from Takemura (1985, 2016). Solid and open stars in Lake Biwa and Osaka Bay represent the 1982–1983 deep drilling site and the 2006 KIX 18-1 drilling site, respectively

The Tokai sedimentary basin in the eastern part of the Kinki district is filled with lacustrine sediments of the Tokai Group (Fig. 1.8). The older Tokai Group is distributed around the southern and eastern parts of the basin, whereas the younger part of the group migrated northward to northwestward (Takemura 1985). The Paleo-Lake Biwa basin in the central Kinki contains lacustrine and fluvial sediments of the Kobiwako Group (Fig. 1.8). The earliest sediments of the group developed within the southern part of the basin, whereas its later sediments are distributed in the northern sector as a result of basinal migration (Yokoyama 1969, 1984).

The Osaka Group filling the Osaka sedimentary basin occupies an extensive region of the western Kinki district (Fig. 1.8) and is characterized by recursive marine invasion during the late Pleistocene under the influence of eustatic sea-level changes (e.g., Ikebe et al. 1970; Itihara 1993), which enables precise chronostratigraphic control based on paleontological evidence and astronomical time calibration. Section 2.2 gives a concise summary of half a century's worth of stratigraphic studies on the Osaka Group.

2.2 Chronology

The Plio-Pleistocene series burying the Osaka sedimentary basin, the Osaka Group, is one of the most intensely studied deposits among contemporaneous strata in the Japanese Islands. This group is approximately 2000 m thick (Itihara 1993) and is mainly composed of fluvio-lacustrine sequences with rhythmical intercalation of marine clay beds in its upper part. Figure 2.2 summarizes the hybrid stratigraphy of the Osaka Group and the oxygen isotope record (Shackleton 1995) compiled after Huzita and Maeda (1985) and Yoshikawa and Mitamura (1999).

2.2.1 Biostratigraphy

The Osaka Group is scarce of age-diagnostic fossils, which is reflective of its dominant sedimentary environments (fluvio-lacustrine and tidal/deltaic). However, changes in the fossil florae (e.g., Momohara 1992; Hongo 2007) reflect the long-term drift of the regional climate and are roughly suggestive of stratigraphic positions. In summary, the lower part of the group, the upper limit of which is assigned as the base of the Ma 3 marine clay bed (Fig. 2.2), yields *Metasequoia* flora, such as *Mellioden-dron*, *Carya*, *Nyssa* sp., *Ginkgo biloba*, *Keteleeria davidiana*, *Pseudolarix kaempferi*, *Liquidambar formosana*, *Pinus fujii*, *Sequoia sempervirens*, *Glyptostrobus pensilis*, *Juglans cinerea* var. *megacinerea*, *Metasequoia disticha*, and *Picea koribai*. Within the upper part of the group assigned to the *Fagus* zone, the Ma 6/7 interval is characterized by *Larix* plant fossils, which are indicative of a cool climate (Huzita and Kasama 1982).

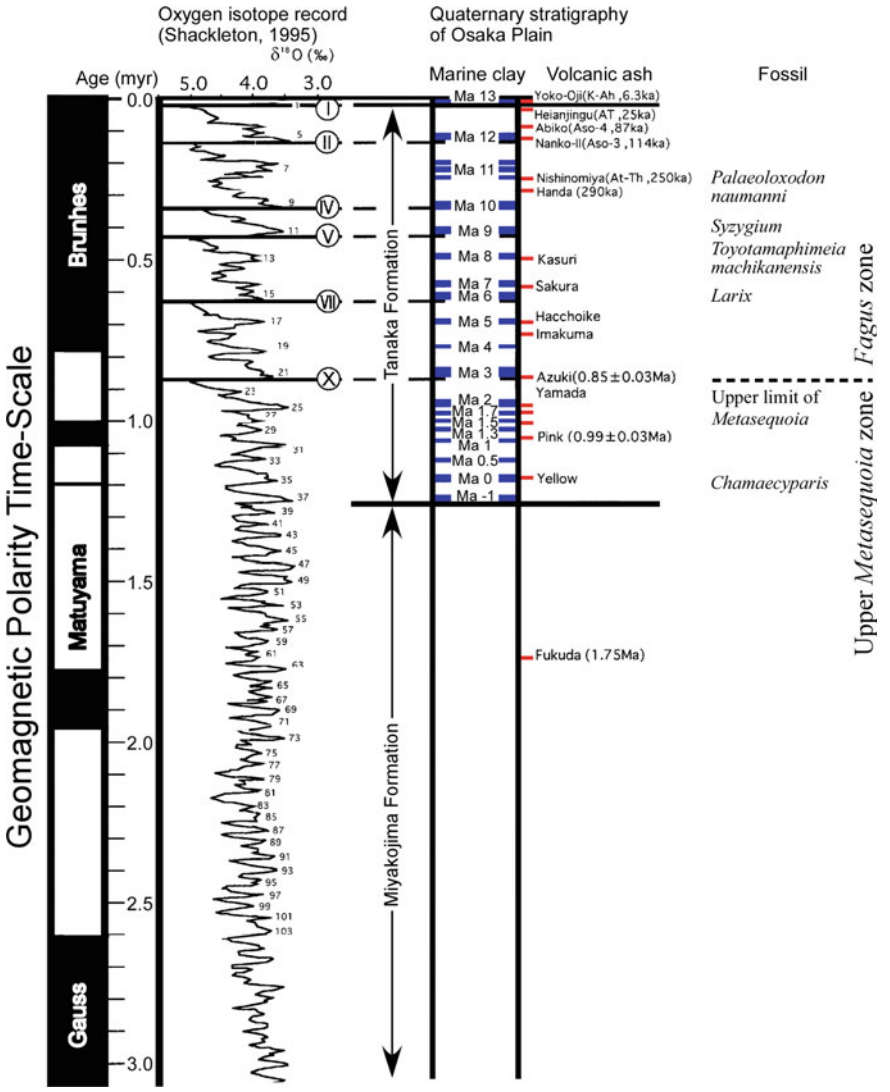

Fig. 2.2 Summary of the biostratigraphy, magnetostratigraphy, and tephrochronology of the Osaka Group and the oxygen isotope record compiled after Huzita and Maeda (1985) and Yoshikawa and Mitamura (1999)

2.2.2 Magnetostratigraphy

As a result of paleomagnetic investigations (e.g., Ishida et al. 1969; Torii et al. 1974; Nishida and Ishida 1975), the Brunhes–Matuyama Chron boundary (0.78 Ma) has been assigned to the basal part of the Ma 4 marine clay. Other boundaries of

subchrons within the Matuyama Chron have been correlated with datum levels as follows: the upper limit of the Jaramillo Subchron (0.98 Ma) with a horizon between the Komyoike III volcanic ash and just below the Ma 2 marine clay, the lower limit of the Jaramillo Subchron (1.05 Ma) with the base of the Ma 1 marine clay, the upper limit of the Olduvai Subchron (1.76 Ma) with a horizon just below the Fukuda volcanic ash, and the lower limit of the Olduvai Subchron (2.00 Ma) with a horizon below the Mitsumatsu volcanic ash.

2.2.3 Tephrochronology

The numerical ages of many volcanic ashes intercalated in the Osaka Group were constrained using fission track (FT) dating in the 1970s and 80s (e.g., Itihara et al. 1986). Although it is a valuable database, a reexamination of the results is necessary because with few exceptions (e.g., Danhara et al. 1997), most of the FT dates were determined before 1990, the year in which a standardized method of FT dating was established (Hurford 1990).

Previous studies have described approximately 50 tephra beds within the Osaka Group (e.g., Yoshikawa 1976), the majority of which are correlated with tephras in other areas (e.g., Yoshikawa et al. 1994). By integrating tephrochronology, magnetostratigraphy, and biostratigraphy, Satoguchi and Nagahashi (2012) compiled a catalog of tephras widespread in Japan. In their rich archive, 15 volcanic ashes in Osaka are recognized as widespread tephras. These are given in ascending sequence as follows, with the corresponding local names in Osaka given in parentheses: Souri-Itayama Tephra (Misaki ash), Tsuchimaru II-Tenjin-ike L2 Tephra (Tsuchimaru II ash), Habutaki I-MT2 Tephra (Habutaki I ash), Habutaki II-Hozoin I Tephra (Habutaki II ash), Asashiro-Tomoda2 Tephra (Asashiro ash), Kd44-Naka Tephra (Mitsumatsu ash), Ebisutoge-Fukuda Tephra (Fukuda ash), Shishimuta-Pink Tephra (Pink ash), Shishimuta-Azuki Tephra (Azuki ash), Sayama-B Tephra (Sayama ash), Hakkoda-Ku1 Tephra (Imakuma I ash), Seiganji-Toga Tephra (Toga ash), Kobayashi-Kasamori Tephra (Sakura ash), Kasuri-E Tephra (Kasuri ash), and Minatojima I-Ks5 Tephra (Minatojima I ash).

2.3 Paleoenvironment

The reliable age control of the Osaka Group enables the reconstruction of an in-depth paleogeographic representation of the study area during recent periods. Figure 2.3 presents a chronicle of the Osaka basin from the youngest interglacial period. In the series of illustrations shown in this figure, the Ma 13 (marine isotope stage (MIS) 1) and Ma 12 (MIS 5) sediments are very useful for mapping the distribution of the marine transgression, whose areal extents have been influenced by the activity of the Ikoma Fault and the Uemachi flexural zone. The former controlled the accommoda-

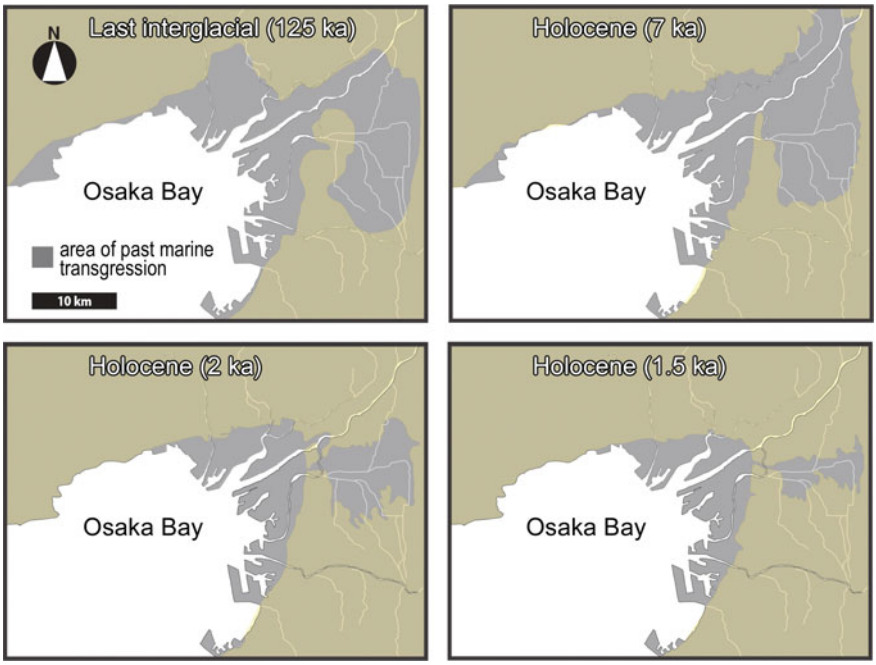

Fig. 2.3 Paleoenvironmental changes around Osaka Bay and Plain during the late Pleistocene and Holocene after Itoh and Takemura (2016)

tion of the embayment located around the eastern part of the present Osaka Plain, and the latter determined the aperture of the sandbar dividing the bay and the fluvial/tidal estuary. In the upper left inset of Fig. 2.3, the Ma 12 distribution represents the paleogeography of the transgression that occurred during the last interglacial period (MIS 5), impressively showing basin domains separated by a north-trending barrier. The rectangular shape of the inlet implies fault-controlled basin development related to an E–W tectonic stress regime. Figure 2.3 (upper right) represents the state during the Holocene marine transgression, in which the compartmentalization of the Osaka basin is still readily observable. Figure 2.3 (lower left) is the paleogeographic map for a retreating stage of the coastline ca. 2 ka, and the existence of a small area of inland water is observable in this map. Finally, the lower right inset of Fig. 2.3 depicts a map corresponding the dawn of the era of human activity ca. 1.5 ka. A narrow lagoonal area was identified based on the results of a drilling survey and the distribution of archaeological sites (Matsuda 2001; Cho et al. 2014). These drastic environmental changes must have been influenced by continued activity on major N–S active faults.

2.4 Deep Boring Survey

2.4.1 Onshore Data

The most accurately age-controlled sedimentary record of land-derived deposits was obtained from present-day Lake Biwa after a labor-intensive deep drilling operation in 1982 and 1983 that struck the basement, which is composed of Mesozoic and Paleozoic sedimentary units. This operation confirmed the existence of a nearly 1-km-thick sediment pile (Fig. 2.4; Horie 1983, 1991; Yokoyama and Takemura 1983; Takemura 1990) in the central part of the lake (ca. 1.3 Ma; Meyers et al. 1993; Danhara et al. 2010). The lithostratigraphy of the unconsolidated sedimentary units in the borehole has been summarized by Takemura et al. (2013) as follows.

Sediments were divided into five units based on differences in their predominant grain-size distributions (Takemura and Yokoyama 1989; Yokoyama and Takemura

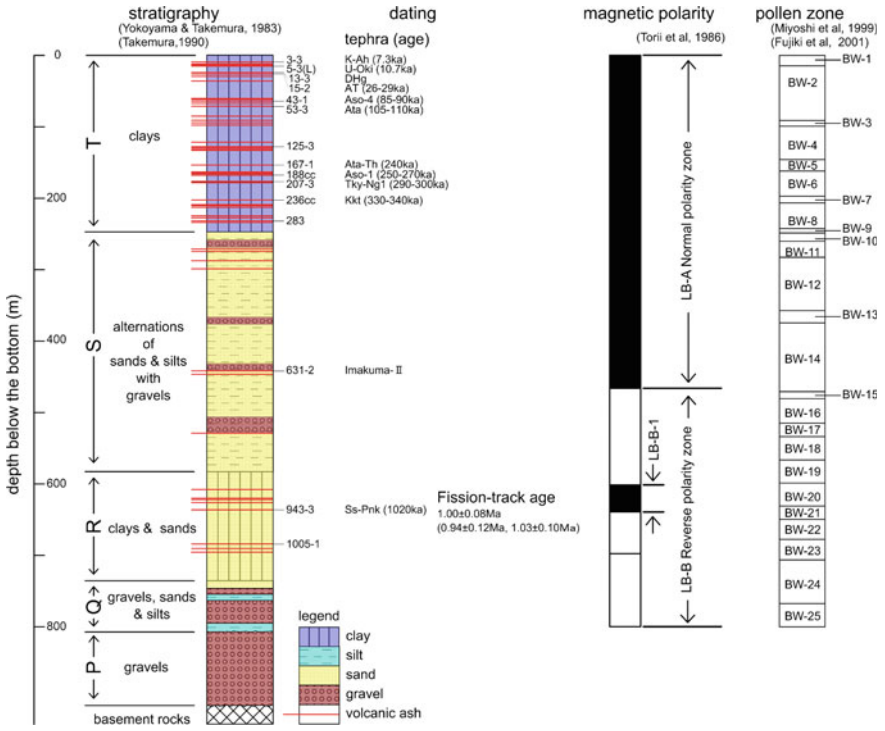

Fig. 2.4 Stratigraphy of the 1982–1983 deep drilling survey in Lake Biwa revised from Takemura (1990). See Fig. 2.1 for the hole location. The lithostratigraphy is after Yokoyama and Takemura (1983) and Takemura (1990). The tephrochronology and fission track ages are after Danhara et al. (2010). The magnetostratigraphy is after Torii et al. (1986). The pollen zonation is after Miyoshi et al. (1999) and Fujiki et al. (2001)

1983). These units have been named the P (approximately 100-m-thick pebble and cobble layer), Q, R, S, and T (fluvial and lacustrine sediments) units in ascending order. The Q unit is a 72.3-m-thick layer 731.8–804.1 m below lake floor (mblf) composed of alternating layers of sand, gravel, and silt. The R unit is 149.9 m thick, 581.9–731.8 mblf, and is considered to be conformable with the S unit above it. Subunits of bluish-gray clay without visible lamination alternate with subunits composed of layers of silt, sand, and sandy gravel at intervals of approximately 10 m throughout this unit. The S unit is 332.4 m thick, 249.5–581.9 mblf, and is believed to be continuous with the overlying T unit. It consists of thin alternations of sands and silts interspersed with sandy gravels. The T unit is 249.5 m thick, 0–249.5 mblf, and is composed of bluish-gray non-laminated clay. These five units contain 54 layers of volcanic ash intercalated throughout (Takemura 1990). The uppermost unit, the T unit, was estimated to have been deposited continuously during the last 430 k year (Meyers et al. 1993).

As for the Osaka Plain, which is east of the target area of the present seismic study, many drilling surveys have been conducted in this region for civil engineering purposes. Their crucial contribution to the present neotectonic analysis is discussed in Sect. 2.5 in light of the burial and exhumation history.

2.4.2 Offshore Data

Among the sedimentological information obtained from boreholes drilled into the Osaka basin, the most representative is the 2006 survey at the Kansai International Airport (KIX 18-1 Editorial Committee 2011). Figure 2.5 shows that the lower and upper parts of the sequence contain lacustrine/fluvial sediments and alternating marine/non-marine sediments, respectively. Age assignment is based on the tephrochronology and paleomagnetism data annotated in the figure. The marine clays are numbered from Ma −1 to 13 in ascending order. The uppermost clay deposit, Ma 13, is synonymous with the Holocene transgressive unit during MIS 1. The clay deposit numbered Ma 12 indicates a marine transgression at MIS 5. The numerical ages of the marine clay beds were determined by Itoh et al. (2000), and the methodology they used is documented in the next section. These marine sequences are very important tools for understanding the subsurface geology and the related tectonic subsidence or uplift in the sedimentary basin.

2.5 Tectonic Movements Deduced from Burial History

Deep boring surveys have revealed the existence of a considerable spatiotemporal difference among the subsidence rates of the Osaka sedimentary basin. As for its land sector (Osaka Plain), Itoh et al. (2000) have attempted to understand the

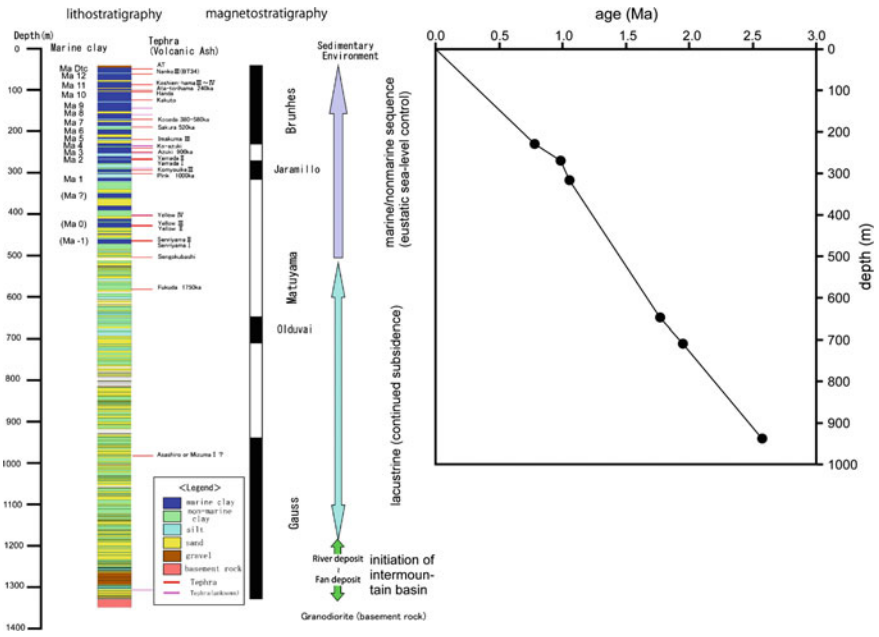

Fig. 2.5 Stratigraphy of deep drilling survey KIX 18-1 in 2006 after KIX 18-1 Editorial Committee (2011) and Itoh and Takemura (2016). See Fig. 2.1 for the hole location

tectonic driving force behind the differential motion of the basement fault blocks. The remainder of this section reviews the basis of their methodology and evaluates its logical strength.

2.5.1 Isotope Stage Boundaries

Continuous cores of the OD-1 deep borehole (see Fig. 2.6) provide a standard record of the upper part of the Osaka Group. As presented in Fig. 2.6, this record confirms the presence of marine clay deposits Ma 0 to 13 in ascending order. The oldest clay, Ma −1, is missing because it was discovered later at other drilling sites (e.g., Mitamura et al. 1998). Warm/cold climate changes corresponding to marine/non-marine environmental oscillations were detected through pollen analysis (Tai 1966a, b).

Because estuary facies deposits of the Osaka Group are absent from age-diagnostic microfossils, the age determination of the sequence has been based on magnetostratigraphy and tephrochronology. Figure 2.6 depicts magnetic reversals (Ishida et al. 1969; Hayashida and Yokoyama 1989; Hayashida et al. 1996) and ash layers with reliable radiometric ages (Machida and Arai 1992; NEDO 1989; Danhara et al.

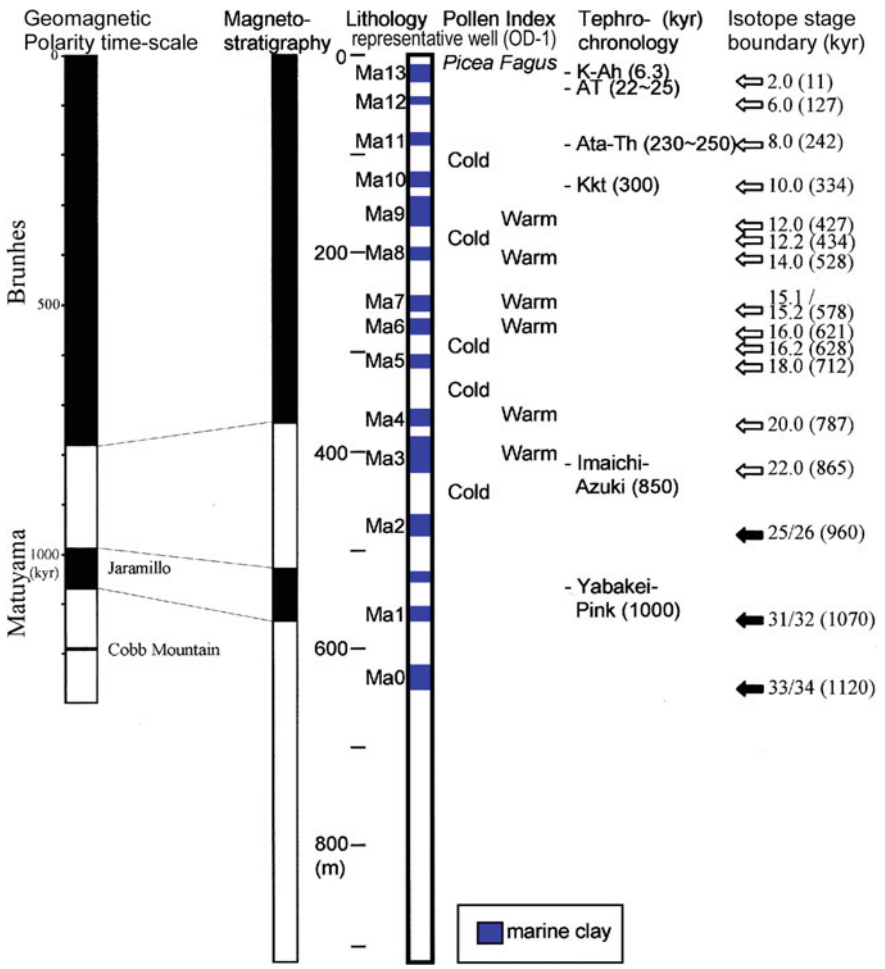

Fig. 2.6 Stratigraphic summary of the Osaka Group and assignment with geomagnetic polarity timescale and oxygen isotope stratigraphy (open arrow: Bassinot et al. 1994; solid arrow: Shackleton et al. 1990 and Farrell et al. 1995). The magnetostratigraphy of the Osaka Group is after Ishida et al. (1969), Hayashida and Yokoyama (1989), and Hayashida et al. (1996). The lithology and pollen analysis of the OD-1 core are after Mitamura et al. (1998) and Tai (1966a, b), respectively. The tephrochronology is after Machida and Arai (1992), NEDO (1989), and Danhara et al. (1997)

1997), which indicate that the upper Osaka Group can be assigned to the upper part of the Matuyama Chron, including the Jaramillo Subchron and the Brunhes Chron.

As explained in Sect. 2.2, Yoshikawa and Mitamura (1999) correlated marine clays intercalated in the Osaka Group with the oxygen isotope stages by compiling subsurface stratigraphy. In contrast, Itoh et al. (2000) focused on lithologic boundaries, which are indispensable in the reconstruction of basin subsidence. Generally, the basal horizons of the marine clays are clearly recognizable by sharp changes in

lithology and microfossil yields and correspond straightforwardly to isotope stage boundaries during marine transgression.

Itoh et al. (2000) adopted the numerical table of isotope stage boundaries by Bassinot et al. (1994) for stage 22 and younger stages. For older stages, boundary ages were calculated from the control points of Farrell et al. (1995), who relied on Shackleton et al. (1990). Figure 2.6 presents the resultant model of the correlation between the stratigraphic records of the upper Osaka Group and the isotope events.

2.5.2 *Subsurface Datum Levels*

Figure 2.7 depicts the datum horizon levels from the mean sea level with their ages determined using the procedure described in the previous section. Interpolation under the assumption of constant sedimentation was adopted for the calculation of the levels of horizons missing in the inspected cores. An interval between two successive datum planes represents a marine transgression/regression cycle. Therefore, the interval accumulation rate obtained from this dataset is not indicative of high-frequency climatic controls on the sedimentation process but likely reflects the rate of subsidence under the effects of tectonic episodes and the activities of faults surrounding the basin.

Well ID (area)	Block	Present	Ma 13	Ma 12	Ma 11	Ma 10	Ma 9	Ma 8	Ma 7	Ma 6	Ma 5	Ma 4	Ma 3	Ma 2	Ma 1	Ma 0	Ma -1	Basement
Geologic age (ka) ⇒		0	11	127	242	334	427	528	578	621	712	787	865	960	1070	1120	1200	3000
IIA (Osaka)	CC	1.7	*1.0*	*-6.2*	-13.3	-48.5	-76.2	*-118.3*	-139.2	-164.9	-191.1	-238.6						
OD-1 (Osaka)	CW	2.9	-23.5	-50.5	-86.3	-127.1	-169.1	-204.1	-254.6	-278.1	-311.6	-370.2	-415.5	-479.1	-564.1	-635.4		
OD-2 (Osaka)	CC	2.8	-16.2	*-20.0*	*-23.8*	*-26.9*	*-29.9*	*-33.3*	*-34.9*	*-36.3*	*-39.3*	*-41.8*	-44.4	-73.5	-124.4	-171.4	-196.4	-653.4
OD-3 (Osaka)	CE	2.6	-15.0	-34.5	*-70.6*	-99.4	-136.9	-167.0	-231.0	-260.7	-298.3	-359.3	-412.7	-477.5	-574.2			
OD-4 (Osaka)	NC	2.0	-17.9	*-32.6*	*-47.2*	*-58.9*	*-70.7*	*-83.5*	*-89.8*	-95.3	-117.0	-149.6	-191.1	-222.8				
OD-5 (Osaka)	NW	2.3	-14.3	-23.0	*-55.6*	-81.7	-111.2	-163.1	-180.9	-210.5	-239.9	-293.1	-334.0	-395.3	-481.0			
OD-6 (Osaka)	NE	0.3	-9.6	-31.3	*-56.5*	-76.6	-114.9	-130.3	-185.7	-222.2	-253.9	-309.1	-361.8	-426.5				
OD-7 (Osaka)	SC	4.3	-6.0	-22.0	*-26.0*	*-29.2*	*-32.4*	*-35.9*	*-37.6*	-39.1	-73.7	-103.2	-135.0	-162.2	-187.7			
OD-8 (Osaka)	NC	5.0	-13.6	*-23.3*	*-32.8*	*-40.5*	*-48.2*	*-56.6*	-60.8	-86.3	-110.4	-160.0	-196.6					
OD-9 (Osaka)	CC	25.0	*24.4*	*18.4*	*12.5*	*7.7*	*2.9*	*-2.4*	*-5.0*	-7.2	-18.5	-43.7	-72.1	-100.7	-152.5			
OT (Osaka)	CC	19.1	*18.5*	*12.5*	*6.5*	*1.7*	*-3.1*	*-8.3*	*-10.9*	*-13.2*	*-17.9*	-21.8	-50.3	-80.3	-126.9	-167.9	-193.5	
TS (Osaka)	SC	-0.3	-21.5	-48.0	-89.5	-137.2	-185.5	-223.1										
YU (Osaka)	SC	20.0	*19.3*	*11.9*	*4.6*	*-1.2*	*-7.1*	*-13.5*	-16.7	-33.0	-46.0	-76.7	-108.3	-143.6	-203.1	-251.7	-280.5	

not penetrated

Fig. 2.7 Subsurface datum (base of marine clays) levels (m) and ages (k year) at drilling sites in the northern Osaka Plain modified from Itoh et al. (2000). Levels identified with thin italicized font are missing datum horizons and were calculated assuming a constant rate of sedimentation. Shaded cells represent horizons that were not penetrated. Block abbreviations are as follows. NW: northern-western, NC: northern-central, NE: northern-eastern, CW: central-western, CC: central-central, CE: central-eastern, SC: southern-central

2.5.3 *Differential Subsidence of Northern Osaka Basin*

It is notable that the majority of the subordinate faults around the Osaka basin are aligned in N–S direction. Their activity results in the formation of warping zones within the basin, as represented by the pink ovals in Fig. 2.8a. Late Pleistocene basin subsidence curves for the northern Osaka basin are presented in Fig. 2.8b. As typified by the data for the OD-2 borehole (red circles), the drill holes on the Uemachi basement high (north-trending warping within the Osaka Plain shown in Fig. 2.8a) show a sign of stagnant subsidence during a later stage, whereas the western (e.g., data for the OD-1 borehole, red squares) and eastern (e.g., data for the OD-3 borehole, red triangles) subbasins are characterized by steady rapid subsidence throughout the monitored interval.

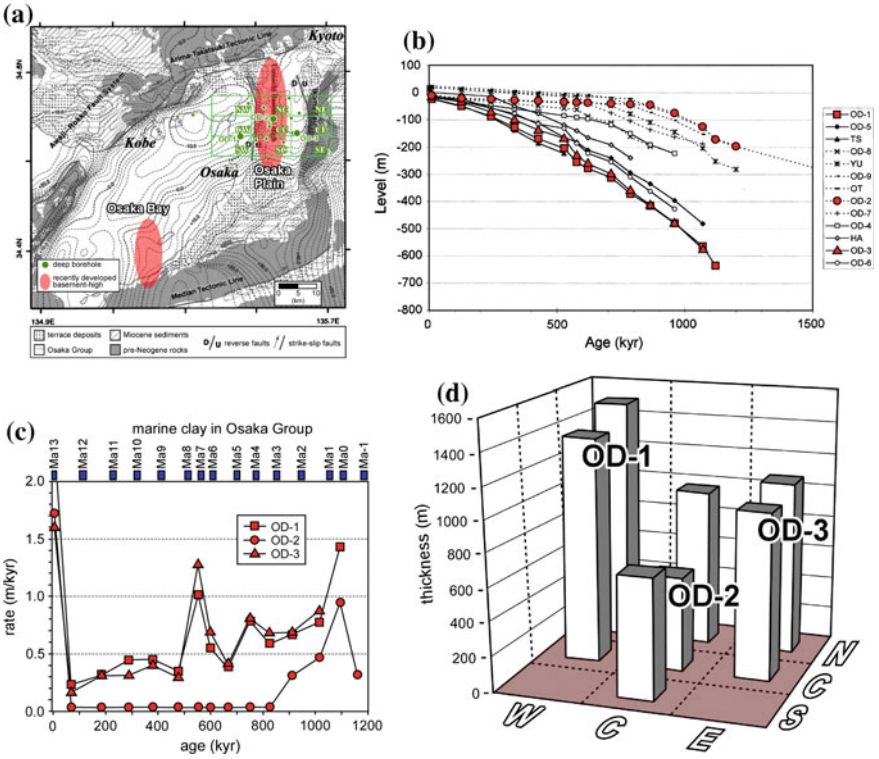

Fig. 2.8 Differential subsidence of the northern Osaka basin compiled after Itoh et al. (2000). **a** Index map of the analyzed blocks. **b** Pleistocene subsidence curves in the northern Osaka basin. Data symbols of key boreholes are highlighted in red. **c** Early to late Pleistocene interval subsidence rates in the northern Osaka basin. **d** Diagram of sediment thickness from the late Pliocene to the early Pleistocene. Names of representative drill holes are attached on bar chart

Three boreholes, OD-1, 2, and 3, were selected here to represent the western subbasin, a N–S basement high, and the eastern subbasin, in this order. Figure 2.8c shows their interval subsidence rates through the late Quaternary. Three short-lived tectonic episodes have been identified within the area. In the considered timeline, the subsidence rates exhibited a sharp drop (the Ma 5/6 interval) in the subbasins on both flanks of the basement high, which seems to have remained stationary since ca. 800 ka. The Uemachi barrier then episodically grew ca. 550 ka (the Ma 7/8 interval), as demonstrated by the synchronous acceleration of subsidence on both flanks of the basement upheaval. The last episode during the Ma 8/9 interval is marked by a decline in subsidence in both of the basinal areas.

The present tectono-sedimentological review of the eastern (onshore) part of the Osaka basin has revealed the differential subsidence of the basement, which is likely controlled by changes in tectonic stress, as delineated by the bar chart in Fig. 2.8d. Note that another basement high is present across the southern coast of Osaka Bay (pink oval in the southwestern part of the basin in Fig. 2.8a). Based on seismic and drilling information available in the coastal zone, Itoh et al. (2001) argued that the N–S warping gradually developed in the period from 1.0 to 0.4 Ma, which controlled the pattern of Pleistocene sedimentation in the western (offshore) part of the Osaka basin. They also identified an environmental impact exemplified by the formation of a lake, named Paleo-Lake Senshu, in present-day southern Osaka Bay between 0.5 and 0.4 Ma. This concludes our overall inspection of the Osaka sedimentary basin. The above discussion indicates that a more regional three-dimensional imaging of the bay area is necessary to comprehend the formation of this tectonic basin, which is the main theme of the following chapters. In these chapters, the basinal architecture is thoroughly studied using a regional dataset of reflection seismic surveys.

References

Bassinot FC, Labeyrie LD, Vincent E, Quidelleur X, Shackleton NJ, Lancelot Y (1994) The astronomical theory of climate and the age of the Brunhes-Matuyama magnetic reversal. Earth Planet Sci Lett 126:91–108

Cho C, Ichikawa H, Takahashi T, Ogura T, Hirata Y, Matsuda J, Tsujimoto Y (2014) Topography in and around Uemachi area and the outline of paleogeographic change. In: Wakita O (ed) Report on JSPS kakenhi kiban kenkyu A 21242031

Danhara T, Kamata H, Iwano H (1997) Fission-track ages of zircons in the Yabakei pyroclastic-flow deposit in central Kyushu and the Pink volcanic ash of the Osaka Group. J Geol Soc Jpn 103:994–997

Danhara T, Yamashita T, Iwano H, Takemura K, Hayashida A (2010) Re-investigation of chronology for the 1400 m sediment core obtained from the Lake Biwa in 1982–1983. Quat Res Jpn 49:101–119

Farrell JW, Murray DW, McKenna VS, Ravelo AC (1995) Upper ocean temperature and nutrient contrasts inferred from Pleistocene planktonic foraminifer $\delta^{18}O$ and $\delta^{13}C$ in the eastern equatorial Pacific. In: Pisias NG, Mayer LA, Janecek TR, Palmer-Julson A, van Andel TH (eds) Proceedings of Ocean Drilling Program, scientific results vol 138. Ocean Drilling Program, College Station, TX, pp 289–319

Fujiki T, Miyoshi N, Morita Y, Horie S, Takemura K (2001) Pollen analysis of an 800 m core sample from Lake Biwa, Japan. In: Proceedings of the IX international palynological congress USA 1996, Houston, pp 367–373

Hayashida A, Yokoyama T (1989) Brunhes/Matuyama polarity epoch boundary in the Osaka Group of the Senri-yama Hills, Southwest Japan. Palaeogeogr Palaeoclimatol Palaeoecol 72:195–201

Hayashida A, Kamata H, Danhara T (1996) Correlation of widespread tephra deposits based on paleomagnetic directions: link between a volcanic field and sedimentary sequences in Japan. Quat Int 34–36:89–98

Hongo M (2007) Stratigraphic distribution of Hemiptelea (Ulmaceae) pollen from Pleistocene sediments in the Osaka sedimentary basin, southwest Japan. Rev Palaeobot Palynol 144:287–299

Horie S (ed) (1983) Paleolimnology of Lake Biwa and the Japanese Pleistocene 11. Inst Paleolimnol Paleoenviron Lake Biwa, Kyoto

Horie S (1991) Die Geschichte des Biwa-See in Japan: seine Entwicklung, dargestellt anhand eines 1400 m langen Tiefbohrkerns. Universitatsverlag, Wagner

Hurford AJ (1990) Standardization of fission track dating calibration: recommendation by the fission track working group of the IUGS subcommission of geochronology. Chem Geol 80:171–178

Huzita K, Kasama T (1982) Geology of the Osaka-Seihokubu district, Quadrangle series, scale 1:50,000. Geol Surv Japan, Tsukuba

Huzita K, Maeda Y (1985) Geology of the Osaka-Seinambu district, Quadrangle series, scale 1:50,000. Geol Surv Japan, Tsukuba

Ikebe N, Iwatsu J, Takenaka J (1970) Quaternary geology of Osaka with special reference to land subsidence. J Geosci Osaka City Univ 13:39–98

Ishida S, Maenaka K, Yokoyama T (1969) Paleomagnetic chronology of volcanic ash of the Plio-Pleistocene series in Kinki district, Japan—the research of younger Cenozoic strata in Kinki district, part 12. J Geol Soc Jpn 75:183–197

Itihara M (ed) (1993) The Osaka Group. Sogensha, Osaka

Itihara M, Ichikawa K, Yamada N (1986) Geology of the Kishiwada district, Quadrangle series, scale 1:50,000. Geol Surv Japan, Tsukuba

Itoh Y, Takemura K (2016) Subsurface structure of the Osaka Plain—its perspective based on geophysical data and future problems. News Osaka Micropaleontol 17:1–74

Itoh Y, Takemura K, Ishiyama T, Tanaka Y, Iwaki H (2000) Basin formation at a contractional bend of a large transcurrent fault: Plio-Pleistocene subsidence of the Kobe and northern Osaka Basins, Japan. Tectonophysics 321:327–341

Itoh Y, Takemura K, Kawabata D, Tanaka Y, Nakaseko K (2001) Quaternary tectonic warping and strata formation in the southern Osaka basin inferred from reflection seismic interpretation and borehole sequences. J Asian Earth Sci 20:45–58

Itoh Y, Tsutsumi H, Yamamoto H, Arato H (2002) Active right-lateral strike-slip fault zone along the southern margin of the Japan Sea. Tectonophysics 351:301–314

KIX 18-1 Editorial Committee (2011) Report on KIX 18-1 in Kansai international airport. KIX 18-1 Editorial Committee, Osaka

Machida H, Arai F (1992) Atlas of tephra in and around Japan. University of Tokyo Press, Tokyo

Matsuda J (2001) Development of tributary of Yamato river and human activity at the alluvial plain in south Kawachi Plain during the late Holocene. In: Abstract at 50th of research committee of buried cultural properties, pp 39–51

Meyers PA, Takemura K, Horie S (1993) Reinterpretation of late Quaternary sediment chronology of Lake Biwa, Japan, from correlation with marine glacial-interglacial cycles. Quat Res 39:154–162

Mitamura M, Yoshikawa S, Ishii Y, Kaito S, Nagahashi Y (1998) Lithology on the OD drilling cores in the Osaka Plain. Bull Osaka Mus Nat Hist 52:1–20

Miyoshi N, Fujiki T, Morita Y (1999) Palynology of a 250-m core from Lake Biwa: a 430,000-year record of glacial-interglacial vegetation change in Japan. Rev Palaeobot Palynol 104:267–283. https://doi.org/10.1016/S0034-6667(98)00058-X

Momohara A (1992) Late Pliocene plant biostratigraphy of the lowermost part of the Osaka Group, southwest Japan, with reference to extinction of plants. Quat Res Jpn 31:77–89
Nakajima T (2013) Late Cenozoic tectonic events and intra-arc basin development in northeast Japan. In: Itoh Y (ed) Mechanism of sedimentary basin formation—multidisciplinary approach on active plate margins. InTech, Croatia, pp 153–189. http://dx.doi.org/10.5772/56706
Nakamura K, Renard V, Angelier J, Azema J, Bourgois J, Deplus C, Fujioka K, Hamano Y, Huchon P, Kinoshita H, Labaume P, Ogawa Y, Seno T, Takeuchi A, Tanahashi M, Uchiyama A, Vigneresse JL (1987) Oblique and near collision subduction, Sagami and Suruga Troughs—preliminary results of the French-Japanese 1984 Kaiko cruise, Leg 2. Earth Planet Sci Lett 83:229–242
NEDO (1989) Report of the nationwide potential survey for geothermal resources on distributions and ages of volcanic rocks in the Turumidake area (Part 3). New Energy Development Organization, Tokyo
Nishida J, Ishida S (1975) Paleomagnetic study of Osaka Group using marine and nonmarine clays near Komyoike, Osaka Prefecture, Japan. Rock Magn Paleogeophys 3:32–35
Satoguchi Y, Nagahashi Y (2012) Tephrostratigraphy of the Pliocene to middle Pleistocene series in Honshu and Kyushu islands, Japan. Island Arc 21:149–169
Shackleton NJ (1995) New data on the evolution of Pliocene climatic variability. In: Vrba ES, Denton DH, Partrige TC, Burckle LH (eds) Paleoclimate and evolution with emphasis on human origins. Yale University Press, New Haven, pp 242–248
Shackleton NJ, Berger A, Peltier WR (1990) An alternative astronomical calibration of the lower Pleistocene time scale based on ODP Site 677. Trans R Soc Edinburgh: Earth Sci 81:251–261
Tai A (1966a) Pollen analysis of the core (OD-1) in Osaka City (I)—the research of younger Cenozoic strata in Kinki province, part 5. Earth Sci (Chikyu Kagaku) 83:25–33
Tai A (1966b) Pollen analysis of the core (OD-1) in Osaka City (II)—the research of younger Cenozoic strata in Kinki province, part 5. Earth Sci (Chikyu Kagaku) 84:31–38
Takemura K (1985) The Plio-Pleistocene Tokai Group and the tectonic development around Ise Bay of central Japan since Pliocene. Mem Fac Sci, Kyoto Univ, Ser Geol Mineral 51:21–96
Takemura K (1990) Tectonic and climatic record of the Lake Biwa, Japan, region provided by the sediments deposited since Pliocene times. Palaeogeogr Palaeoclimatol Palaeoecol 78:185–193
Takemura K (2016) Tectonic implication of basin formation on the basis of paleogeography using stratigraphy and shallow subsurface structure from a drilling data base. In: Itoh Y (ed) Research frontiers of sedimentary basin interiors—a case study and methodological review on an oblique convergent margin. Nova Science Publishers Inc., NY, pp 71–88
Takemura K, Yokoyama T (1989) Sedimentary facies of the 1,400 m drilling sample from Lake Biwa with reference to the discontinuity in the sedimentary sequence. IPPCCE Newslett 5:36–48
Takemura K, Haraguchi T, Kusumoto S, Itoh Y (2013) Tectonic basin formation in and around Lake Biwa, central Japan. In: Itoh Y (ed) Mechanism of sedimentary basin formation—multidisciplinary approach on active plate margins. InTech, Croatia, pp 209–229. http://dx.doi.org/10.5772/56667
Torii M, Yoshikawa S, Itihara M (1974) Paleomagnetism on the water-laid volcanic ash layers in the Osaka Group, Sennan and Senpoku hills, southwestern Japan. Rock Magn Paleogeophys 2:34–37
Torii M, Shibuya H, Hayashida A, Katsura I, Yoshida S, Tagami T, Otofuji Y, Maeda Y, Sasajima S, Horie S (1986) Magnetostratigraphy of sub-bottom sediments from Lake Biwa. Proc Jpn Acad 62:333–336
Yokoyama T (1969) Tephrochronology and paleogeography of the Plio-Pleistocene in the eastern Setouchi geologic province, southwest Japan. Mem Fac Sci, Kyoto Univ, Ser Geol Mineral 36:19–85
Yokoyama T (1984) Stratigraphy of the Quaternary system around Lake Biwa and geohistory of the ancient Lake Biwa. In: Horie S (ed) Lake Biwa. Dr. W. Junk, The Hague, pp 43–128

Yokoyama T, Takemura K (1983) Geologic column obtained by the deep drilling from the bottom surface of Lake Biwa, Japan. IPPCCE Newslett 3:21–23
Yoshikawa S (1976) The volcanic ash layers of the Osaka Group. J Geol Soc Jpn 82:497–515
Yoshikawa S, Mitamura M (1999) Quaternary stratigraphy of the Osaka Plain, central Japan and its correlation with oxygen isotope record from deep sea cores. J Geol Soc Jpn 105:332–340
Yoshikawa S, Tateishi M, Kazaoka O (1994) Correlation of Fukuda volcanic ash layer in the Osaka Group and Tsujimatagawa volcanic ash layer in the Uonuma Group, central Japan. J Geol Soc Jpn 100:486–494

Chapter 3
Reflection Seismic Data

Abstract A systematic seismic investigation of Osaka Bay is presented in this chapter. Multichannel reflection records from 19 lines totaling 456 km in length were acquired by the Geological Survey of Japan, National Institute of Advanced Industrial Science and Technology (AIST); the Hydrographic and Oceanographic Department of the Japan Coast Guard (JCG); and the Hyogo Prefecture and Osaka Soil Test Laboratory of the Geo-Research Institute (GRI). These records span the entire tectonic basin region; however, they have not been comprehensively understood to date. The consistency of the present seismic interpretation was confirmed based on the correlation between the conspicuous reflectors observed in the 19 profiles and the stratigraphy of transgressive marker horizons (marine clays), which are under the control of eustasy, confirmed in deep boreholes tied with the seismic lines. At the beginning of the analytical procedure, the trends of the gravity and geomagnetic anomalies were observed along a single profile, and the basic seismic characteristics of the corresponding survey track were determined. Noteworthy subsurface structures were identified on the assessed sections and quantitatively evaluated with regard to vertical separations on select horizons. This analysis delineates the architecture of faults concealed mainly in peripheral parts of the basin. The growth of the deformation of some marine clays in the Osaka Group inevitably suggests Quaternary activity on the majority of the detected faults. The temporal migration of depocenters within Osaka Bay is visually represented by structural maps of interpreted seismic horizons assigned to the basin development and compartmentalization stages that have occurred in the past 1 Myr. Based on a detailed volumetric analysis of the neotectonic basin, we have confirmed a late Pleistocene event of descending subsidence rates synchronous with that previously found in the Osaka Plain.

Keywords Osaka Bay · Seismic survey · Gravity anomaly · Geomagnetic anomaly · Active fault

A disastrous earthquake in 1995 centered at the northwestern flank of the Osaka basin forced public officials to launch geophysical research projects to elucidate the architecture of the fault-studded tectonic region. In the land sector, Itoh et al. (2013, 2015, 2017), Itoh and Takemura (2016), and Itoh (2016) have performed structural

Y. Itoh and K. Takemura, *Three-Dimensional Architecture and Paleoenvironments of Osaka Bay*, Advances in Geological Science,
https://doi.org/10.1007/978-981-13-0577-1_3

interpretations, although further effort is necessary to achieve a comprehensive understanding of the formation history of the terrestrial component of the basin (Osaka Plain). However, the offshore sector (Osaka Bay) has never been studied beyond localized analyses conducted by corporations that organized seismic shooting. In this book, the authors present the first-ever complete description of seismic data obtained from the Osaka Bay area, the structural interpretation of which is supported by the stratigraphic records of key boreholes tied with the seismic survey lines considered in this chapter.

3.1 Dataset

In the present study, we utilized multichannel seismic reflection data acquired by the Geological Survey of Japan, National Institute of Advanced Industrial Science and Technology (AIST); the Hydrographic and Oceanographic Department of the Japan Coast Guard (JCG); Hyogo Prefecture; and the Osaka Soil Test Laboratory of the Geo-Research Institute (GRI). Figures 3.1, 3.2, and 3.3 show the distribution of the seismic survey lines in and around Osaka Bay together with the terrestrial

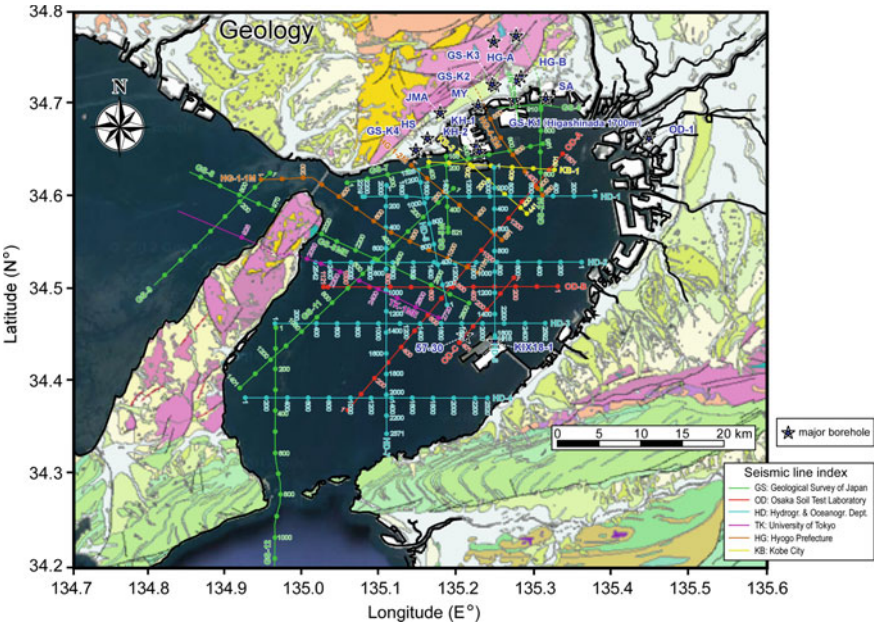

Fig. 3.1 Seismic line index showing the terrestrial geology after the Geological Survey of Japan (2012). The magenta unit fringing the study area represents the Cretaceous granitic rocks that underlie the Osaka sedimentary basin

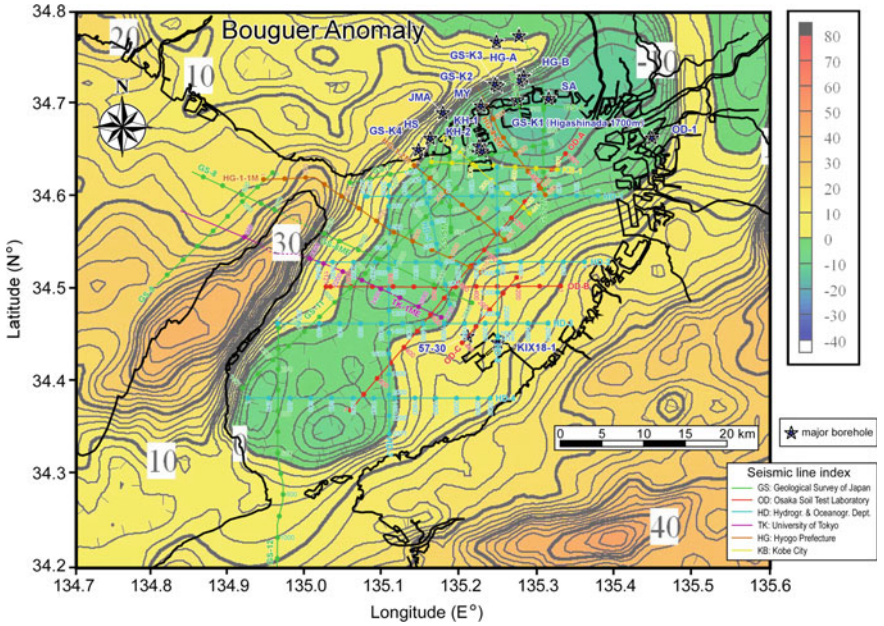

Fig. 3.2 Seismic line index showing the Bouguer gravity anomaly after the Geological Survey of Japan (2004). The color scale is in units of milligals

geology (Geological Survey of Japan 2012) and the gravity (Geological Survey of Japan 2004) and geomagnetic (Nakatsuka and Okuma 2005) anomaly distribution, respectively.

The seismic shooting performed by the Geological Survey of Japan, AIST, has the largest coverage. Although the survey lines GS-8 and GS-9 are allocated along the west coast of Awaji Island, the focus of this study was on the data obtained within Osaka Bay, where the reliability of the seismic interpretation can be confirmed by the geologic control of deep borehole data. The N–S line GS-12 runs through the Kitan Strait between the southeastern coast of Awaji Island and Osaka, where it is expected that the deep architecture of an arc-bisecting fault (the Median Tectonic Line) can be observed. Reflection data acquired by the Hydrographic and Oceanographic Department, JCG, also spread over a wide range of Osaka Bay, and the determination of the subsurface structure of the southern part of the bay is dependent on this dataset. Special attention was paid to HD-6 because this survey track is connected with a reference borehole at its southern end. Three seismic lines in Hyogo Prefecture are located around the northern portion of the bay. These cross significant NE–SW-trending faults, such as the Osaka Bay Fault on the eastern coast of Awaji Island and the northern extension of the Nojima Fault, which constitutes the seismogenic zone of the 1995 Kobe earthquake. Seismic data obtained by the Osaka

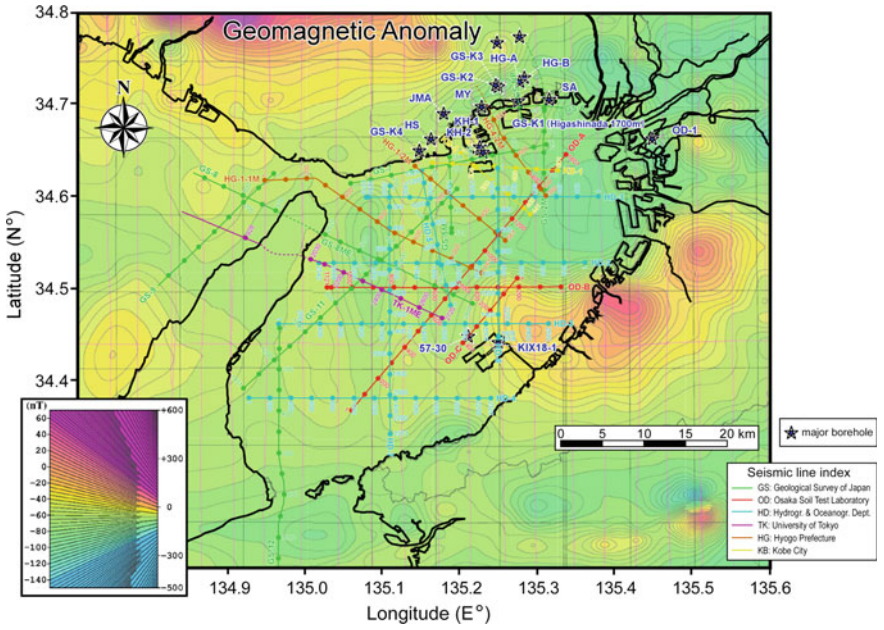

Fig. 3.3 Seismic line index showing the geomagnetic anomaly after Nakatsuka and Okuma (2005). The color scale is in units of nanoteslas

Soil Test Laboratory (GRI) are key in verifying the consistency of the present seismic interpretation because they are connected with all the other institutional data. Thus, the available dataset sufficiently covers approximately 1500 km^2 of the bay area.

3.2 Correlation Between Subsurface Datum Planes and Seismic Horizons

Crucial data for the correlation between remarkable seismic reflectors and subsurface datum levels have been given by Yokokura et al. (1999) based on stratigraphic information of the GS-K1 borehole at Higashinada, which penetrated unconsolidated sediment piles and basement rocks to a depth of 1700 m (Research Committee on Ground in Kansai 1998). Their inspection method is depicted in Fig. 3.4. First, they correlated select horizons of marine clay beds with events in sonic logging data. Then, the depth axis was converted into the domain of two-way time based on the interval velocity curve. The marker horizons are traced on time sections of the crossing lines GS-NP and GS-6 (see Figs. 3.1, 3.2 and 3.3).

In its eastern part, GS-6 is connected with the composite onshore–offshore line GS-2 (Fig. 3.4; Yokokura et al. 1996). After the selected reflectors were confirmed, they were identified along a depth-converted profile of the same survey track, and the

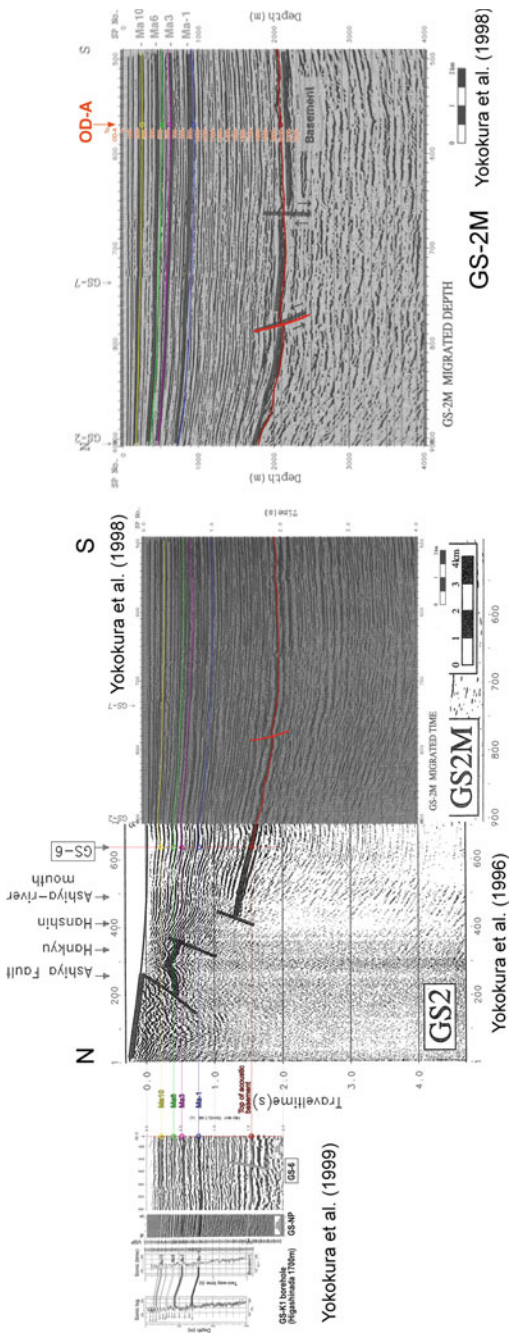

Fig. 3.4 Correlation between datum levels confirmed in boreholes and seismic horizons identified on shallow water seismic profiles, which is compiled after Yokokura et al. (1996, 1998, 1999)

characteristics of seismic features were confirmed throughout the offshore segment (GS-2M). Horizon picking was conducted on the crossing line OD-A to HD-6, the southernmost tip of which is tied with the deep drilling of KIX 18-1 described in Chap. 2 (Sect. 2.4.2). Figure 3.5 shows that the markers in the Osaka Group have been consistently traced in the study area. On this robust basis for analysis, the seismic datasets are discussed one by one in the following section with the marine clays Ma 3, 6, and 10 adopted as indicators of the incipient, climax, and diminishing stages of basin compartmentalization, as shown in Chap. 2 (Sect. 2.5.3).

3.3 Systematic Descriptions

3.3.1 Data Acquired by Geological Survey of Japan, AIST

In 1995, an extensive offshore seismic survey was conducted in Osaka Bay by the Geological Survey of Japan (AIST). According to Yokokura et al. (1998), 48 channels of hydrophones installed at intervals of 12.5 m recorded the energy released from an approximately 11-l airgun array during the shooting of survey lines totaling 136 km in length with a shooting interval of 25 m. Raw seismic data were stacked and then subjected to a post-stack processing sequence to enhance the resolution.

3.3.1.1 Line GS-2M

Figure 3.6 shows a N–S-trending raw seismic profile of the approximately 10,500-m-long line GS-2M. The Bouguer gravity anomaly map along this section (Fig. 3.2) is characterized by negative anomaly values reaching −15 mGal at its northernmost tip, which is at the coastline. Itoh et al. (2015) calculated the dimensionality index *I* (Beiki and Pedersen 2010) and the shape index *Si* (Cevallos 2014) around the Osaka basin using gravity gradient tensors and determined that *I* exceeds 0.7 and *Si* is nearly −1 around the northern coast of the bay. These results imply that the gravity minimum is caused by a three-dimensional bowl-like structure. The geomagnetic anomaly along this section (Fig. 3.3) does not show any notable trends.

Regarding the reflection patterns in the raw seismic profile, a strong continuous reflector, indicative of the surface of the acoustic basement, was recorded at a depth of approximately 2000 m, and its depth tends to decrease northward. The upper horizons show thin parallel reflections.

Figure 3.7 shows the interpreted seismic profile of GS-2M. Notable subsurface structures along this profile include a reverse fault at shot point (Sp.) 780. The vertical separation of the basement surface on this fault is 50 m. The deformation of the Ma 3, 6, and 10 marine clays on this fault is negligible. The reflectors at the bottom of these sedimentary units partially onlap small bumps in the acoustic basement. The three marine clays show subtle curvature and reach their greatest depths at approximately Sp. 600.

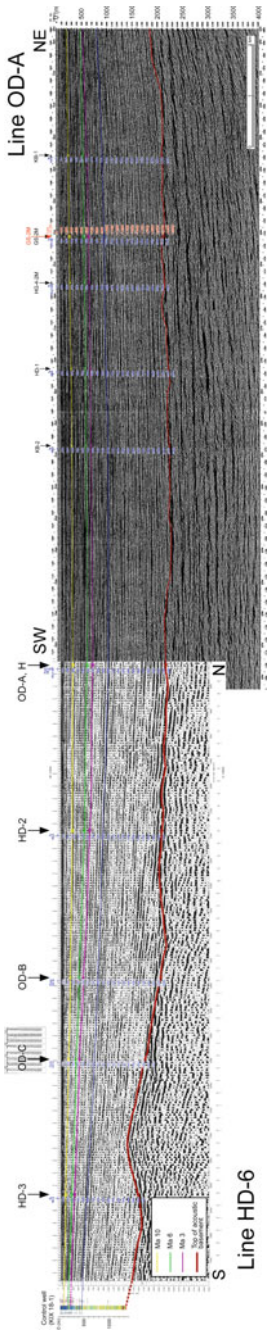

Fig. 3.5 Correlation between seismic horizons traced on offshore seismic profiles and datum levels in the deep KIX 18-1 borehole, which is compiled after Iwasaki et al. (1994) and Iwabuchi et al. (2000)

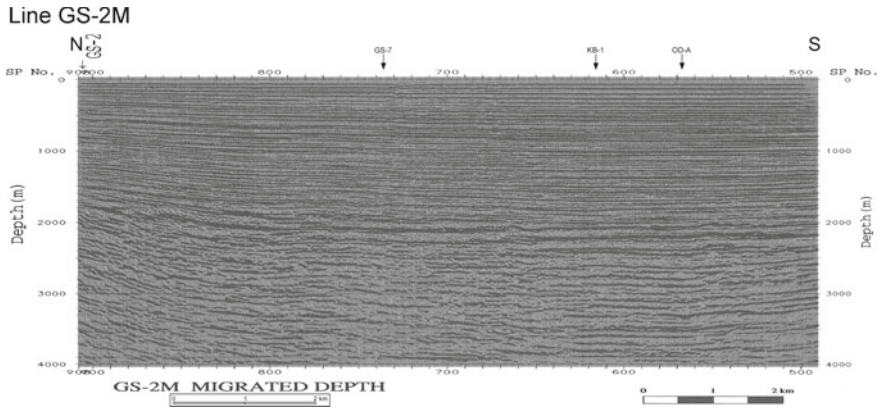

Fig. 3.6 Raw seismic profile of GS-2M (Yokokura et al. 1998) without vertical exaggeration. See Figs. 3.1, 3.2, and 3.3 for line location

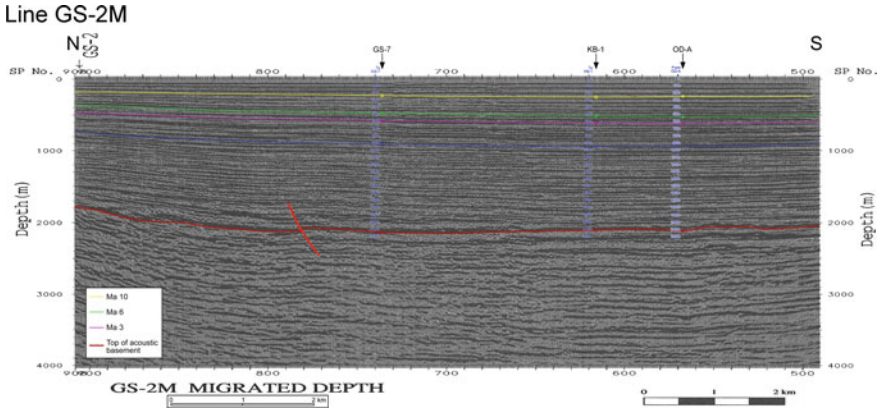

Fig. 3.7 Interpreted seismic profile of GS-2M without vertical exaggeration. See Figs. 3.1, 3.2, and 3.3 for line location

3.3.1.2 Line GS-5M

Figure 3.8 shows the N–S-trending raw seismic profile of the approximately 9100-m-long line GS-5M. The Bouguer gravity anomaly along this section (Fig. 3.2) reaches a minimum (approximately −9 mGal) in the southern portion of the section (Sp. 400). The geomagnetic anomaly along this section (Fig. 3.3) is fairly constant.

Regarding the reflection patterns in the raw seismic profile, a strong basement-indicative reflector was observed to descend northward. After reaching a maximum depth (approximately 3000 m) at Sp. 300, it abruptly travels approximately 1000 m upward in the northern part. Such a pattern, together with the similar undulation of the overriding units, suggests active faulting.

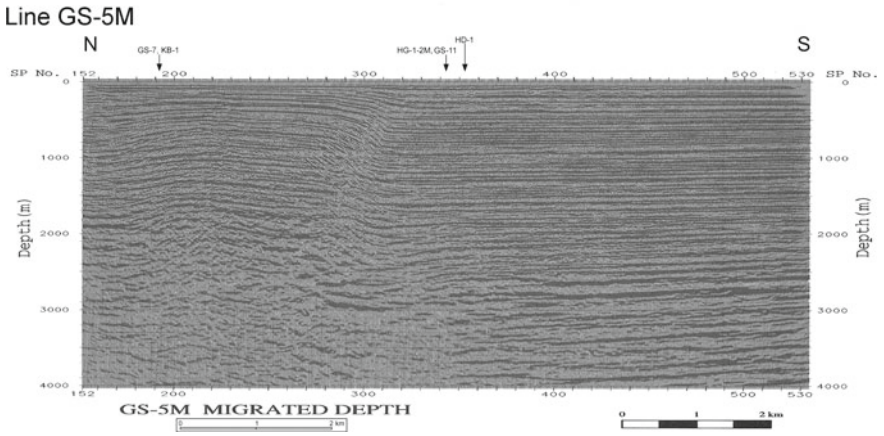

Fig. 3.8 Raw seismic profile of GS-5M (Yokokura et al. 1998) without vertical exaggeration. See Figs. 3.1, 3.2, and 3.3 for line location

Figure 3.9 shows the interpreted seismic profile of GS-5M. Notable subsurface structures along this profile include a fault-bounded pop-up block between Sp. 180 and 300. The vertical separations of the basement surface on a south-dipping fault (Sp. 175–210) and variably tilted swarm of faults (Sp. 280–310) are 100 m and a total of 1000 m, respectively. The Ma 3 and 6 marine clays show small (10–20 m) displacements along the fault swarm. The faults between Sp. 280 and 310 collectively show reverse separation and have an upward-splaying appearance. Changes in the relative upthrown side and fault dip direction are suggestive of transcurrent motions along these faults. The reflectors in the lowermost part of the sediments are flat-lying on top of the basement. The Ma 3, 6, and 10 marine clays can be traced with little ambiguity. Their curvatures around the faulted terrace suggest that the structure grew simultaneously with the basin development.

3.3.1.3 Line GS-7

Figure 3.10 shows the E–W-trending raw seismic profile of the approximately 24,000-m-long Line GS-7. The Bouguer gravity anomaly along this section (Fig. 3.2) is characterized by a trend of westerly increase, which roughly corresponds to the zone of a low-angle structure deduced from gravity gradient tensor analysis (see Chap. 1, Sect. 1.4.3.1). The geomagnetic anomaly along this section (Fig. 3.3) does not show any notable trends.

Regarding the reflection patterns in the raw seismic profile, the depth of the basement reflector decreases westward by more than 1000 m with ups and downs suggestive of displacements along several faults. The cumulative deformation of the upper strata implies the growth of faults during the deposition of the Quaternary sediments.

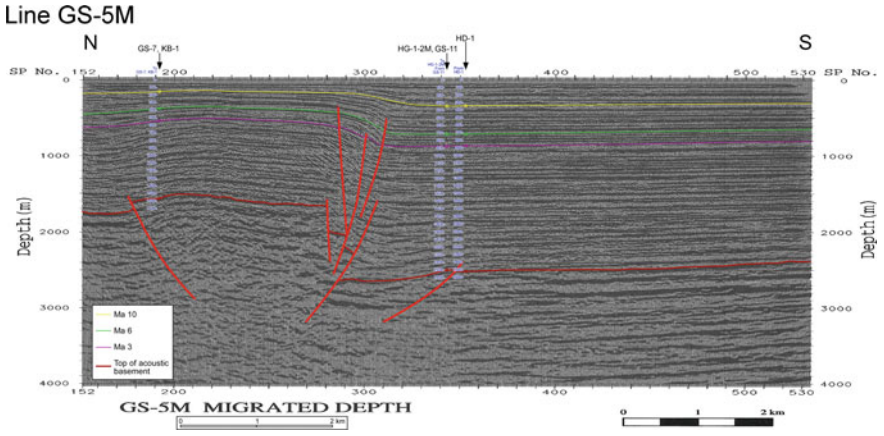

Fig. 3.9 Interpreted seismic profile of GS-5 M without vertical exaggeration. See Figs. 3.1, 3.2, and 3.3 for line location

Figure 3.11 shows the interpreted seismic profile of GS-7. Notable subsurface structures along this profile include basement-involving reverse faults. The vertical separations of the basement surface on the faults at Sps. 495, 640, 670, and 740 are 150, 200, 70, and 230 m, respectively. Although the separation on a fault in the westernmost part of the section seems to be the largest, it is indeterminable because no seismic horizon was identified on the hanging wall. Along with the discrete separations, the long-wavelength undulation of the basement suggests prevailing contraction. The reflectors in the lowermost part of the sediments are generally flat-lying on top of the basement and partly onlap preexisting basement heaves. The morphology of the Ma 3, 6, and 10 marine clays simulates the basal movements. Toward the Akashi Strait, they are drawn upward on the westernmost fault (Sp. 65), indicating vigorous fault activity.

3.3.1.4 Line GS-8ME

Figure 3.12 shows the WNW–ESE-trending raw seismic profile of the approximately 19,500-m-long line GS-8ME. The Bouguer gravity anomaly along this section (Fig. 3.2) is characterized by gentle changes. Moving westward, it reaches a minimum (approximately −5 mGal) near Sp. 2500 and then increases toward the westernmost point (10 mGal). The geomagnetic anomaly along this section (Fig. 3.3) reaches a local maximum (approximately −40 nT) near Sp. 2500, where the line crosses a north-trending anomaly ridge. A west-adjoining trough in the geomagnetic anomaly is expressed as a local minimum (approximately −90 nT) near Sp. 2200–2300.

Regarding the reflection patterns in the raw seismic profile, strong continuous paired reflectors give a clear indication of the upper limit of the acoustic basement. These reflectors descend westward from 2000 to 3500 m deep and then discontinu-

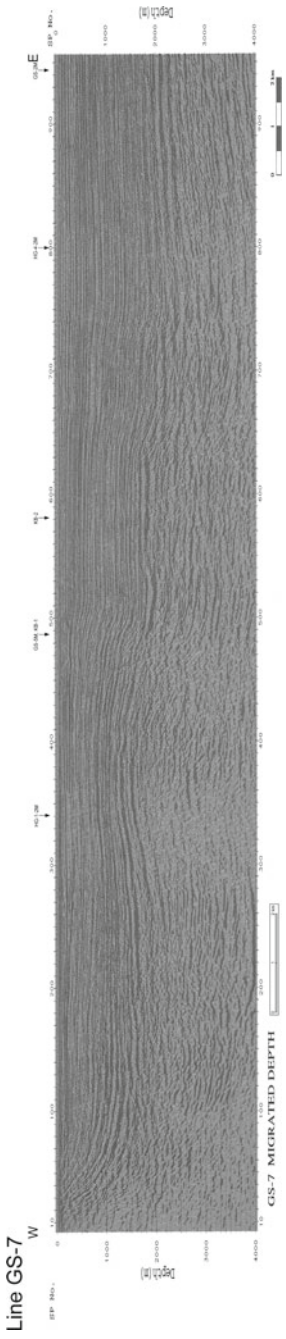

Fig. 3.10 Raw seismic profile of GS-7 (Yokokura et al. 1998) without vertical exaggeration. See Figs. 3.1, 3.2, and 3.3 for line location

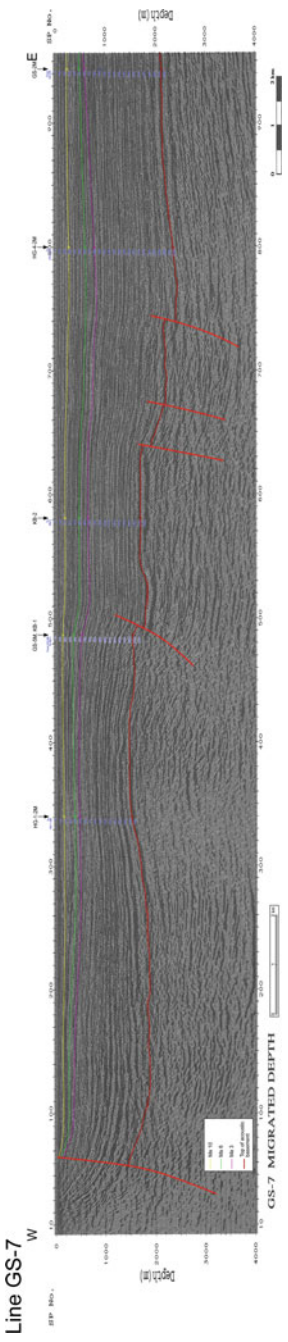

Fig. 3.11 Interpreted seismic profile of GS-7 without vertical exaggeration. See Figs. 3.1, 3.2, and 3.3 for line location

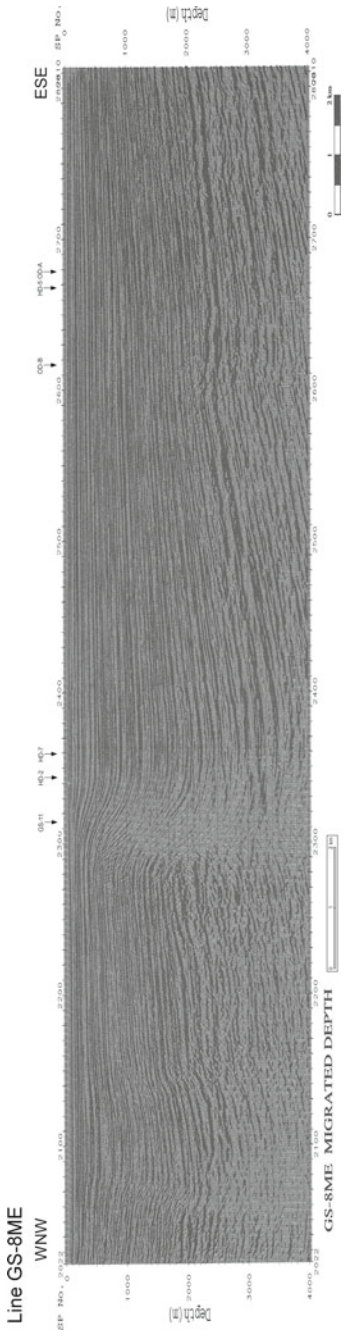

Fig. 3.12 Raw seismic profile of GS-8ME (Yokokura et al. 1998) without vertical exaggeration. See Figs. 3.1, 3.2, and 3.3 for line location

ously pop up near Sp. 2300. The western terrace of the basement has a rough surface undulating with a small amplitude. Thinly laminated reflectors originating from the basin-filling sediments show obvious draping and syn-sedimentary growth over the periods of basement ascent and descent in the western part.

Figure 3.13 shows the interpreted seismic profile of GS-8ME. Notable subsurface structures along this profile include a series of faults in the western half. The vertical separations of the basement surface on the faults at Sps. 2060, 2067, 2150, 2250, 2296, 2330, and 2352 are 150, 130, 50, 120, 40, 200, and 100 m, respectively. At Sp. 2080, the Ma 3 and 6 marine clays show separations of 50 and 30 m, respectively. The architectural characteristics are indicative of reverse faulting. As for the faults near Sp. 2250–2352, their flowerlike shape and change in separation sense may be related to strike-slip movements. It should be noted that strong continuous reflectors are distributed beneath the basement surface in the eastern part of the profile. Because the reliability of the present seismic interpretation was verified against tied profiles, the deep-seated reflections may suggest the existence of an older sedimentary basin. The reflectors in the lowermost part of the Quaternary sediments are generally flat-lying on top of the basement and partly onlap preexisting basement highs. The undulating shape of the Ma 3, 6, and 10 marine clays represents the basal vertical movements.

3.3.1.5 Line GS-11

Figure 3.14 shows the NE–SW-trending raw seismic profile of the approximately 35,000-m-long line GS-11. The Bouguer gravity anomaly along this section, which runs along the northwestern flank of the regional gravity low in the central part of the basin (Fig. 3.2), is characterized by subtle fluctuations with a maximum (approximately 1 mGal) at Sp. 900 and a minimum (approximately −8 mGal) at Sp. 1. The geomagnetic anomaly along this section (Fig. 3.3) has two cycles of drift with an amplitude of 40 nT reflecting N–S-aligned anomaly maxima and minima.

Regarding the reflection patterns in the raw seismic profile, the depth of a strong reflector indicative of the basement surface fluctuates from 3000 m to less than 2000 m. Upper fine reflectors in the sedimentary basin exhibit gentle draping over the basement heaves.

Figure 3.15 shows the interpreted seismic profile of GS-11. Notable subsurface structures along this profile include reverse faults at long intervals. The vertical separations of the basement surface on the faults at Sps. 1180, 1120, 985, 928, 820, 710, 480, and 440 are 230, 200, 200, 100, 150, 320, 160, and 480 m, respectively. Although such large separations indicate the tectonic significance of these faults, the architectural features may be seriously skewed because this survey line runs along the flank of a buried NE–SW trough in central Osaka Bay, as indicated by a negative gravity anomaly (see Fig. 3.2). Thus, the structural description was determined using tied seismic lines crossing the general trend at a right angle. The reflectors in the lowermost Quaternary sediments are generally flat-lying on top of the basement and partly onlap preexisting basement slopes. The gently undulating shape of the Ma 3, 6, and 10 marine clays reflects the vertical motions of the acoustic basement.

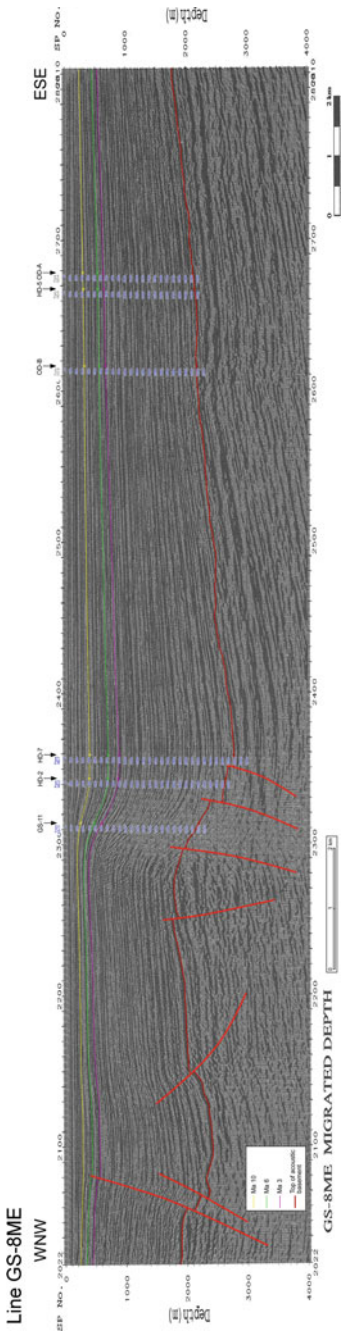

Fig. 3.13 Interpreted seismic profile of GS-8ME without vertical exaggeration. See Figs. 3.1, 3.2, and 3.3 for line location

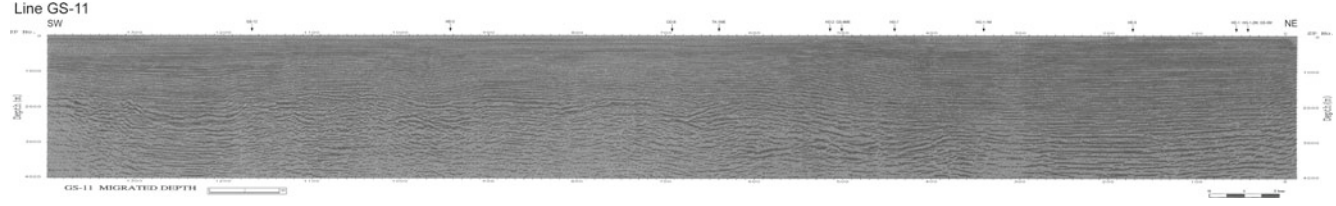

Fig. 3.14 Raw seismic profile of GS-11 (Yokokura et al. 1998) without vertical exaggeration. See Figs. 3.1, 3.2, and 3.3 for line location

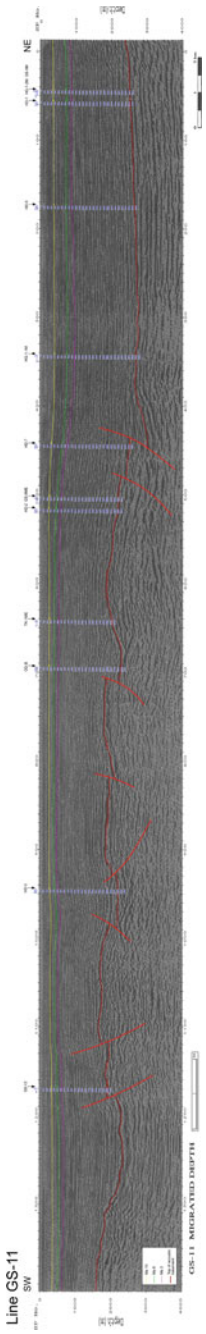

Fig. 3.15 Interpreted seismic profile of GS-11 without vertical exaggeration. See Figs. 3.1, 3.2, and 3.3 for line location

3.3.1.6 Line GS-12

Figure 3.16 shows a N–S-trending raw seismic profile of the approximately 37,500-m-long line GS-12. The Bouguer gravity anomaly along this section (Fig. 3.2) is characterized by lows in the northern part (−6 mGal at minimum) and highs in the southern part (exceeding 10 mGal). The geomagnetic anomaly along this section (Fig. 3.3) shows subtle changes and has a local minimum (approximately −90 nT) on the southern side of the Kitan Strait (Sp. 1000).

Regarding the reflection patterns in the raw seismic profile, the depth of the surface of the acoustic basement was considerably reduced from more than 2000 m in the northern part to just below the seabed around the Kitan Strait (Sp. 800–900). The most remarkable discontinuity of the basement–sediment interface is located around Sp. 1000, where the vertical displacement reaches 2000 m. To the south of this structure, the basement tends to ascend southward with some upheavals. Divided by the basement mound between Sp. 800 and 1000, fine reflectors originating from the Osaka Group show gentle draping over deeper structures in the northern flank, whereas the same unit overlies the rugged surface of the basement without deformation in the southern flank. Within the zone of the largest vertical separation, upper reflectors exhibit uneven deformation, implying a complex fracture geometry.

Figure 3.17 shows the interpreted seismic profile of GS-12. Because the tectonic context of the flowerlike fault on the southern flank of the basement mound is discussed in Chap. 4 (Sect. 4.2.3), this section concentrates on the seismic characteristics within Osaka Bay. Notable subsurface structures along this profile include stepwise south-dipping reverse faults (Sp. 285–370) and a north-dipping reverse fault (Sp. 150). The vertical separations of the basement surface on these faults are a total of 600 and 460 m, respectively. Although these large separations indicate the tectonic significance of these faults, their architectural features may be seriously skewed because this survey line runs along a flank of a buried N–S elongate depocenter in southern Osaka Bay represented by negative gravity anomaly (Fig. 3.2). Thus, the structural description was determined using a tied seismic line crossing the local trend at a right angle. The reflectors in the lowermost Quaternary sediments are generally flat-lying on the basement surface and partly onlap the preexisting rugged surface of the basement. The Ma 3, 6, and 10 marine clays are gently tilted and thin out on the basement mound.

3.3.2 Data Acquired by Hydrographic and Oceanographic Department, JCG

After the 1995 Kobe earthquake, an offshore seismic survey was conducted in Osaka Bay by the Hydrographic and Oceanographic Department, JCG. According to Iwabuchi et al. (2000), 24 channels of hydrophones installed at intervals of 12.5 m were used to record the energy released from an approximately 2.5-l GI-type

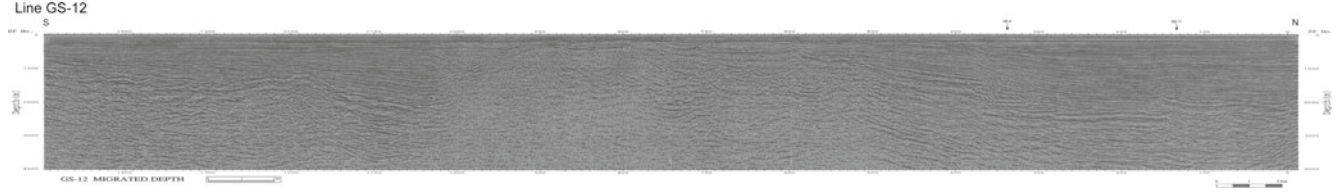

Fig. 3.16 Raw seismic profile of GS-12 (Yokokura et al. 1998) without vertical exaggeration. See Figs. 3.1, 3.2, and 3.3 for line location

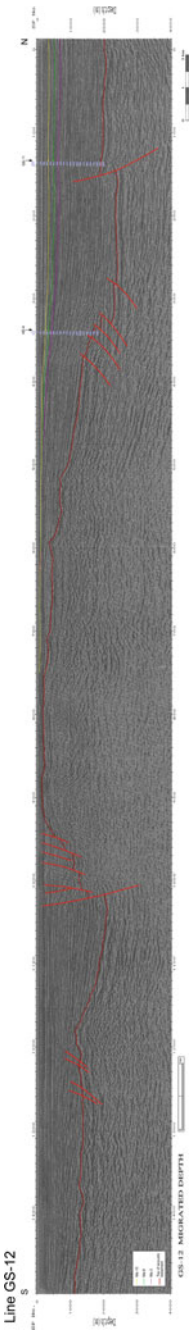

Fig. 3.17 Interpreted seismic profile of GS-12 without vertical exaggeration. See Figs. 3.1, 3.2, and 3.3 for line location

airgun during the shooting of survey tracks totaling 187 km in length with a shooting interval of 12.5 m. Raw seismic data were stacked and then subjected to a post-stack processing sequence to enhance the resolution.

3.3.2.1 Line HD-1

Figure 3.18 shows the E–W-trending raw seismic profile of the approximately 27,700-m-long line HD-1. The Bouguer gravity anomaly along this section (Fig. 3.2) is characterized by asymmetric changes; that is, the anomaly gradually decreases westward. After reaching a minimum (approximately −9 mGal) at Sp. 1200, it increases with a steeper gradient until the western end of the line, which corresponds to the zone of a low-angle structure identified through gravity gradient tensor analysis (see Chap. 1, Sect. 1.4.3.1). The geomagnetic anomaly along this section (Fig. 3.3) has a local maximum (approximately −40 nT) and a local minimum (approximately −80 nT) in the western (Sp. 1800) and eastern (Sp. 200) parts, respectively.

Regarding the reflection patterns in the raw seismic profile, the deeper horizons in this section are rich in strong reflectors, which may be related to frequent influx of coarse-grained material (e.g., talus deposits) at the foot of the Rokko Mountains. The lowermost strong reflector, which is assumed to represent the surface of the acoustic basement, reaches a depth of 2500 m in the western portion and shows an asymmetric morphology (gently sloping eastern wing and steep western wing). Chaotic reflections near the crossing point with HD-5 (Sp. 1600) accompany basal displacement and imply the presence of faults. Because thin reflectors in the upper horizons are also disturbed around the same interval, the predicted faults may have experienced recent activity.

Figure 3.19 shows the interpreted seismic profile of HD-1. Notable subsurface structures along this profile include a group of reverse faults (Sp. 1630–1715) and a west-dipping reverse fault (Sp. 1510). The vertical separations of the basement surface on these faults are a total of 600 and 60 m, respectively. The architecture of the western fault swarm is characterized by an upward-splaying flowerlike shape, implying transcurrent activity. Together with the reverse displacement sense on each branch, this architecture indicates a positive wrench fault system. The reflectors within the lowermost Quaternary sediments are flat-lying on top of the basement in the western part, whereas they partly downlap the eroded surface of the basement in the eastern part. The morphology of the Ma 3, 6, and 10 marine clays follows the basal movements caused by the strike-slip fault.

3.3.2.2 Line HD-2

Figure 3.20 shows the E–W-trending raw seismic profile of the approximately 31,800-m-long line HD-2. The Bouguer gravity anomaly along this section (Fig. 3.2) is characterized by gentle westerly declination. A local minimum (approximately

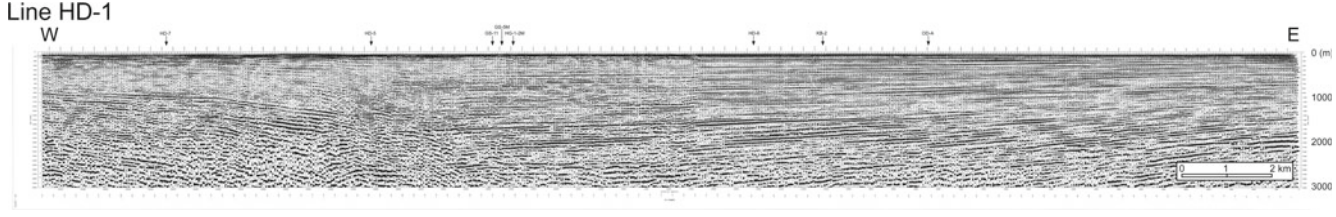

Fig. 3.18 Raw seismic profile of HD-1 (Iwabuchi et al. 2000) without vertical exaggeration. See Figs. 3.1, 3.2, and 3.3 for line location

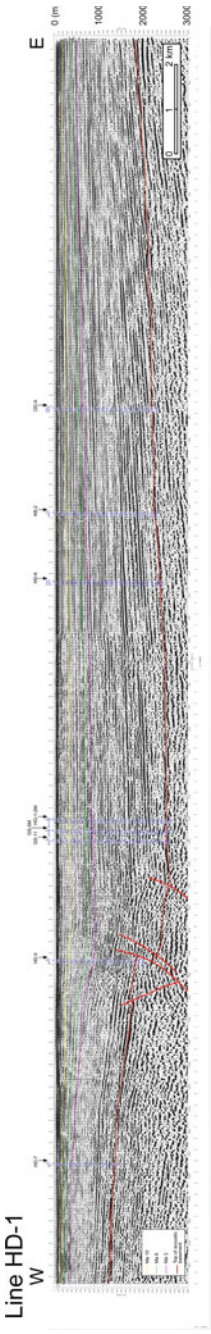

Fig. 3.19 Interpreted seismic profile of HD-1 without vertical exaggeration. See Figs. 3.1, 3.2, and 3.3 for line location

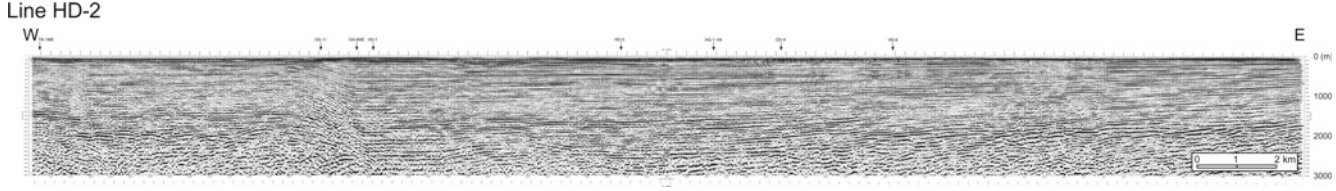

Fig. 3.20 Raw seismic profile of HD-2 (Iwabuchi et al. 2000) without vertical exaggeration. See Figs. 3.1, 3.2, and 3.3 for line location

−6 mGal) is located around Sp. 1600. The geomagnetic anomaly along this section (Fig. 3.3) is fairly constant except for trivial oscillations.

Regarding the reflection patterns in the raw seismic profile, the depth of the surface of the acoustic basement consistently increases westward from less than 2000 m to nearly 3000 m. After passing through a disturbed bottom around Sp. 1800–2000, the basement shows a stepwise upturn toward its western end. Thinly laminated upper horizons show growing undulation, indicating that the disturbed zone was active through the Quaternary.

Figure 3.21 shows the interpreted seismic profile of HD-2. Notable subsurface structures along this profile include faults in the western part. The vertical separations of the basement surface on these faults at Sps. 2464 and 1978–1892 are 450 and a total of 600 m, respectively. Between these faults, there are smaller faults at long intervals (Sps. 2150–2390). The separations on these faults range 30–50 m. Although a portion of the smaller fault swarm shows an irregular separation sense, they generally have characteristics of reverse faults. The reflectors in the lowermost Quaternary sediments are flat-lying on top of the basement and partly onlap the preexisting roughness of the basement. The deformation of the Ma 3, 6, and 10 marine clays suggests that the eastern faults (Sp. 1892–1978) were more active than the westernmost fault (Sp. 2464) in the later stages of the Quaternary basin development.

3.3.2.3 Line HD-3

Figure 3.22 shows the E–W-trending raw seismic profile of the approximately 32,400-m-long line HD-3. The Bouguer gravity anomaly along this section (Fig. 3.2) is characterized by asymmetric changes with the anomaly value gradually decreasing westward. After reaching a minimum (approximately −3 mGal) at Sp. 800, it increases with a steeper gradient until the westernmost point of the survey line in the vicinity of the eastern coast of Awaji Island. The geomagnetic anomaly along this section (Fig. 3.3) reaches a local maximum (approximately −10 nT) near the eastern end of the line (Sp. 2400–2500). This maximum represents the western wing of a remarkable geomagnetic high on the Osaka Bay coast (Fig. 3.3), the origin of which has not been identified.

Regarding the reflection patterns in the raw seismic profile, the surface of the acoustic basement seems to be cut by minor faults because the basement-indicative strong reflectors exhibit a fragmented distribution. The gentle undulation of thin superficial reflectors in the western part of the profile implies recent activity on these faults.

Figure 3.23 shows the interpreted seismic profile of HD-3. From west to east, the notable subsurface structures along this profile are a pair of faults forming a pop-up block (Sp. 40–274), divergent faults around a gentle basement swell (Sp. 332–780), and a solitary reverse fault (Sp. 1690). The relative heights of the pop-up block and the gentle basement swell are 670 and 270 m, respectively. The vertical separations of the basement surface on the reverse fault at Sp. 1690 are 180 m. The fault architecture around the eastern end of the gentle basement swell is characterized by changes

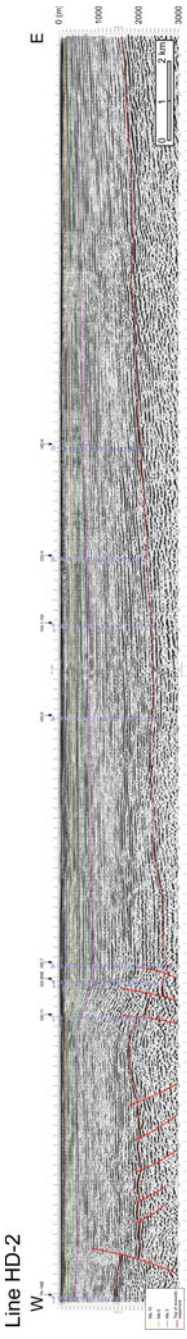

Fig. 3.21 Interpreted seismic profile of HD-2 without vertical exaggeration. See Figs. 3.1, 3.2, and 3.3 for line location

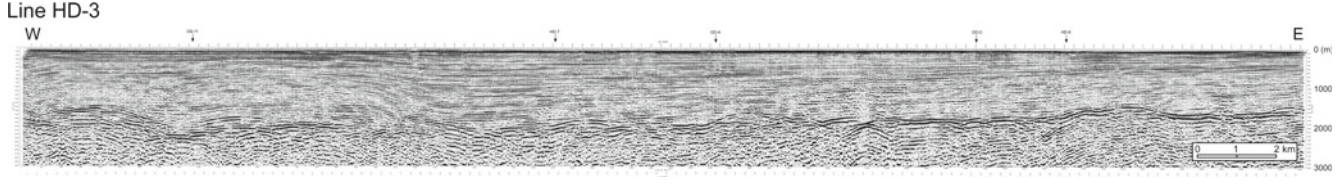

Fig. 3.22 Raw seismic profile of HD-3 (Iwabuchi et al. 2000) without vertical exaggeration. See Figs. 3.1, 3.2, and 3.3 for line location

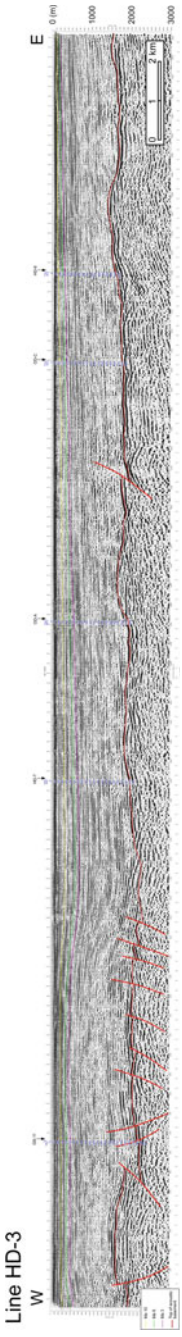

Fig. 3.23 Interpreted seismic profile of HD-3 without vertical exaggeration. See Figs. 3.1, 3.2, and 3.3 for line location

in the dipping direction at depths, implying transcurrent motions. The reflectors in the lowermost Quaternary sediments are flat-lying on top of the basement and partly onlap the preexisting topography of the basement. The moderate deformation of the Ma 3, 6, and 10 marine clays suggests that the easternmost portion of the gentle basement swell was active through the later stages of the Quaternary basin development.

3.3.2.4 Line HD-4

Figure 3.24 shows the E–W-trending raw seismic profile of the approximately 29,000-m-long line HD-4. The Bouguer gravity anomaly along this section (Fig. 3.2) continues to decrease westward with a local maximum (approximately 7 mGal) at Sp. 1900–2000 and local minima (approximately −5 and −7 mGal) at Sp. 1000 and 100, respectively. In the area of the maximum, Itoh et al. (2015) calculated the dimensionality index *I* (Beiki and Pedersen 2010) and shape index *Si* (Cevallos 2014) from the gravity gradient tensors and found them to be less than 0.5 and 0.2–0.3, respectively. These results suggest that the anomaly may have originated from a two-dimensional ridge-like structure. The geomagnetic anomaly along this section (Fig. 3.3) is fairly constant and shows no systematic changes.

Regarding the reflection patterns in the raw seismic profile, the depth of the high-amplitude seismic horizon of the surface of the acoustic basement is 800–900 m at the eastern end of the line and increases westward, showing some bumps. In the western half of the profile, this horizon seems to be discontinuous because of basement-cutting faults. A strong convex-upward reflector resides within the eastern part of the basement (Sp. 1600–1900) at a depth of 2000–3000 m. This reflector roughly coincides with the area of the local gravity maximum mentioned above. Shallow reflectors of the Quaternary sediments are deformed and somewhat discontinuous in the western part, indicative of recent fault activity.

Figure 3.25 shows the interpreted seismic profile of HD-4. Notable subsurface structures along this profile include a fault-bounded pop-up terrace in the west (Sp. 357–848) and a deep-seated anticline within the acoustic basement in the east (Sp. 1550–1880). The relative height of the pop-up terrace is 620 m. The total vertical separations of the basement surface and the Ma 3, 6, and 10 marine clays on the paired reverse faults along the western margin of this terrace are 520, 100, 70, and 40 m, respectively. Although the eastern anticline, which is situated at a large depth, is located around the N–S-warping region described in Chap. 2 (Sect. 2.5.3), it is not accompanied by the detectable deformation of the Quaternary strata. Reflectors settling on the basement–sediment interface exhibit an onlapping pattern because the basement surface shows frequent ups and downs along this section. The draping pattern of the Ma 3, 6, and 10 marine clays over the pop-up terrace suggests that the western marginal fault has maintained a higher level of activity than its eastern counterpart through the Quaternary basin development.

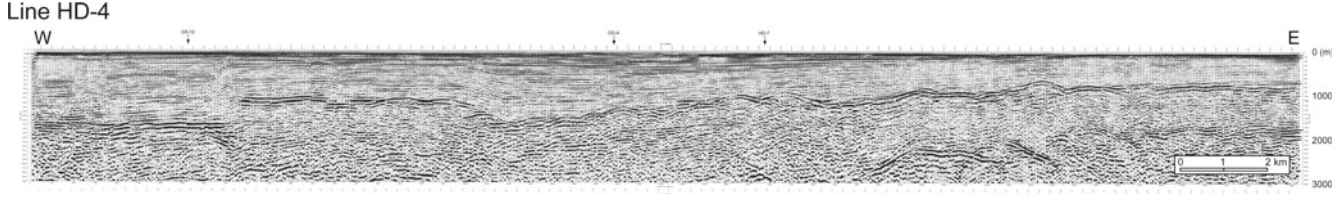

Fig. 3.24 Raw seismic profile of HD-4 (Iwabuchi et al. 2000) without vertical exaggeration. See Figs. 3.1, 3.2, and 3.3 for line location

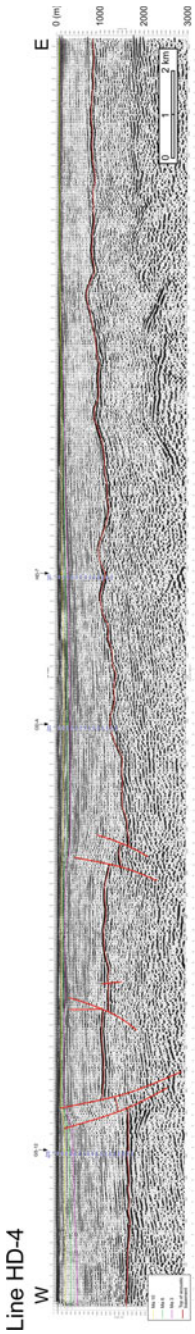

Fig. 3.25 Interpreted seismic profile of HD-4 without vertical exaggeration. See Figs. 3.1, 3.2, and 3.3 for line location

3.3.2.5 Line HD-5

Figure 3.26 shows the N–S-trending raw seismic profile of the approximately 16,600-m-long line HD-5. The Bouguer gravity anomaly along this section (Fig. 3.2) is highest (approximately 0 mGal) on either end of the line and reaches a local minimum (approximately −8 mGal) at Sp. 900. The gradient of the anomaly value is steeper in the northern part in a region corresponding to the zone of a subsurface low-angle structure identified from gravity gradient tensor analysis (see Chap. 1, Sect. 1.4.3.1). The geomagnetic anomaly along this section (Fig. 3.3) is fairly constant and shows no systematic changes.

Regarding the reflection patterns on the raw seismic profile, a strong seismic horizon corresponding to the surface of the acoustic basement resides at a depth of 2000 m at its southern end and descends northward to its minimum depth at Sp. 900. Then, it ascends in a stepwise fashion toward the northern end of the line. The discontinuity around Sp. 1100 is related to vertical displacements on the fault planes. In the same interval, upper fine reflectors show a clear undulation similar to the basement topography. In the northern half of the section, many strong reflectors are present in the upper sedimentary unit; these may be related to the frequent influx of coarse-grained material (e.g., talus deposits) near the foot of the Rokko Mountains.

Figure 3.27 shows the interpreted seismic profile of HD-5. Notable subsurface structures along this profile include a reverse fault at Sp. 920 and a group of upward-splaying faults around Sp. 1045–1136. The vertical separations of the basement surface on the southern solitary fault and the northern fault swarm (represented by the north-dipping fault with the largest shift) are 150 and 610 m, respectively. The architecture of the northern cluster has the characteristics of a positive flower structure; that is, the tapered fault slices within the steep master zone of deformation join at depth. The reflectors in the lowermost Quaternary sediments are generally flat-lying on top of the basement and partly onlap the preexisting rugged surface of the basement. The curvatures of the Ma 3, 6, and 10 marine clays indicate the steady growth of the active structure.

3.3.2.6 Line HD-6

Figure 3.28 shows the N–S-trending raw seismic profile of the approximately 20,200-m-long line HD-6. The Bouguer gravity anomaly along this section (Fig. 3.2) is characterized by a steady southerly increase from −10 mGal at the northern end to 8 mGal at the southern end. The geomagnetic anomaly along this section (Fig. 3.3) reaches a maximum (approximately −40 nT) at Sp. 1400, where the line passes through the western flank of a circular positive anomaly.

Regarding the reflection patterns in the raw seismic profile, the depth of the lowermost strong reflector originating from the basement decreases southward from 2500 to 1500 m. An upheaval with a relative height of 300 m is present in the same interval as the above-mentioned geomagnetic local maximum. The upper fine reflections in

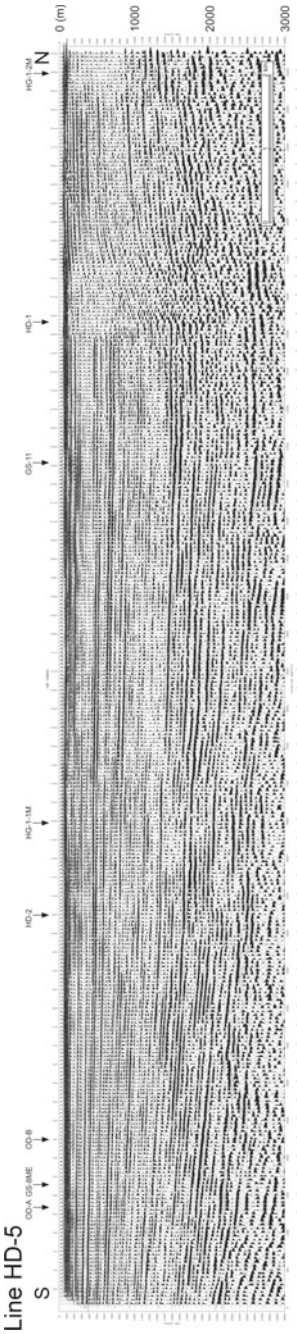

Fig. 3.26 Raw seismic profile of HD-5 (Iwabuchi et al. 2000) without vertical exaggeration. See Figs. 3.1, 3.2, and 3.3 for line location

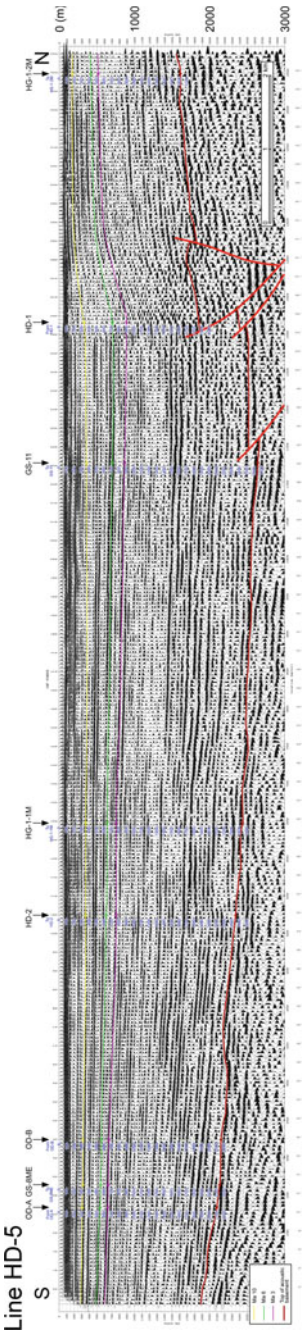

Fig. 3.27 Interpreted seismic profile of HD-5 without vertical exaggeration. See Figs. 3.1, 3.2, and 3.3 for line location

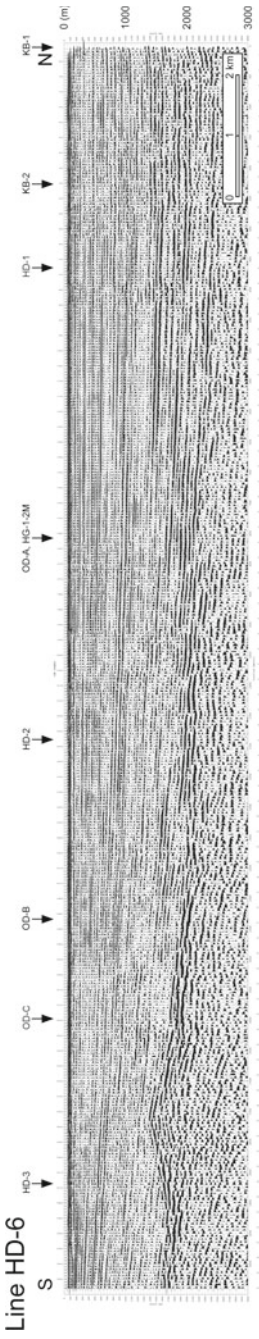

Fig. 3.28 Raw seismic profile of HD-6 (Iwabuchi et al. 2000) without vertical exaggeration. See Figs. 3.1, 3.2, and 3.3 for line location

the sedimentary unit descend monotonically toward the northern sector, where many strong reflectors related to the frequent influx of coarse-grained material reside.

Figure 3.29 shows the interpreted seismic profile of HD-6. As explained in Sect. 3.2, the key horizons are successfully tied with the marine clay beds, which were deposited under the control of eustasy, in the KIX 18-1 borehole adjacent to the southernmost tip of the survey line. No notable structural disturbances were detected in this section. The reflectors within the lowermost Quaternary sediments are generally flat-lying on top of the basement and onlap the preexisting basement slope in the southern part. The Ma 3, 6, and 10 marine clays tilt gently northward.

3.3.2.7 Line HD-7

Figure 3.30 shows the N–S-trending raw seismic profile of the approximately 29,600-m-long line HD-7. The Bouguer gravity anomaly along this section (Fig. 3.2) is characterized by subtle ups and downs because this survey line obliquely traverses a NE–SW-trending regional gravity trough in the central part of Osaka Bay. The geomagnetic anomaly along this section (Fig. 3.3) is fairly constant and shows no systematic changes.

Regarding the reflection patterns in the raw seismic profile, a reflector indicative of the basement surface is present at a depth of 1200 m at the northern end and gradually descends southward. Its depth shows a sharp decline around Sp. 600–700 and reaches 3000 m at Sp. 900–1000. After reaching its minimum depth, the horizon ascends southward to 1000 m without clear disruption. The upper fine reflections present in the sedimentary unit show growing undulations on the basement cliff, suggestive of active faulting in the northern sector.

Figure 3.31 shows the interpreted seismic profile of HD-7. Notable subsurface structures along this profile include a series of faults between Sps. 752 and 605. The total vertical separation of the basement surface on this fault swarm is 1050 m. This series of faults shows variation in separation senses and bedding attitudes, features that are characteristic of narrow fault slices. Upward-splaying fault branches seem to join at large depths, although such depths are outside the scope of the present seismic record. This suggests that the structure underwent lateral movement. The reflectors in the lowermost Quaternary sediments are generally flat-lying on top of the basement and partly onlap the preexisting ups and downs of the basement. The morphology of the Ma 3, 6, and 10 marine clays points to the temporal transition of active traces. Namely, the lower part of the basin-filling Quaternary exhibits an obvious flexure over the southern strand of the fault system, whereas the three seismic horizons in the upper part remain undeformed in the same interval. However, the northern fault strand became active in the beginning of the marine transgression stage, as indicated by the spatial changes in the curvatures of the reflectors throughout the structure.

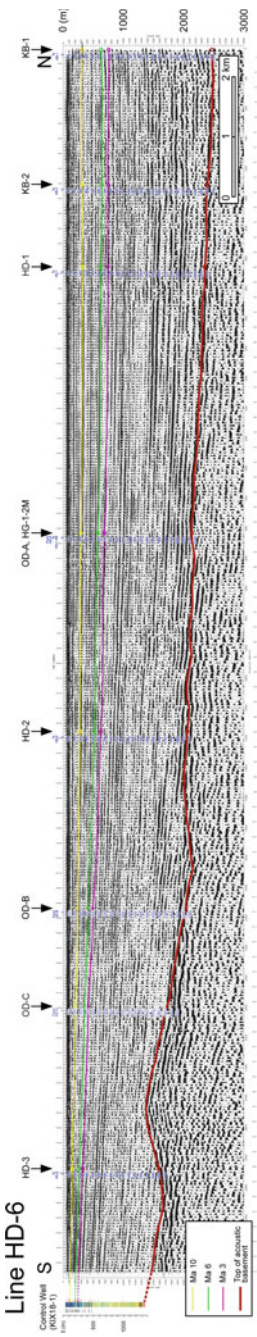

Fig. 3.29 Interpreted seismic profile of HD-6 without vertical exaggeration. See Figs. 3.1, 3.2, and 3.3 for line location

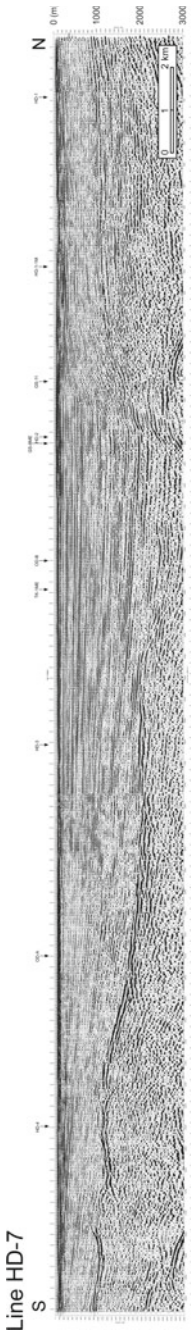

Fig. 3.30 Raw seismic profile of HD-7 (Iwabuchi et al. 2000) without vertical exaggeration. See Figs. 3.1, 3.2, and 3.3 for line location

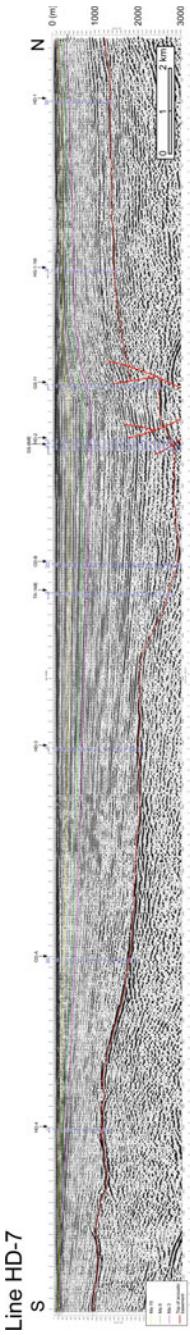

Fig. 3.31 Interpreted seismic profile of HD-7 without vertical exaggeration. See Figs. 3.1, 3.2, and 3.3 for line location

3.3.3 Data Acquired by Hyogo Prefecture

In 1995, an offshore seismic survey was conducted by Hyogo Prefecture in Osaka Bay. According to Yokota et al. (1997), 48 channels of hydrophones installed at intervals of 12.5 m were used to record the energy released from an approximately 12-l airgun array during the shooting of offshore lines totaling 55 km in length with a shooting interval of 25 m. Raw seismic data were stacked and then subjected to a post-stack processing sequence to enhance the resolution.

3.3.3.1 Line HG-1-1M

Figure 3.32 shows the WNW–ESE-trending raw seismic profile of the approximately 30,000-m-long line HG-1-1M. The Bouguer gravity anomaly along this section (Fig. 3.2) is characterized by prominent positive (approximately 22 mGal) and negative (approximately −7 mGal) peaks in the western and eastern parts, respectively. On the eastern flank of the anomaly maximum, a steep gradient zone is present around Sp. 390–470 (10,400–12,400 m from the western end), corresponding to faults or structural boundaries with high dip angles (some of which exceed 70°; see Chap. 1, Sect. 1.4.3.1), as identified by Itoh et al. (2015) and Kusumoto (2016). Furthermore, a basin-side gentle slope around Sp. 500–700 (13,300–18,300 m from the western end) is coincident with the general zone of a low-angle structure identified from gravity gradient tensor analysis (see Chap. 1, Sect. 1.4.3.1). The geomagnetic anomaly along this section (Fig. 3.3) tends to be high on both ends of the line (approximately −40 nT at the highest) and low around the center (approximately −70 nT at the lowest).

Regarding the reflection patterns in the raw seismic profile, signals from the acoustic basement were obscured on the western side of Awaji Island (0–8000 m from the western end of the survey line), whereas the basement reflector is clearly observable on the eastern side. Two notable separations of the surface of the basement are identifiable on the eastern margins of above-mentioned steep and gentle slopes of the gravity anomaly. They are accompanied by the growing deformation of the overlying thinly laminated reflectors, implying recent activity on concealed faults.

Figure 3.33 shows the interpreted seismic profile of HG-1-1M. Notable subsurface structures within Osaka Bay include fault swarms around Sp. 390–470 (10,400–12,400 m from the western end) and Sp. 685–755 (17,900–19,600 m from the western end). The total vertical separations of the basement surface on these fault swarms are 1100 and 1250 m, respectively. Both of these systems have features that are indicative of transcurrent faulting, namely downward-converging high-angle ruptures with a variable sense of separation and tilting attitude. Together with a considerable amount of cumulative vertical slip, these features indicate the faults are positive wrench faults that have controlled basin development under a transpressive regime. The reflectors in the lowermost Quaternary sediments are generally flat-lying on top of the basement and partly onlap the preexisting basement

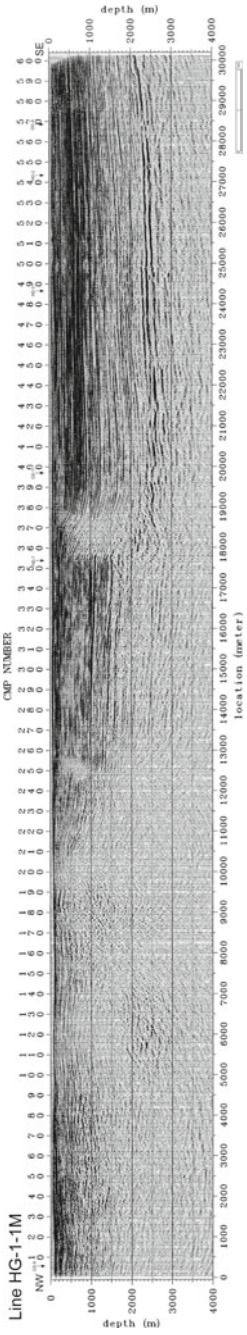

Fig. 3.32 Raw seismic profile of HG-1-1M (Yokota et al. 1997) without vertical exaggeration. See Figs. 3.1, 3.2, and 3.3 for line location

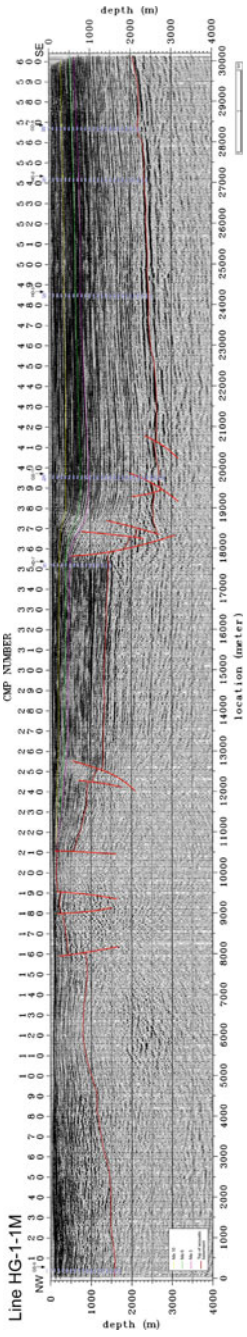

Fig. 3.33 Interpreted seismic profile of HG-1-1M without vertical exaggeration. See Figs. 3.1, 3.2, and 3.3 for line location

slopes. The morphological features of the Ma 3, 6, and 10 marine clays indicate that the southeastern (basin-side) fault system has maintained a higher activity level than its northwestern (coast-side) counterpart.

3.3.3.2 Line HG-1-2M

Figure 3.34 shows the NW–SE-trending raw seismic profile of the approximately 14,000-m-long line HG-1-2 M. The Bouguer gravity anomaly along this section (Fig. 3.2) follows as a concave curve with maxima on both ends of the line (approximately −2–0 mGal) and a minimum at the center (approximately −9 mGal). The northwestern flank of the negative anomaly trough corresponds to a subsurface low-angle structural zone identified from gravity gradient tensor analysis (see Chap. 1, Sect. 1.4.3.1). The geomagnetic anomaly along this section (Fig. 3.3) is fairly constant and shows no systematic changes.

Regarding the reflection patterns in the raw seismic profile, deep strong reflectors indicative of the surface of the acoustic basement can be traced throughout the section. A remarkable disturbance to this seismic horizon is present in the northwest near Sp. 150 (10,500 m from the southeastern end of the line). Diffuse reflections in the upper sedimentary unit were observed around the same interval, strongly suggesting active faulting.

Figure 3.35 shows the interpreted seismic profile of HG-1-2M. Notable subsurface structures along this profile include a peculiar fault swarm around Sp. 180–150 (9800–10,500 m from the southeastern end of the line). The total vertical separation of the basement surface on this swarm is 300 m. The fault architecture has characteristics typical of wrench faults. A steep master fault splays upward. Changes in separation sense and tilting attitude were observed within narrow fault slices and are accompanied by a chaotic pattern of reflections, implying the presence of subordinate fractures. The reflectors in the lowermost Quaternary sediments are generally flat-lying on top of the basement and partly onlap the preexisting basement slopes. The sinuous shape of the Ma 3, 6, and 10 marine clays over the described structure is an indication of the complexity of the deformation in the wrench fault zone.

3.3.3.3 Line HG-4-2M

Figure 3.36 shows the NW–SE-trending raw seismic profile of the approximately 11,000-m-long line HG-4-2 M. The Bouguer gravity anomaly along this section (Fig. 3.2) has a local minimum (approximately −13 mGal) around Sp. 700–800 (8500–11,000 m from the southeastern end of the line). The geomagnetic anomaly along this section (Fig. 3.3) shows no systematic changes.

Regarding the reflection patterns in the raw seismic profile, the deformation of the basement rocks evaluated on the basis of the separations of a deep strong reflector indicative of the surface of the acoustic basement seems to be modest except for a

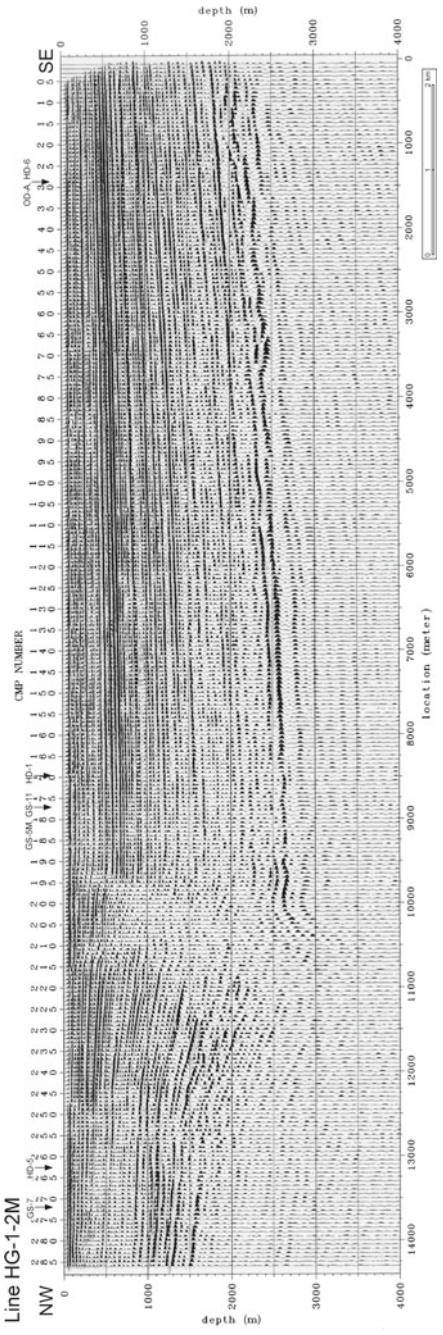

Fig. 3.34 Raw seismic profile of HG-1-2M (Yokota et al. 1997) without vertical exaggeration. See Figs. 3.1, 3.2, and 3.3 for line location

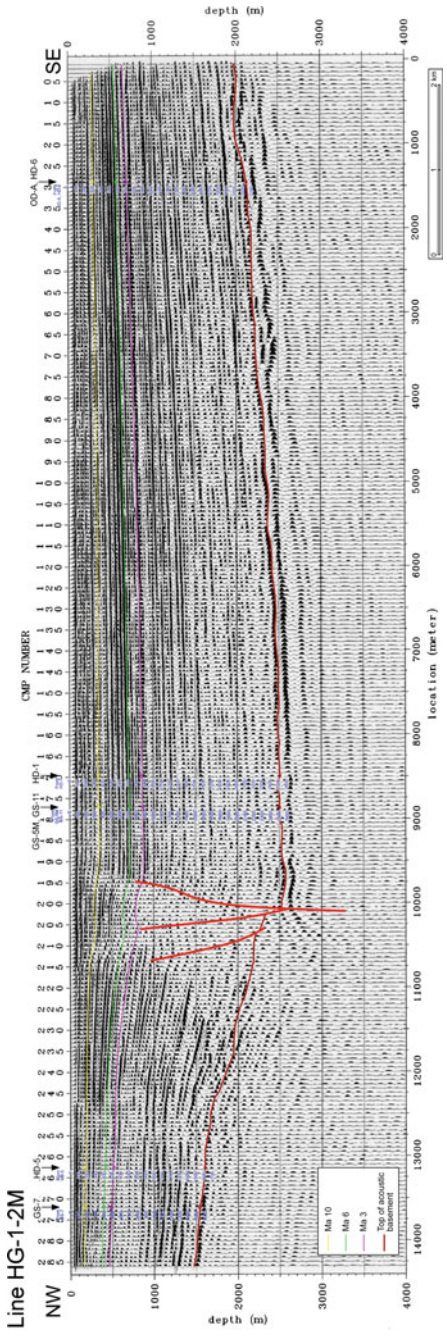

Fig. 3.35 Interpreted seismic profile of HG-1-2M without vertical exaggeration. See Figs. 3.1, 3.2, and 3.3 for line location

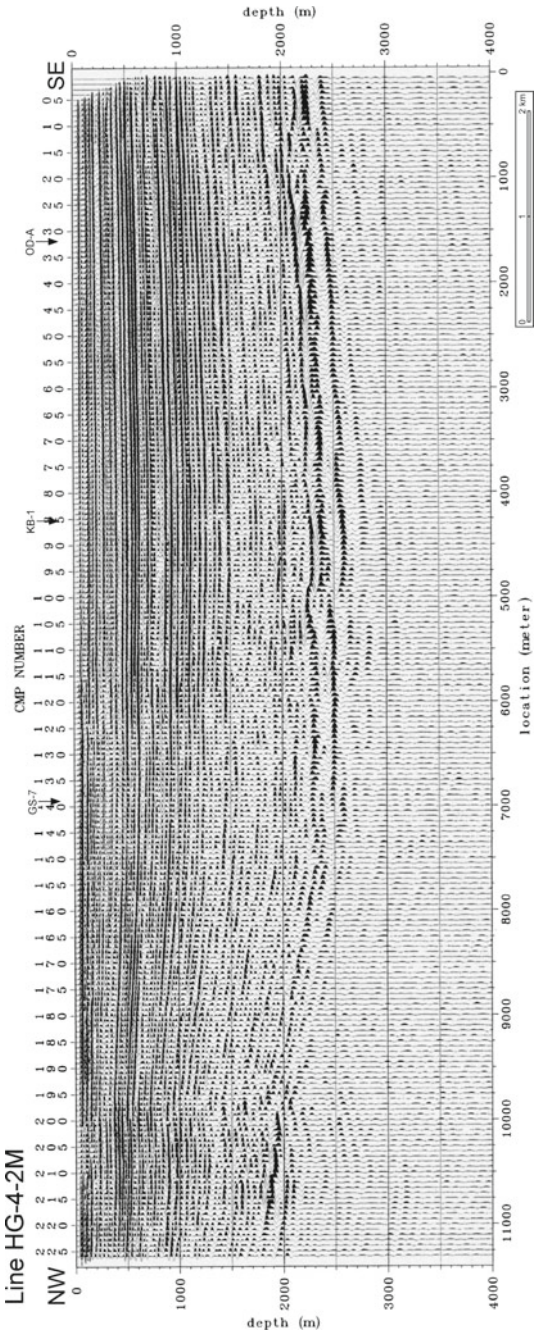

Fig. 3.36 Raw seismic profile of HG-4-2M (Yokota et al. 1997) without vertical exaggeration. See Figs. 3.1, 3.2, and 3.3 for line location

steplike shape near the northwestern end. The deformation of the younger reflectors in the upper sedimentary unit is also subtle.

Figure 3.37 shows the interpreted seismic profile of HG-4-2M. Notable subsurface structures along this profile include small faults between Sp. 740 and 775 (9800–10,600 m from the southeastern end of the line). The vertical separations of the surface of acoustic basement on these faults range from 40 to 60 m. The reflectors in the lowermost Quaternary sediments are generally flat-lying on top of the basement and partly onlap the preexisting rugged surface of the basement. The morphological features of the Ma 3, 6, and 10 marine clays suggest that neotectonic disturbances are minimal on this section.

3.3.4 Data Acquired by Osaka Soil Test Laboratory, GRI

In 1989, an offshore seismic survey was conducted in Osaka Bay by Osaka Soil Test Laboratory, GRI. According to Iwasaki et al. (1994), 20 channels of hydrophones placed at intervals of 25 m were used to record the energy released from an approximately 9.8-l airgun array during the shooting of survey lines totaling 78 km in length with a shooting interval of 25 m. Raw seismic data were stacked and then subjected to a post-stack processing sequence for the enhancement of resolution.

3.3.4.1 Line OD-A

Figure 3.38 shows the NE–SW-trending raw seismic profile of the approximately 40,000-m-long line OD-A. The Bouguer gravity anomaly along this section (Fig. 3.2) reaches a minimum (approximately −11 mGal) at the northeastern end of the line and is characterized by subtle ups and downs because the survey line runs parallel to a NE–SW regional gravity trough in the central part of Osaka Bay. The geomagnetic anomaly along this section (Fig. 3.3) is fairly constant and shows no systematic changes.

Regarding the reflection patterns in the raw seismic profile, a strong continuous reflector suggestive of the surface of the acoustic basement shows gentle undulations between depths of 1200 and 2200 m. The basement terrace around the southwestern end (Sp. 1–200) of the line accompanies a negative gravity anomaly (Fig. 3.2). The fine reflectors in the upper sediments are generally flat-lying and do not show draping over the southwestern basement high.

Figure 3.39 shows the interpreted seismic profile of OD-A. No notable subsurface structures were observed on this section. The reflectors in the lowermost Quaternary sediments are generally flat-lying on top of the basement and partly onlap the preexisting rugged surface of the basement. The Ma 3, 6, and 10 marine clays remain intact and reach the greatest depths around the central part of the bay.

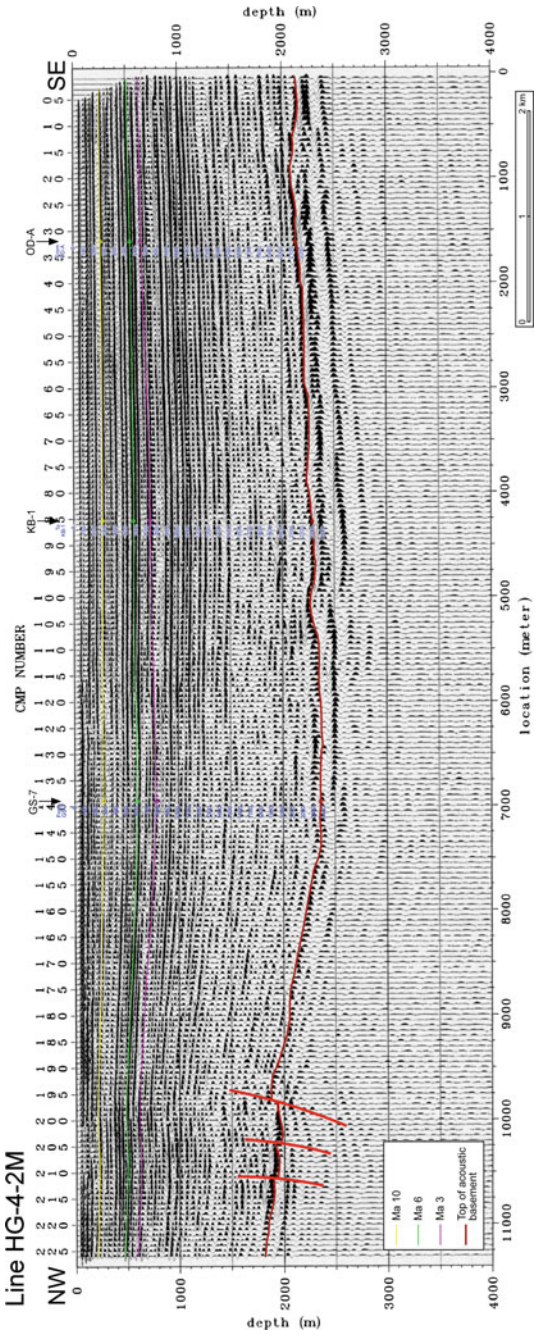

Fig. 3.37 Interpreted seismic profile of HG-4-2M without vertical exaggeration. See Figs. 3.1, 3.2, and 3.3 for line location

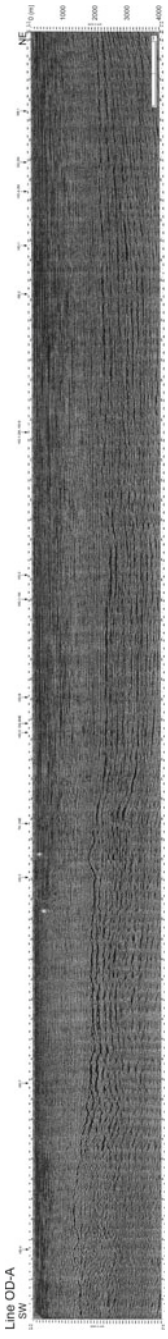

Fig. 3.38 Raw seismic profile of OD-A (Iwasaki et al. 1994) without vertical exaggeration. See Figs. 3.1, 3.2, and 3.3 for line location

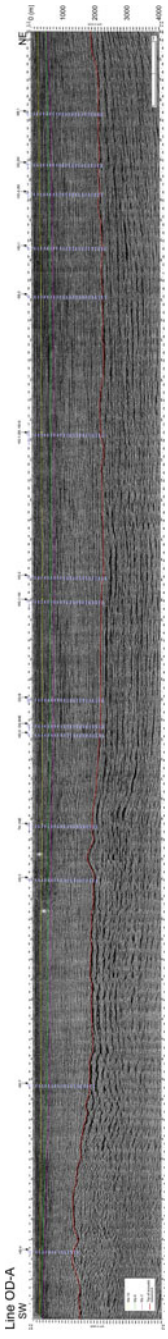

Fig. 3.39 Interpreted seismic profile of OD-A without vertical exaggeration. See Figs. 3.1, 3.2, and 3.3 for line location

3.3.4.2 Line OD-B

Figure 3.40 shows the E–W-trending raw seismic profile of the approximately 28,000-m-long line OD-B. The Bouguer gravity anomaly along this section, which passes through a regional gravity trough in the central part of Osaka Bay (Fig. 3.2), follows a concave curve with a local minimum (approximately −5 mGal) in its western portion (Sp. 700–800). The geomagnetic anomaly along this section (Fig. 3.3) reaches a maximum (approximately −30 nT) at Sp. 200–300, where the line meets the northern flank of a circular peak centered around the coast.

Regarding the reflection patterns in the raw seismic profile, the depth of the rugged surface of the basement increases westward from 1500 to 3200 m and then decreases stepwise up to 1800 m. Fragmented basal reflectors in the western part (Sp. 900–1100) are indicative of a broad fault zone. Thinly laminated reflectors in the upper unit form a kinked band over the largest separation of the basement rocks (Sp. 900–930).

Figure 3.41 shows the interpreted seismic profile of OD-B. Notable subsurface structures along this profile include divergent faults around Sp. 930–1090. The vertical separations of the basement surface on these faults range from 40 to 360 m and reach 1200 m in total. Their architecture shows characteristics of wrench faults, such as an upward-splaying shape, spatial changes in separation senses, and varied tilting attitudes in fault-bounded narrow slices. The reflectors in the lowermost Quaternary sediments are generally flat-lying on top of the acoustic basement and partly onlap the preexisting roughness of the interface. The remarkable flexure of the Ma 3, 6, and 10 marine clays indicates that the Quaternary activity of the contractional wrench fault zone peaked at its easternmost point.

3.3.4.3 Line OD-C

Figure 3.42 shows the NE–SW-trending raw seismic profile of the approximately 10,000-m-long line OD-C. The Bouguer gravity anomaly along this section, which lies on the southeastern flank of a regional gravity trough (Fig. 3.2), shows no systematic changes. The geomagnetic anomaly along this section (Fig. 3.3) reaches a maximum (approximately −30 nT) at Sp. 100, where the line meets the northern flank of a circular peak centered around the coast.

Regarding the reflection patterns in the raw seismic profile, the rugged appearance of the basement reflector recalls an eroded surface in a terrestrial environment. The parallel thin reflectors in the upper unconsolidated sediments do not display any distinguishable deformation.

Figure 3.43 shows the interpreted seismic profile of OD-C. Near the southwestern termination, an auxiliary borehole (57-30) is tied with the survey line. Although the well did not reach the basement, key seismic horizons in the sedimentary unit were successfully correlated with marine clay beds deposited under the control of eustatic change of sea level and confirmed in borehole 57-30. No notable subsurface structures

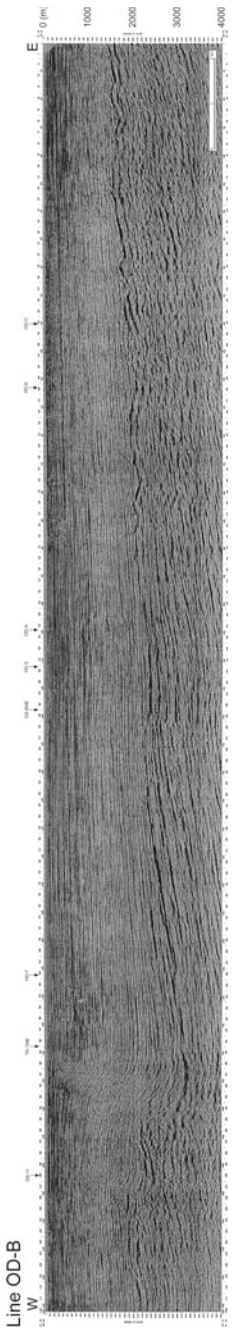

Fig. 3.40 Raw seismic profile of OD-B (Iwasaki et al. 1994) without vertical exaggeration. See Figs. 3.1, 3.2, and 3.3 for line location

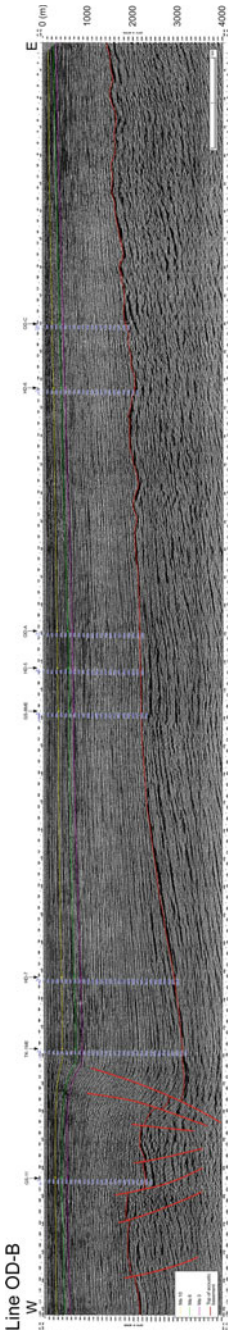

Fig. 3.41 Interpreted seismic profile of OD-B without vertical exaggeration. See Figs. 3.1, 3.2, and 3.3 for line location

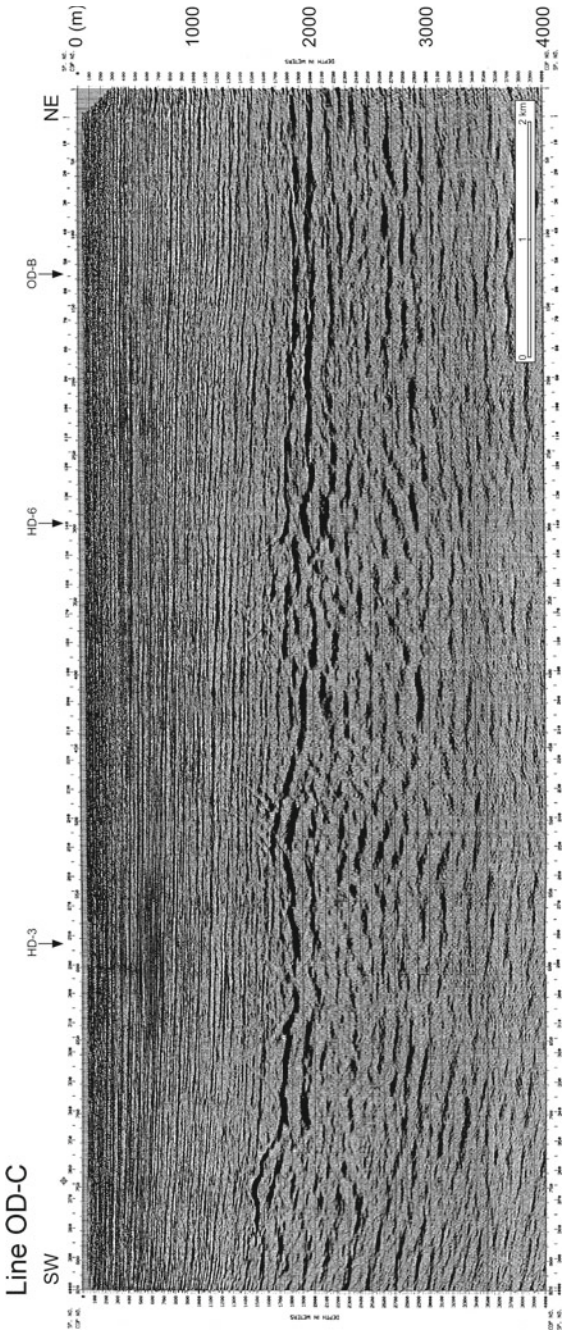

Fig. 3.42 Raw seismic profile of OD-C (Iwasaki et al. 1994) without vertical exaggeration. See Figs. 3.1, 3.2, and 3.3 for line location

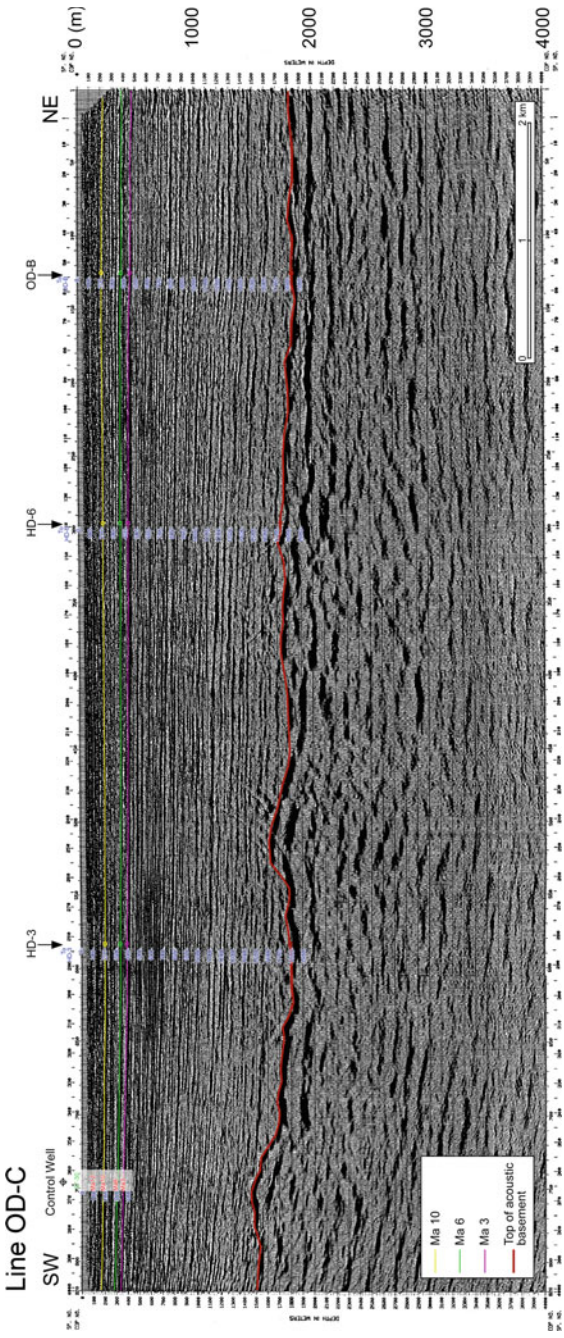

Fig. 3.43 Interpreted seismic profile of OD-C without vertical exaggeration. See Figs. 3.1, 3.2, and 3.3 for line location

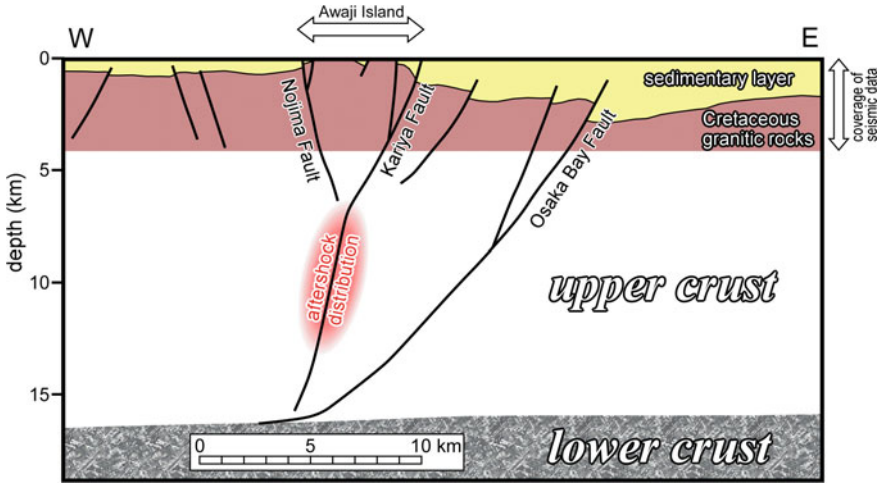

Fig. 3.44 Deep structure of active faults along the coasts of Awaji Island after Sato et al. (1998)

were observed in this section. Reflectors settling on the basement–sediment interface exhibit a flat-lying or onlapping appearance. The Ma 3, 6, and 10 marine clays are nearly horizontal.

3.3.5 Auxiliary Data

In 1996, hybrid onshore–offshore seismic data were acquired across the northern part of Awaji Island (TK-1ME in Fig. 3.1) by the JAPEX Geoscience Institute, Inc. (JGI). According to Sato et al. (1998), 48 channels of hydrophones installed at intervals of 12.5 m were used to record the energy released from approximately 12-l GI-type airguns during the shooting of the offshore segment with a shooting interval of 25 m. The raw seismic data were stacked and then subjected to a post-stack processing sequence to enhance the resolution.

As shown by Sato et al. (1998), the eastern coast of Awaji Island is cut by a number of active faults. The surface traces of these faults are named the Higashiura and Kariya faults, and they show dominant dextral and reverse displacements, respectively (Research Group for Active Faults 1991). It is also noteworthy that step-down shelves have been observed on the eastern flank of the island. The easternmost margin of these shelves is coincident with the Osaka Bay Fault previously visualized by means of offshore sounding surveys (Research Group for Active Faults 1991). Based on the hypocentral distribution of the aftershocks of the 1995 Kobe earthquake, Sato et al. (1998) hypothesized that these faults, together with the Nojima Fault on the western coast, constitute a common seismogenic master fault in the middle of the upper crust, as illustrated in Fig. 3.44.

3.4 Results

3.4.1 Structural Architecture

Our structural interpretation of the Osaka basin is presented as isochron maps from Figs. 3.45, 3.46, 3.47, 3.48. The morphology of the surface of acoustic basement of the bay area (Fig. 3.45) is characterized by fault-related two depressions. The major one is an asymmetric deep adjacent to the Osaka Bay Fault, and its bottom reaches 3000 m below sea level. If we assume that the fault has been activated since the earliest Pleistocene (see Fig. 1.8), average slip rate on it exceeds 1 mm/year. To the west, gently undulate shelf lies alongside, and cut by a sharp escarpment of the Awaji–Rokko Fault System. The minor round-bottomed sag exists off the southeastern coast of the Awaji Island and bordered by a sinuate fault, cumulative separation on which is approximately 1000 m. Another noted feature is broad wavelet near the southern Osaka shoreline. It is the root of N–S warping that gave a paleoenvironmental impact as discussed in Chap. 2 (Sect. 2.5.3; Fig. 2.8).

Isochrons of three marker horizons in the Osaka Group basically simulate structural architecture of the basement. The two remarkable depocenters have been subsiding during the late Pleistocene. The boundary faults are responsible for flexures of the sedimentary layers but do not make clear ruptures. Based on the height of scarp of the Osaka Bay Fault for the Ma 10 marine clay (see Fig. 3.48), average slip rate is calcu-

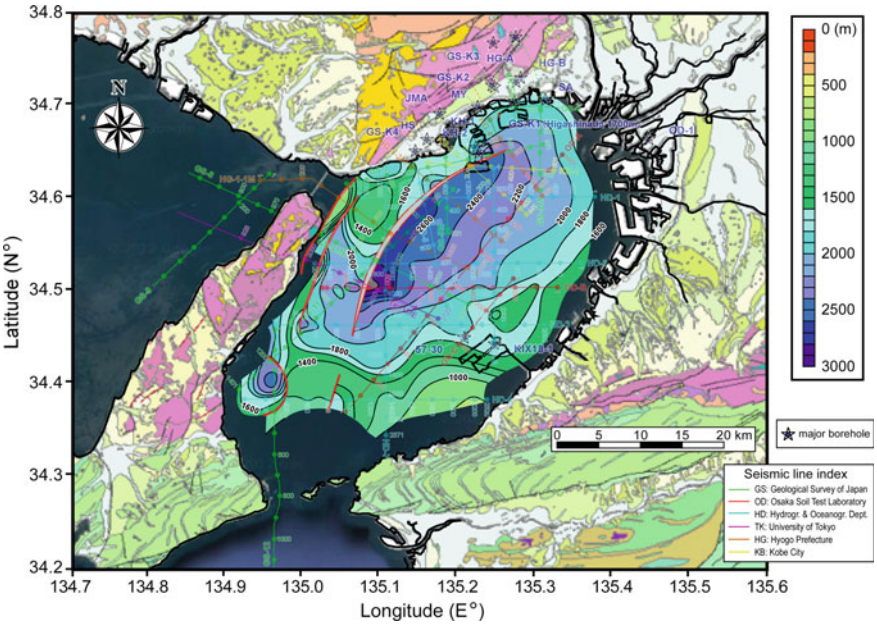

Fig. 3.45 Structural map of the surface of the acoustic basement of the Osaka Bay area

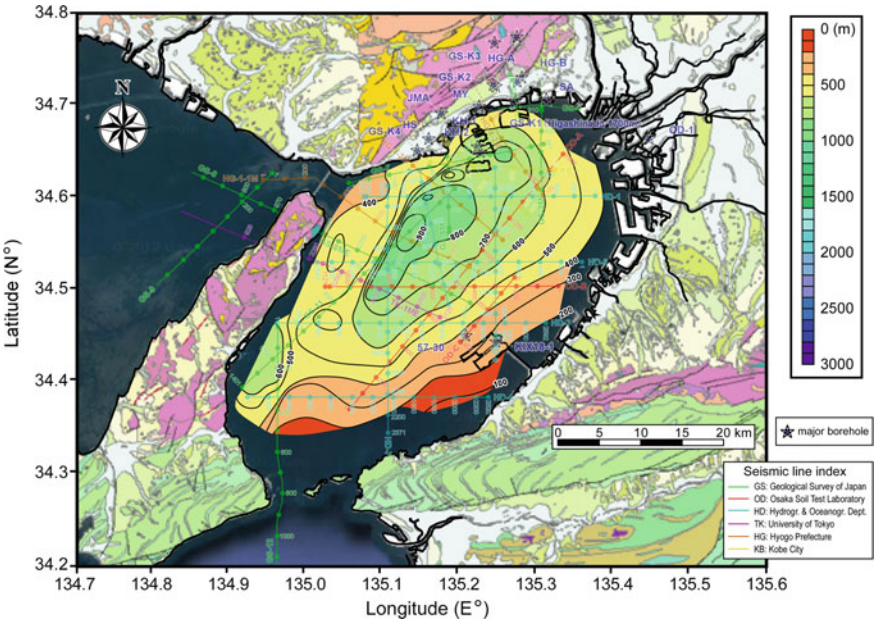

Fig. 3.46 Structural map of the Ma 3 marine clay horizon in the Osaka Bay area

lated as much as 0.6 mm/year, which may suggest recent decline of the fault activity level. As for the N–S warping on the southern shoreface, its signature is detectable in subtle trends of the Ma 3 (Fig. 3.46) and 6 (Fig. 3.47) marine clays. In contrast, map for the Ma 10 (Fig. 3.48) does not show related deformation, which is concordant with the notion that the warping ceased to develop ca. 0.4 Ma (Chap. 2, Sect. 2.5.3).

3.4.2 Basin Accommodation

Regarding previous volumetric analysis, Itoh et al. (2013) reported a rough estimate as explained in Chap. 1 (Sect. 1.4.3.2; Fig. 1.11). The total volume (9.1×10^2 km^3) was deduced from density contrast between the basement and basin fill (400 kg/m^3) and mass deficiency, which was given by gravity anomaly based on Gauss's theorem (e.g., Wangen 2010). Although scarce information of infill sediments forced them to assume a constant density, the present study has demonstrated that the pre-Quaternary basement around Osaka consists of several rock types with varied densities. It is also noted that offshore reflection seismic data have visualized gigantic neotectonic depression as deep as 3000 m, in which considerable compaction inevitably causes early density increase. For example, Itoh et al. (1994) described Neogene stratigraphy of a well on the Japan Sea shelf and found that average density determined on borehole logging exceeds 2.5 g/cm^3 over 2000 m below sea level.

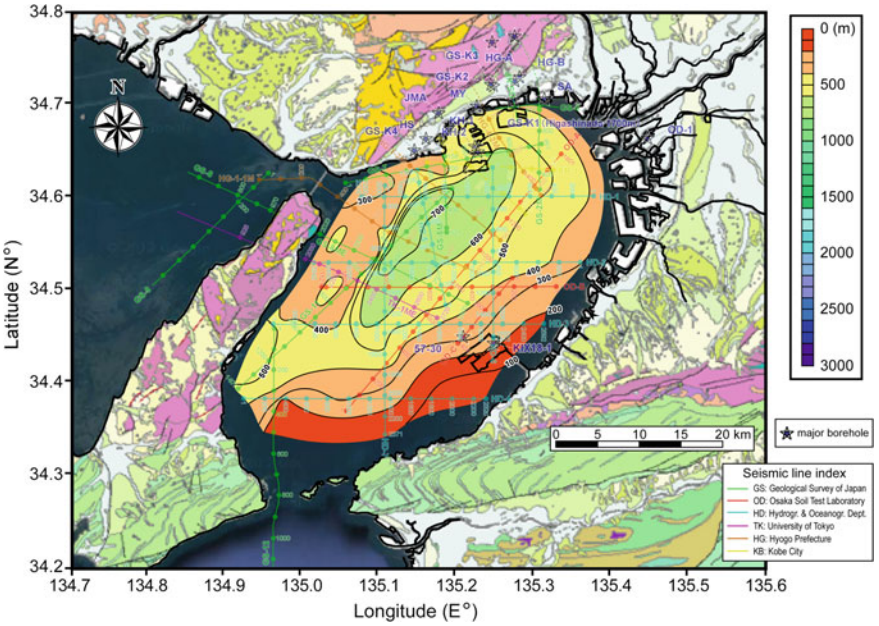

Fig. 3.47 Structural map of the Ma 6 marine clay horizon in the Osaka Bay area

The authors, hence, attempt to assess the spatiotemporal variation of basin accommodation utilizing structural maps of selected seismic horizons described above. First, Osaka Bay is divided into eastern, central, and western parts that represent ramp margin of the asymmetric basin, major trough along the Osaka Bay Fault and the Awaji shelf accompanied by multi-azimuthal undulations, respectively (see Fig. 3.49). The total dimension of the basement depression is a sum of volumes of three rectangular areas in Fig. 3.49a. It was calculated to be 1.3×10^3 km^3 from depth data given on the mesh with a 2-km interval by using the Gauss-Legendre numerical integration (e.g., Davis and Rabinowitz 2007). The present estimate is nearly 50% larger than the result by Itoh et al. (2013), which is probably related to prompt density increase in great depth as stated in the previous paragraph.

Next, we calculate subtotal accommodations for each time slice. Figure 3.50 depicts subsidence curves of three blocks of the Osaka Bay, together with their sum-upped volumes, since the late Pliocene. In the figure, the sedimentary basin is assumed to have begun subsiding at ca. 3 Ma based on the paleogeographic discussion in Chap. 1 (Sect. 1.4.1; Fig. 1.8). It seems that the tectonic subbasins have steadily deepened since their initiation. However, a closer looking shows that interval accumulation rates descend between the marker horizons Ma 3 and Ma 6 without exception (see inset data of Fig. 3.50), which accords well with temporal change in subsidence pattern in the eastern half of the basin, Osaka Plain, as explained in Chap. 2 (Sect. 2.5.3; Fig. 2.8).

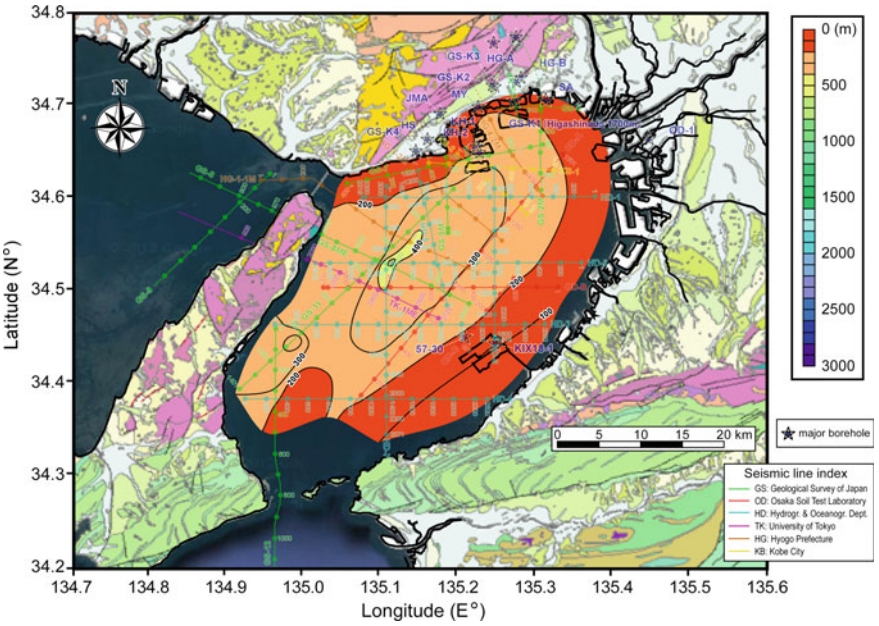

Fig. 3.48 Structural map of the Ma 10 marine clay horizon in the Osaka Bay area

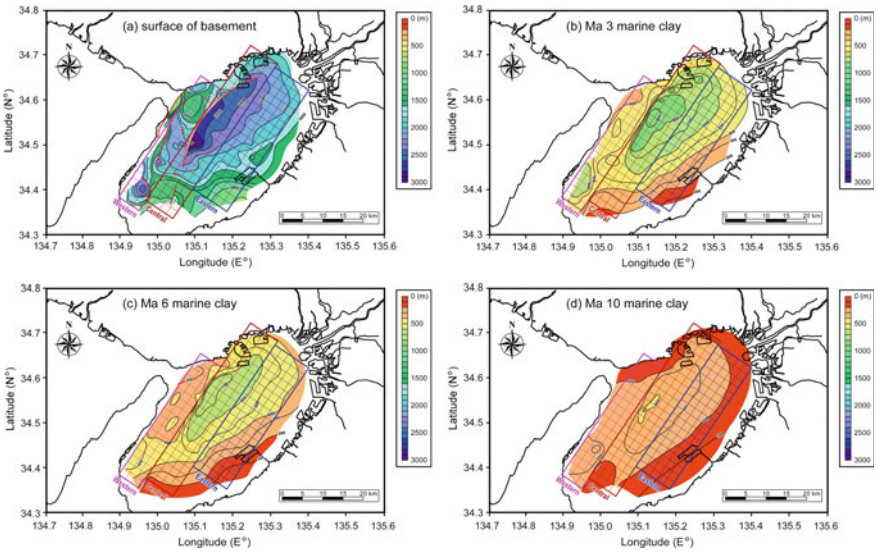

Fig. 3.49 Volumetric analysis of the Osaka Bay area. **a** Structure of the surface of the acoustic basement. **b** Structure of the Ma 3 marine clay. **c** Structure of the Ma 6 marine clay. **d** Structure of the Ma 10 marine clay. Grids show data points

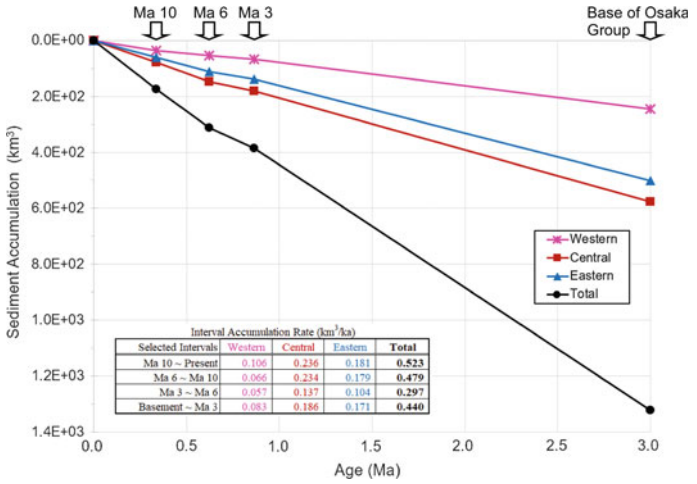

Fig. 3.50 Subsidence from late Pliocene through Pleistocene in the Osaka Bay area. Eastern, central, and western areas correspond to rectangular grids in Fig. 3.49

References

Beiki M, Pedersen LB (2010) Eigenvector analysis of gravity gradient tensor to locate geologic bodies. Geophysics 75:I37–I49. https://doi.org/10.1190/1.3484098

Cevallos C (2014) Automatic generation of 3D geophysical models using curvatures derived from airborne gravity gradient data. Geophysics 79:G49–G58

Davis PJ, Rabinowitz P (2007) Methods of numerical integration, 2nd edn. Dover, New York

Geological Survey of Japan (2004) Gravity CD-ROM of Japan, ver 2, digital geoscience map P-2. Geological Survey of Japan AIST, Tsukuba

Geological Survey of Japan (ed) (2012) Seamless digital geological map of Japan 1:200,000 (July 3, 2012 ver), research information database DB084. National Institute of Advanced Industrial Science and Technology (AIST), Tsukuba

Itoh Y (2016) Subsurface structure of Osaka sedimentary basin and its tectonic evolution. In: Itoh Y (ed) Research frontiers of sedimentary basin interiors—a case study and methodological review on an oblique convergent margin. Nova Science Publishers Inc., NY, pp 27–70

Itoh Y, Takemura K (2016) Subsurface structure of the Osaka Plain—its perspective based on geophysical data and future problems. News Osaka Micropaleontol 17:1–74 (in Japanese)

Itoh Y, Yamashita T, Danhara T, Nagasaki Y, Watanabe M, Arato H (1994) Miocene volcanic rocks in MITI "Kanazawa-oki" well: a description of syn-rifting volcanism. J Jpn Assoc Pet Technol 59:509–518

Itoh Y, Kusumoto S, Takemura K (2013) Characteristic basin formation at terminations of a large transcurrent fault—basin configuration based on gravity and geomagnetic data. In: Itoh Y (ed) Mechanism of sedimentary basin formation—multidisciplinary approach on active plate margins. InTech, Croatia, pp 255–272. http://dx.doi.org/10.5772/56702

Itoh Y, Kusumoto S, Takemura K (2015) Tectonically controlled asymmetric basin formation and evolution: an example from an active plate margin. In: Veress B, Szigethy J (eds) Horizons in Earth science research, vol 14. Nova Science Publishers Inc., NY, pp 123–141

Itoh Y, Iwata T, Takemura K (2017) Three-dimensional architecture of the Median Tectonic Line in southwest Japan based on detailed reflection seismic and drilling surveys. In: Itoh Y (ed)

Evolutionary models of convergent margins—origin of their diversity. InTech, Croatia, pp 51–71. http://dx.doi.org/10.5772/67434

Iwabuchi Y, Nishikawa H, Noda N, Yukimatsu T, Taga M, Miyano M, Sakai K, Fukazawa M (2000) Basement and active structures revealed by the seismic reflection survey in Osaka Bay. Rep Hydrogr Res 36:1–23

Iwasaki Y, Kagawa T, Sawada S, Matsuyama N, Ohshima K, Ikawa T, Onishi M (1994) Basement structure by airgun reflection survey in Osaka Bay, southwest Japan. J Seismol Soc Jpn 46:395–403

Kusumoto S (2016) Estimations of subsurface structures by gravity anomaly and gravity gradient tensor. In: Itoh Y (ed) Research frontiers of sedimentary basin interiors—a case study and methodological review on an oblique convergent margin. Nova Science Publishers Inc., NY, pp 9–26

Nakatsuka T, Okuma S (2005) Aeromagnetic anomalies database of Japan, digital geoscience map P-6. Geological Survey of Japan AIST, Tsukuba

Research Committee on Ground in Kansai (1998) Shin-Kansai jiban (Ground of Kansai)—from Kobe to Hanshin. Association of Research on Geotechnical Information in Kansai, Osaka

Research Group for Active Faults (1991) The active faults in Japan: sheet maps and inventories, rev edn. University of Tokyo Press, Tokyo

Sato H, Hirata H, Ito T, Tsumura N, Ikawa T (1998) Seismic reflection profiling across the seismogenic fault of the 1995 Kobe earthquake, southwestern Japan. Tectonophysics 286:19–30

Wangen M (2010) Physical principles of sedimentary basin analysis. Cambridge University Press, London

Yokokura T, Kano N, Yamaguchi K, Miyazaki T, Ikawa T, Ohta Y, Kawanaka T (1996) On fault systems and basement structures in and around the epicentral region of the 1995 Hyogo-ken Nanbu earthquake: a brief report. Butsuri-Tansa 49:435–451

Yokokura T, Kano N, Yamaguchi K, Miyazaki T, Ikawa T, Ohta Y, Kawanaka T, Abe S (1998) Seismic profiling of deep geological structure in the Osaka Bay area. Bull Geol Surv Jpn 49:571–590

Yokokura T, Yamaguchi K, Kano N, Miyazaki T, Ikawa T, Ohta Y, Kawanaka T, Abe S (1999) Seismic profiling of deep geological structure in the Kobe and Ashiya areas. Bull Geol Surv Jpn 50:245–267

Yokota H, Ikawa T, Sano M, Takemura K (1997) Chapter 2: seismic reflection profiles across the northern part of Osaka Bay and Rokko Mountain foothill. In: Museum of Nature and Human Activities, Hyogo (ed) The great Hanshin-Awaji earthquake disaster and Rokko movements —report on the research of active tectonics around the damaged area by the 1995 Hyogoken-Nanbu earthquake. Kobe Civil Engineering Office, Kobe, pp 57–89

Chapter 4
Discussion—Origin and Evolution of the Osaka Basin

Abstract On the basis of the seismic interpretation presented in the previous chapter, the subsurface architecture of Osaka Bay in southwest Japan is described in detail in this chapter. Although this Plio-Pleistocene basin has a two-layered simple system of Cretaceous granitic basement and fluvio-tidal/deltaic sediments as a first approximation, discrepancies between the gravitational and seismic analyses imply the existence of concealed pre-Neogene basins within the northern part of the acoustic basement. The main findings regarding the three-dimensional characteristics of significant structural trends are summarized as follows. (1) A number of active faults fringing the northwestern margin of Osaka Bay have been classified into the Awaji–Rokko Fault System to the west and the Osaka Bay Fault to the east accompanied by dextral and reverse displacements, respectively. However, the present research shows that both lateral and vertical slips occur on each of the continuous fault strands, which are collectively regarded as a buffer zone of prevailing transpressive tectonic stress. (2) Among sporadic basement highs acting as domain boundaries of the late Pleistocene basin, a N–S warping zone on the southern coast extends into the bay area and has the most important paleoenvironmental influence, as exemplified by the formation of a freshwater lake ca. 500–400 ka. (3) A seismic section passing through the Kitan Strait shows upward-splaying faults. Together with the specific separation senses of the faulted blocks, they are interpreted as constituting a large transcurrent fault. Its connectivity with onshore active fault traces indicates that the observed rupture is a part of the Median Tectonic Line (MTL) with dominant right-lateral motions through the late Quaternary. In an open sea half-graben, the northern depocenter of which is cut by the MTL, there is a conspicuous sedimentary interface, on which a truncation pattern of reflection terminations was clearly identified. On the basis of the neotectonic history of southwest Japan, this unconformable boundary is related to intermittent N–S contractional events dating to the Pliocene. (4) Gentle horsts and grabens off the southeastern coast of Awaji Island are aligned in a N–S trend and regarded as a wide shortening zone under E–W compression. Although a remarkable negative gravity anomaly around this structure suggests longstanding cumulative deformation, the development of Holocene depocenters on the gravity minimum points to ongoing structural buildup. A chronological table of the Plio-Pleistocene noted tectonic events around the Kinki Triangle suggests occa-

Y. Itoh and K. Takemura, *Three-Dimensional Architecture and Paleoenvironments of Osaka Bay*, Advances in Geological Science,
https://doi.org/10.1007/978-981-13-0577-1_4

sional changes of regional tectonic regimes, which have occurred at shorter intervals since ca. 1 Ma. Finally, the authors present a structural model of the present Osaka sedimentary basin as a fault-surrounded active tectonic region.

Keywords Osaka Bay · Sedimentary basin · Quaternary · Active fault Tectonics

4.1 Comparison Between Proximal and Peripheral Parts of the Basin

As explained in Chap. 1 (Sect. 1.4.3.1), analysis of the gravity gradient tensors has provided an excellent view of the unreachable interior of the sedimentary basin. As depicted in Fig. 1.10b, solution clouds given by the tensor Euler deconvolution after Kusumoto (2016) indicate that the northern part of Osaka Bay is three to four times deeper than the southern part. Such an estimate qualitatively accords with the notion that the northern proximal and southern peripheral parts of the Plio-Pleistocene basin have formed an entrapped inlet affected by recurrent marine invasions.

However, it seems that the structural dimension deduced from the mass deficiency is much larger than that expected from the seismic interpretation. This is exemplified by the seismic line GS-2M, which travels through a gravitationally detected gigantic sag on the northern coast. The profile obtained from GS-2M shows a flat basement surface as deep as 2000 m (Chap. 3, Sect. 3.3.1.1; see Fig. 3.7). This indicates that the acoustic basement of the northern proximal basin does not consist of a simple continuum of granitic rocks but a mixture of some lithofacies with varied densities.

Figure 4.1 presents a working hypothesis to reconcile the contradiction between the gravitational and seismic analyses. As shown in Fig. 4.1a, the northern basin is accompanied by high dimensionality index values; together with the shape index for the same area, these are indicative of a bowl-like depression (Itoh et al. 2015). This region is bordered by the Awaji–Rokko Fault System and the Arima–Takatsuki Tectonic Line. Based on numerical modeling, Kusumoto et al. (2001) predicted an extreme pair of subsidence and uplift on the southern and northern sides of the connected faults, respectively (see Fig. 1.12). According to a regional geologic map (Fig. 4.1b; Geological Survey of Japan 2012), the area of exhumation to the north of the fault junction is occupied by a thick Paleogene sedimentary unit named the Kobe Group (Geological Society of Japan 2009). Therefore, it is plausible that the Quaternary basin is underlain by a Paleogene basin and characterized by a considerably negative gravity anomaly.

Regarding the basement constituents of the southern portion of Osaka Bay, available information is restricted because of scarce subsurface surveys. On the southern coast, the Kanku–Maejima observatory well confirmed granodiorite at depths exceeding 1300 m (Itoh et al. 2017a, b). An analogy with the geology of adjacent land points to Early Cretaceous granitic rocks as the dominant component of the

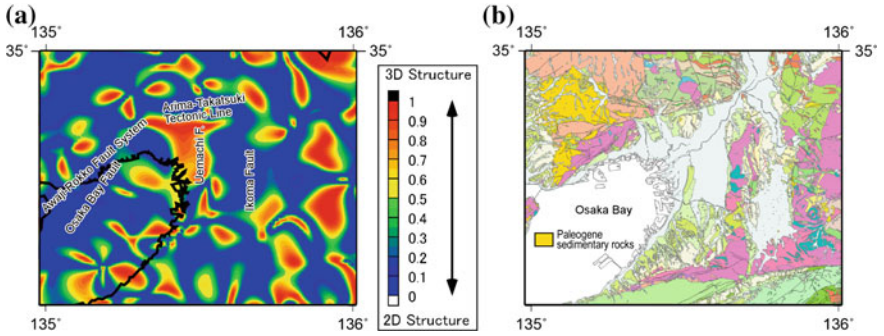

Fig. 4.1 **a** Subsurface structural trends in and around the Osaka basin on the basis of analysis of gravity gradient tensors (dimensionality index *I*; Beiki and Pedersen 2010) after Itoh et al. (2015). **b** Surface geology around the Osaka basin after the Geological Survey of Japan (2012)

basement with a minor contribution of Late Cretaceous marine sediments (Izumi Group) on the northern side of the Median Tectonic Line (MTL), as described by Itoh and Iwata (2017) and Itoh et al. (2017a, b).

4.2 Marine–Land Connectivity of Major Structural Trends

4.2.1 Awaji–Rokko Fault System and Osaka Bay Fault

A series of active faults running along the eastern coast of Awaji Island and the southern flank of the Rokko Mountains is collectively called the Awaji–Rokko Fault System. This system is 2–3 km in width and shows a straightforward trend (Research Group for Active Faults 1991). The seismic interpretation presented in Chap. 3 has revealed a number of faults on the western shelf of Osaka Bay and delineated their broad distribution (exceeding 5 km) and considerable diversity in architectural styles. This section discusses the landward connectivity of noteworthy subseafloor structures and presents an evaluation of their activity levels and motion senses.

Figure 4.2 presents the structural interpretations of Osaka Bay derived in the previous studies and the present study. It is noteworthy that previous researchers (Yokota et al. 1997; Yokokura et al. 1996, 1998, 1999; Iwabuchi et al. 2000) have assumed the presence of bifurcated fault ends around the northern coast of the bay without exception. This concept originates from nearshore boring and echo sounding surveys. Huzita and Maeda (1984) recognized two superficial ruptures based on the discontinuity of the Ma 12 marine clay and named the Wadamisaki and Maya Faults, which correspond to the western and eastern branches of the Osaka Bay Fault (Fig. 4.2), respectively. However, the tectonic importance of these features should be carefully verified. To the north, extensions of these faults have not been found under

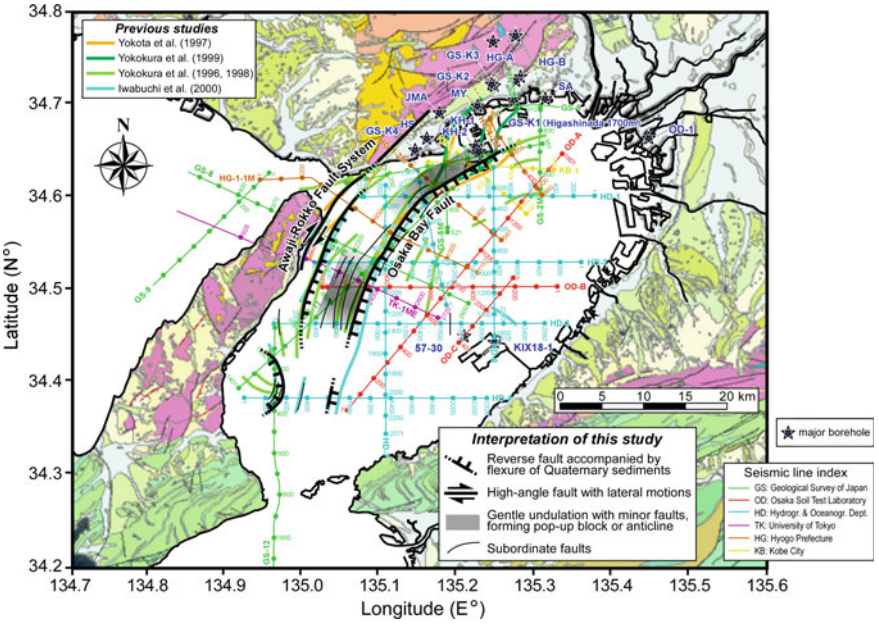

Fig. 4.2 Comparison of fault interpretations of previous studies. The surface geology is after the Geological Survey of Japan (2012)

the alluvial plain (e.g., Research Group for Active Faults 1991; Huzita and Kasama 1983). The present offshore survey also did not yield remarkable subsurface structures. From south to north, a wrench fault at the junction of the supposed branches was identified in the present study on HG-1-2M, and reverse faults with separations up to 150 and 230 m were observed on GS-7 in locations where the Wadamisaki and Maya Faults have been confirmed. However, HG-4-2M, which is the line nearest to land, shows negligible effects of faults within the upper Quaternary and suggests that the Osaka Bay Fault rapidly diminishes its activity level toward the coast. Therefore, in our interpretation, a solitary trace of the significant fault terminates off Kobe.

As explained in Chap. 3, the westernmost strand of the offshore faults along the Awaji coast has a high-angle appearance indicative of strike-slip motions and is interpreted as a member of the Awaji–Rokko Fault System, whereas the eastern Osaka Bay Fault is featured by divergent and varied architectures. From the seismic profiles along the across-fault lines GS-8ME, HD-2, OD-B, and HD-3 from north to south, this fault system shows the highest neotectonic activity on its eastern margin judging from the deformation trend of the late Pleistocene sediments. Figure 4.3 presents the relationship between the fault interpretation conducted in the present study and the gravitationally estimated dip angles of the faults and/or structural boundaries around the Osaka basin after Kusumoto (2016). As discussed for specific cases in Chap. 3 (e.g., Sect. 3.3.3.1), the high-angle fault strand near the eastern margin of the Awaji–Rokko Fault System and broad traces of the Osaka Bay Fault correspond to

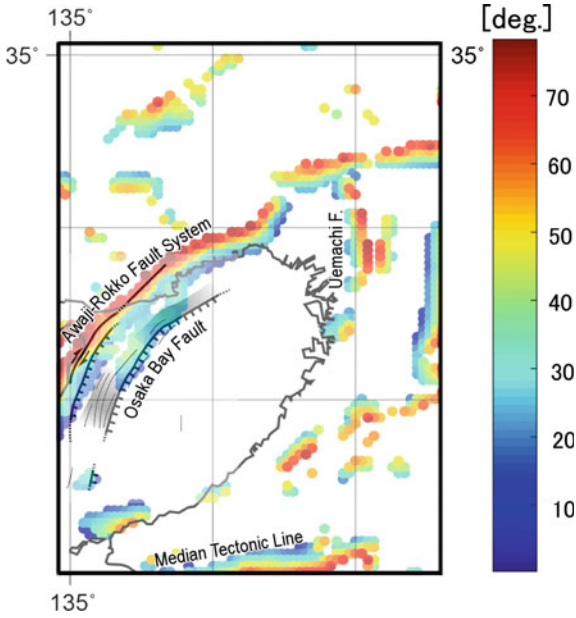

Fig. 4.3 Relationship between the fault interpretation performed in the present study and the gravitationally estimated dip angles of faults and/or structural boundaries around the Osaka basin after Kusumoto (2016)

faults or structural boundaries with high dip angles and a wide low-angle structural zone, respectively. Figure 4.4 visually indicates the diversity of fault architecture around the western margin of the Osaka sedimentary basin. This mixed appearances of reverse and strike-slip faults indicates the ability of this structure to accommodate transpressive neotectonic stress as a whole.

4.2.2 N–S Warping Zones

As discussed in Chap. 2 (Sect. 2.5.3; see Fig. 2.8), two north-trending warping zones are present in the Osaka sedimentary basin. It is widely accepted that a warping structure within the Osaka Plain called the Uemachi basement high is accompanied by an active fault on its western flank named the Uemachi Fault. The present gravity gradient tensor analysis (Chap. 1, Sect. 1.4.3.1) clarified that the dip angles of the Uemachi Fault range between 55° and 65° (Fig. 1.10). Because the fault is located in the Osaka metropolis, many surveys have been conducted to assess the seismic hazard. For example, the Disaster Prevention Research Institute (2013) argued that the fault has active branches extending toward the bay area. It is detectable as a low-angle structure in Fig. 1.10a. However, Itoh and Takemura (2016) found that the flexures are not observable on a seismic line along the coast. Thus, it was concluded from the present results that the Uemachi basement high is not linked with structural development within Osaka Bay.

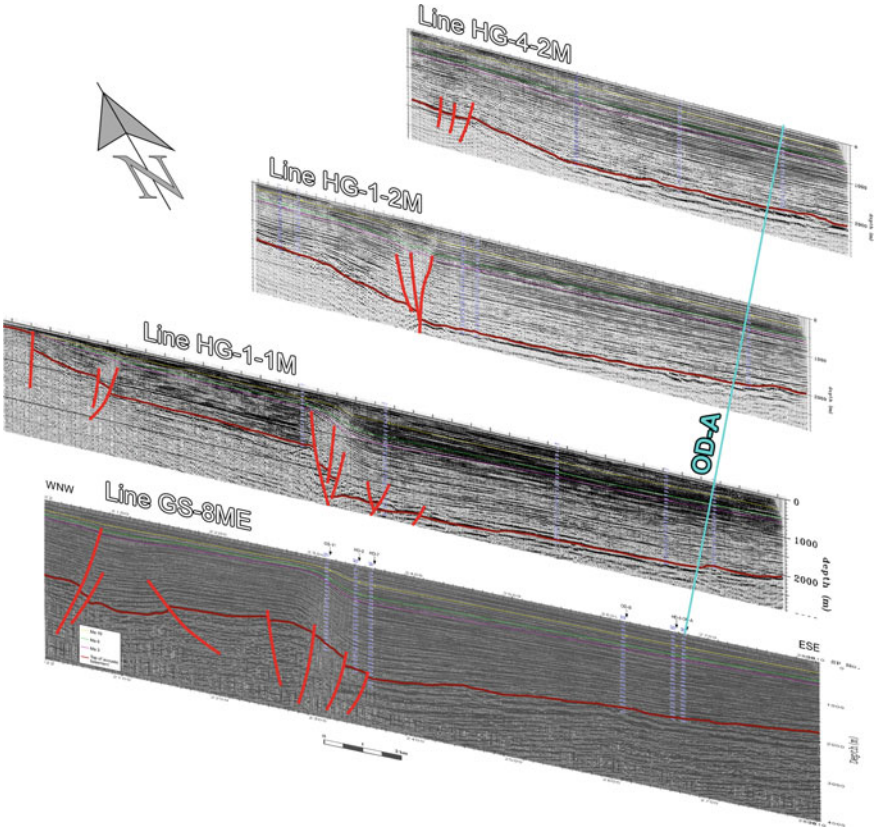

Fig. 4.4 Bird's-eye view of the subsurface architecture of the Awaji–Rokko Fault System and the Osaka Bay Fault. See Figs. 3.1, 3.2, and 3.3 for line locations

Another notable warping zone exists in the southern part of the basin and extends into the offshore areas (colored oval in Fig. 2.8a); this zone was first described by Itoh et al. (2001), and a refined description around the Kansai International Airport has been reported by Inoue et al. (2012). Although some insist that the Uemachi Fault reaches the southernmost part of the Osaka Plain and crosses the onshore sector of the N–S warping zone (e.g., Kondo et al. 2015), the azimuth of the conceived fault is contradictory to the trend of regional warping. Hence, a more reasonable structural model is proposed herein.

As explained in Chap. 2 (Sect. 2.5.3), Itoh et al. (2001) argued that the N–S warping gradually developed from 1.0 to 0.4 Ma and eventually dammed the big inlet to form a lake (Paleo-Lake Senshu) between the stages of the Ma 8 and 9 marine clays (500–400 ka), the diatom assemblages of which contain a lacustrine habitant (*Melosira* sp.). The termination of the E–W compressive regime deduced from the intra-basinal structural buildup has not been definitively dated, but Itoh et al.

(2017b) noted the possibility of the ongoing growth of the tectonic warping based on the homoclinal tilting of shallow sediments in a land seismic section parallel to the shoreline.

Apart from the prominent upheavals, the southern coast of Osaka Bay is rich in geomorphological diversity. Figure 4.5a shows the results of structural analysis performed around the coast of the bay. It is noteworthy that the structure of the surface of the acoustic basement (Disaster Prevention Research Institute 2013) and that represented by a widespread tephra at 1 Ma (Itihara et al. 1986) closely resemble one another with regard to the shape of the broad N–S anticline surrounded by surface geomorphic trends. The stratigraphy of the upper part of the Osaka Group in a coast-parallel borehole array (Fig. 4.5b; Research Committee on Ground in Kansai 2007) and the seismic interpretation of the coast-normal Takaishi–Sakai Line (Fig. 4.5c) led Itoh (2016) to infer the presence of a neotectonic depression with a bowl-like shape. An unusual sag is located at northern tip of the above-mentioned north-trending nose, where local tensile stress inevitably exists. Thus, a widespread E–W compression seems to have been present in the southern half of the late Pleistocene basin.

A different cause for the rough basement surface is proposed here based on the gravity gradient tensor analysis by Itoh et al. (2015). Figure 4.5a presents the spatial distribution of the shape index *Si* (Cevallos 2014). An area where *Si* is near unity implies the presence of a domal mass excess on the coast, the deep structure of which was visualized using the seismic record of the Otsugawa Line (Fig. 4.5d). The profile shows an active rupture, named the Kumedaike Fault (Okada and Togo 2000), around common midpoint (CMP) 1700–1800 and delineates strong reflectors above the basement surface on the downthrown side of the fault. These seismic features are accompanied by a positive geomagnetic anomaly (Fig. 3.3) and were interpreted here as a buried Neogene volcanic mound similar to that described by Itoh et al. (2013) around an inland area of the Osaka Plain. The above discussion indicates that local pre-Quaternary elements should be taken into account in the course of the seismic interpretation of the Osaka sedimentary basin.

4.2.3 Median Tectonic Line

Figure 4.6 shows a close-up view of the seismic profile of GS-12 (southern half). In this profile, high-angle faults with an upward-splaying "flower" appearance are visible around Sp. 950–1030. The relative upthrown side and/or separation senses of these faults are variable at depth, which is in accordance with the criteria for the identification of strike-slip faults (e.g., Harding 1990). In reference to the onshore distribution of active faults (Research Group for Active Faults 1991), the observed rupture is considered to be a part of the MTL with dominantly dextral slips during the Quaternary.

It is rather exceptional that such an obvious indication of lateral movement is confirmed in seismic records obtained across the regional fault on land. Itoh et al. (2017b) described an E–W-trending low-angle north-dipping fault along the southern

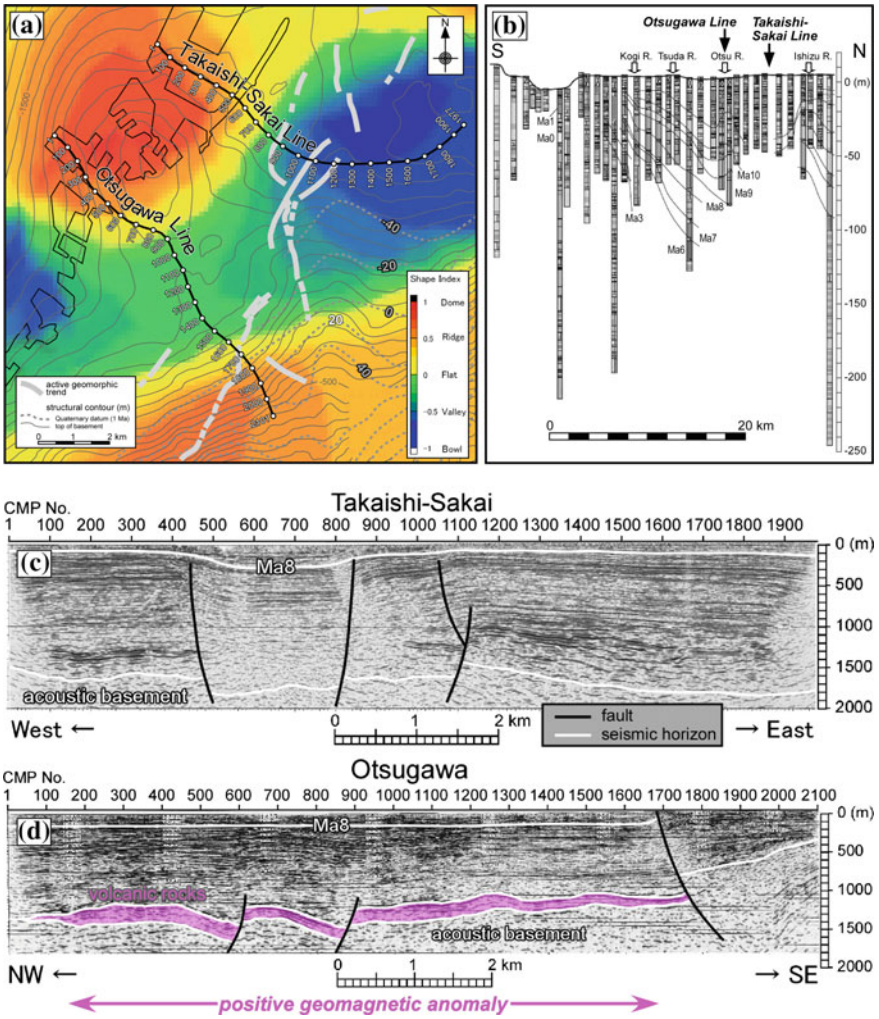

Fig. 4.5 **a** Analysis of gravity gradient tensors (shape index *Si*; Cevallos 2014) around the coast of Osaka Bay and subsurface topography compiled by Itoh (2016). **b**, **c**, **d** Borehole and seismic information around the area mapped in (a) after Itoh (2016)

foot of the Izumi Mountains and a watershed along the southern margin of the Osaka sedimentary basin. They argued that the low-angle break is a material boundary in the upper crust and is irrelevant to the high-angle mechanical boundary accommodating recent prevalent shear stress.

Aside from the lateral motion, evidence of an older contraction phase can be found in a half-graben on the southern side of the MTL, in which thinly laminated reflectors suggestive of normal sediments are widely observed. It should be noted that a sequence boundary (truncated surface; orange horizon in Fig. 4.6) is defined

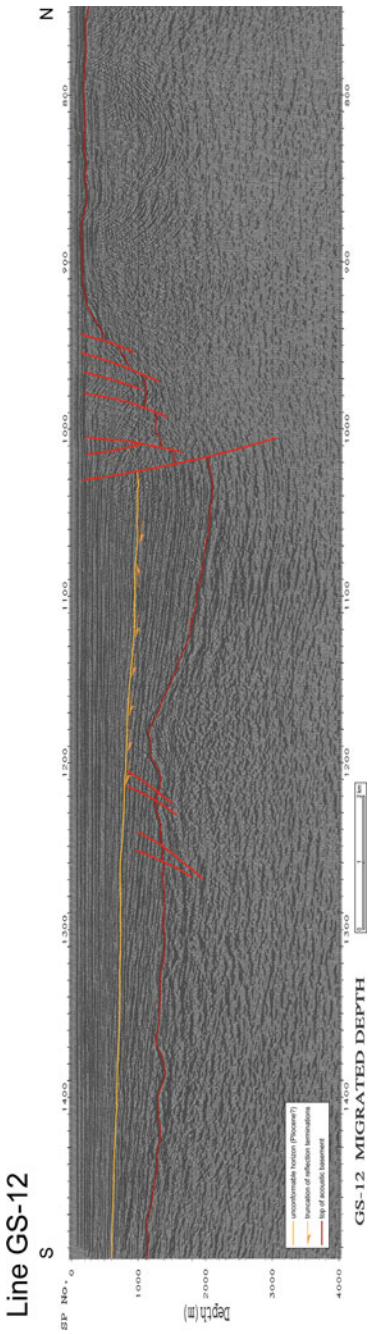

Fig. 4.6 Close-up view of the seismic line GS-12 crossing the Median Tectonic Line. See Figs. 3.1, 3.2, and 3.3 for the line location

in the basin fill. This unconformable boundary is likely linked to the deformation events of the island arc. The evolutionary process of the Izumi divide tells us that two phases of contractional episodes have occurred around the Osaka basin since the Pliocene. The initial uplift of the main range was brought about under regional N–S compression ca. 2.9 Ma (Oka 1978), when an influx of schist gravels (Fig. 1.9) from metamorphosed terranes south of the MTL ceased. After a dormant period in the early Pleistocene, the uplift of the northern Izumi foothill was provoked by the resumption of a compressive regime at the stage of Ma 3 marine clay (0.87 Ma; Oka 1978). As a result of this tectonic episode, exhumed Cretaceous granites are distributed as fault-bounded blocks, as identified through the gravity gradient tensor analysis discussed in Chap. 1 (dotted oval in Fig. 1.10a). Further investigation is needed to elucidate the tectonic context of the formation of an unconformity observed on the seismic line GS-12.

4.2.4 Broad Contractional Horsts off the Eastern Coast of Awaji Island

A N–S-trending broad horst/graben structure exists beneath the southwestern shelf of Osaka Bay. It is quite different from the trend of the adjoining Awaji Island, which is characterized by a narrow fault-bounded northern bulge and a southern latitudinal basis uplifted during contractional activities on the MTL (Fig. 4.7; Oka and Sangawa 1981) in a manner analogous with the Izumi range (Sect. 4.2.3). From the morphology of deep-rooted faults observed in seismic data, this subsea structural trend seems to have developed under E–W compression.

The evolutionary processes of the tectonic zone remain enigmatic. Around the area of the present study, an E–W shortening is regarded as the latest tectonic epoch (1.0–0.4 Ma with an episodic climax ca. 0.5 Ma), as explained in Chap. 2 (Sect. 2.5.3) and argued by Itoh (2016). However, it would be difficult to generate the mass defect estimated from the negative gravity anomaly around the area of the structure (Fig. 3.2) through a process of subsidence and burial in such a short period. As discussed in Chap. 1 (Fig. 1.8; Sect. 1.4.1), the migration of intra-arc basins (Tokai and Lake Biwa) in the Pleistocene is related to the waxing and waning of E–W compressive stress. That being the case, the gentle dent off Awaji Island may have been involved in an earlier phase of evolution.

On the other hand, a close look at the distribution of the Holocene sediments provides insight into the active development of the structure. Figure 4.8 shows the depths of the base of Ma 13 marine clay ca. 11 ka (Huzita and Maeda 1985), which clearly delineates an incised valley network of the "Paleo-Osaka River" running through the terrestrially exposed bay bottom in the last glacial period. Apart from the buried channel system, obvious lows were located within a notable area of negative gravity anomaly. Although the precision of the subsurface topography based on outdated

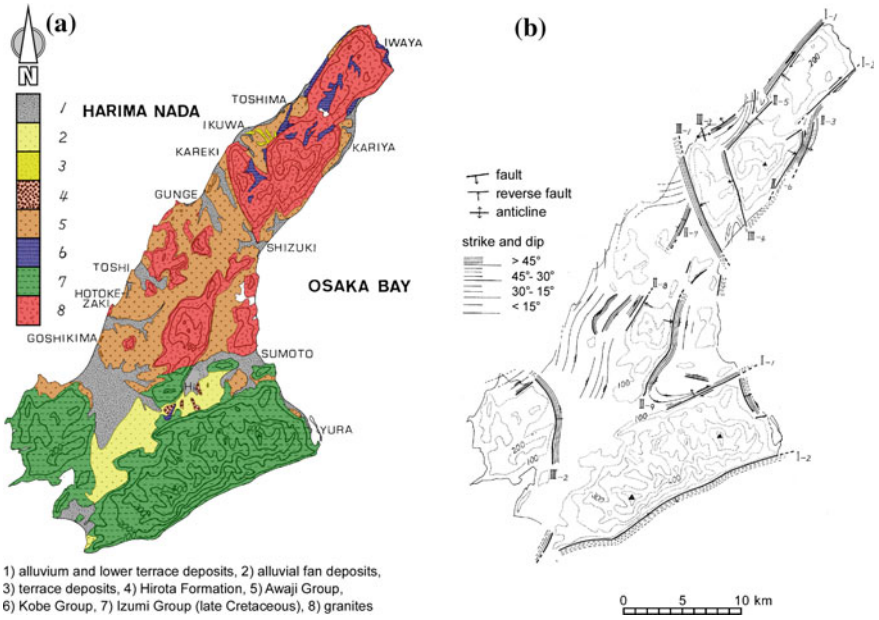

Fig. 4.7 Tectonic features of Awaji Island after Oka and Sangawa (1981). **a** Geology and summit level contours. **b** Faults and structure of the late Cenozoic strata

echo sounding recordings taken in the 1960s should be carefully reexamined, the striking resemblance between the topographic and gravitational downwarp indicates that the growth of this subbasin is still underway.

4.3 Evolutionary Process of the Osaka Basin—A Tectonic Model

4.3.1 A Synthesis of the Plio-Pleistocene Tectonic Events

Basin formation processes in the Kinki Triangle are described in the context of regional tectonic regimes which are chronicled in Fig. 4.9. As stated in Chap. 1 (Sect. 1.2.2; Fig. 1.6), Pliocene of southwest Japan was heralded by an inversion event. Although contraction seems to have been more intense on the backarc side (e.g., Itoh and Nagasaki 1996), Itoh et al. (2017a) detected a synchronous forearc uplift based on apatite fission track analysis (AFTA). Such a regional deformation on the convergent margin may be related to resume northward subduction of the Philippine Sea Plate.

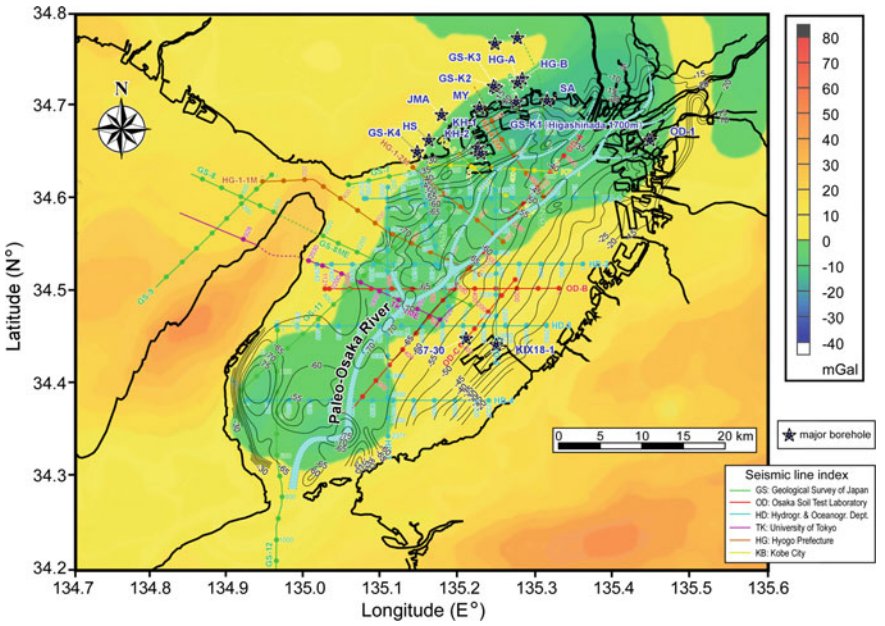

Fig. 4.8 Depth contours of the base of Ma 13 marine clay bed in the Osaka Bay area (Huzita and Maeda 1985). The Paleo-Osaka River system on the eroded surface of the uppermost Pleistocene is shown as a pale blue zone. The background color scale represents the Bouguer gravity anomaly in milligal after the Geological Survey of Japan (2004)

N–S compressive regime may have lingered through the Pliocene considering development of the Tokai basin. The oldest E–W elongate lake in the Kinki Triangle formed on an arc-parallel divide and was migrated northerly just like pushed away from the uplifting mountain ranges, which is fully explained in Chap. 1 (Sect. 1.4.1; Fig. 1.8).

Continued subduction of the Philippine Sea Plate is also supported by episodic contraction phenomena on the forearc side, namely formation of a watershed along the Median Tectonic Line (uplift of Izumi range; Oka 1978) and succeeding uplift of forearc basins (Takano et al. 2009).

Longstanding north to northwestward migration and deformation history of the Lake Tokai and Paleo-Lake Biwa basins may imply emergence of an E–W compressive stress around the end of the Pliocene as argued in Chap. 1 (Sect. 1.4.1; Fig. 1.8), which may have linkage with convergence of the Pacific Plate (Huzita 1980).

As for the growing E–W compression, paleoenvironmental studies give a significant temporal constraint. Ikebe et al. (1971) and Mitamura (1992) found that the Ma 1 and 2 marine clays in the Nara basin (see Fig. 4.10). Younger evidence for transgression has not been established. It is a phenomenon that initial compartmentalization of the proto-Osaka basin began under emergence of a N–S watershed (Ikoma Mts.) as a result of activation of the Ikoma Fault since ca. 1 Ma.

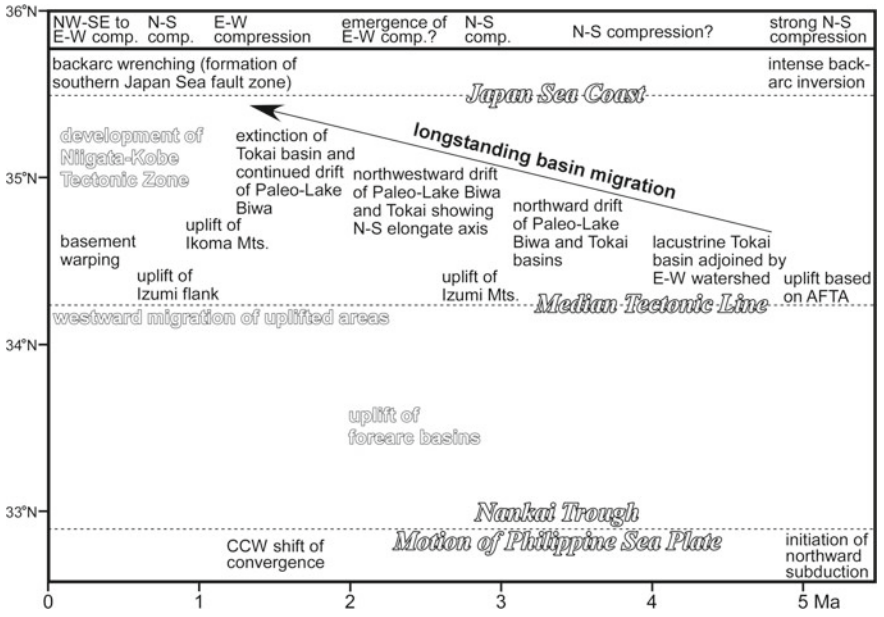

Fig. 4.9 A chronology of tectonic events in and around the Kinki Triangle. Regional episodes are shown by outline characters

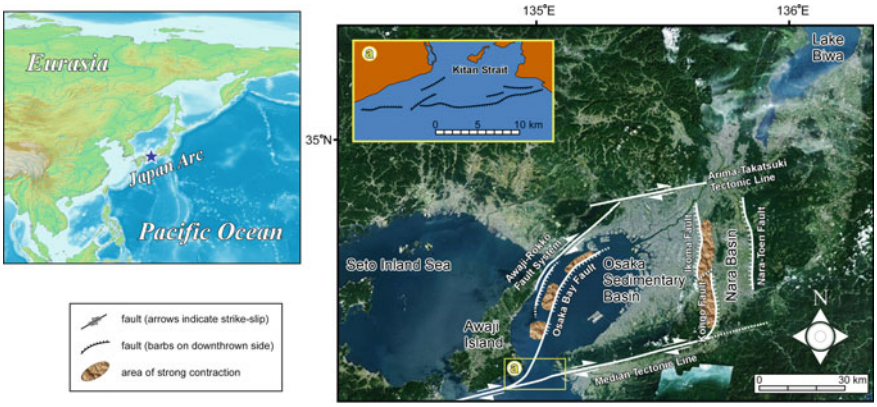

Fig. 4.10 Structural model of the present Osaka sedimentary basin. A star in the regional map indicates the study area. Images are after Geoscience, NTT DATA, RESTEC. Fault architecture of the Kitan Strait (inset a) is after Yoshikawa et al. (1996) and Mitsuhashi et al. (2000)

Since 1 Ma, stress state in the Kinki Triangle seems to have been quite changeable. Although the authors suspect that some of them can be coexistent reflecting complicated tectonic framework under the influence of the Philippine Sea Plate and Pacific Plate, stratigraphic data are not sufficient to verify synchronism among local

events. Therefore, we submit a chronological table on the assumption that the known tectonic episodes and their driving force were prevalent within the studied region.

After the episodic uplift of the Ikoma Mountains, a signature of N–S compression is observed on the Median Tectonic Line. Based on provenance study of gravels in the late Pleistocene, Oka (1978) argued that the northern Izumi flank was uplifted at 0.87 Ma (depositional age of the Ma 3 marine clay). From more regional point of view, onset timing of watershed formation along the arc-bisecting fault was reviewed by Itoh (2015) based on gravel compositions indicative of cessation of schist influx from forearc metamorphosed terranes (see Fig. 1.9), which found that the rise of contraction is younger going westward. He attributed the transient tectonic regimes to changing convergence modes of the Philippine Sea Plate.

The most recent event around the study area was an E–W compression, under which the compartmentalization of the Osaka sedimentary basin occurred alongside the emergence of basement bulges. Simultaneously, a shear deformation zone traversing the island arc (Niigata–Kobe Tectonic Zone; Fig. 1.9) developed and backarc wrenching was getting stronger to eventual formation of the Southern Japan Sea Fault Zone (Figs. 1.6 and 1.9). These episodes may be related to counterclockwise shift of convergence of the Philippine Sea Plate from 2 to 1 Ma (Nakamura et al. 1987).

4.3.2 Structural Framework of the Present Osaka Basin

Our final structural model of the Osaka sedimentary basin is presented as Fig. 4.10. The study area is surrounded by active faults. As stated in Chap. 1 (Sect. 1.4.3.3; Fig. 1.12), dextral and/or reverse slips on these faults result in vigorous basin formation at an inherently confining left-step of the right-lateral MTL (Kusumoto et al. 2001).

In addition to the well-known MTL's branching into the Kongo and Ikoma Faults (e.g., Research Group for Active Faults 1991), we introduced a turnout track to the Osaka Bay Fault around the Kitan Strait. Although scarce multichannel seismic records in the southernmost part of the bay hinder us from figuring out deep-rooted structure, Yoshikawa et al. (1996) and Mitsuhashi et al. (2000) delineated divergent strands of the MTL around the gullet (see inset a of Fig. 4.10) based on reflection survey using uniboom and water gun as energy sources. They suggested that the MTL is not a single continuous fault, but is regarded as a combination of ruptures showing clear difference in morphology and activation age in their survey area.

As shown in our paleogeographic reconstruction (Fig. 1.8), the Awaji–Rokko Fault System and the Osaka Bay Fault have been active since the late Pliocene initiation of the proto-Osaka basin. Their dextral movement is a part of development of the Niigata–Kobe Tectonic Zone (Fig. 1.9) and reverse movement is responsible for ongoing deformation off the eastern coast of Awaji Island (Sect. 4.2.4; Fig. 4.8). Delayed reverse activity on the Ikoma and Kongo Faults provoked uplift of a N–S watershed (Sect. 4.3.1; Fig. 4.9) getting the start of continued basin compartmentalization through the late Quaternary period.

References

Beiki M, Pedersen LB (2010) Eigenvector analysis of gravity gradient tensor to locate geologic bodies. Geophysics 75:I37–I49. https://doi.org/10.1190/1.3484098

Cevallos C (2014) Automatic generation of 3D geophysical models using curvatures derived from airborne gravity gradient data. Geophysics 79:G49–G58

Disaster Prevention Research Institute (2013) Integrated research project for the Uemachi active fault system by METI. Kyoto University (DPRI), Uji

Geological Society of Japan (ed) (2009) Geology of Japan: 5 Kinki district. Asakura-Shoten, Tokyo

Geological Survey of Japan (2004) Gravity CD-ROM of Japan, ver 2, digital geoscience map P-2. Geological Survey of Japan AIST, Tsukuba

Geological Survey of Japan (ed) (2012) Seamless digital geological map of Japan 1:200,000 (July 3, 2012 ver), research information database DB084. National Institute of Advanced Industrial Science and Technology (AIST), Tsukuba

Harding TP (1990) Identification of wrench faults using subsurface structural data: criteria and pitfalls. AAPG Bull 74:1590–1609

Huzita K (1980) Role of the Median Tectonic Line in the Quaternary tectonics of the Japanese islands. Mem Geol Soc Jpn 18:129–153

Huzita K, Kasama T (1983) Geology of the Kobe district, Quadrangle series, scale 1:50,000. Geol Surv Japan, Tsukuba

Huzita K, Maeda Y (1984) Geology of the Suma district, Quadrangle series, scale 1:50,000. Geol Surv Japan, Tsukuba

Huzita K, Maeda Y (1985) Geology of the Osaka-Seinambu district, Quadrangle series, scale 1:50,000. Geol Surv Japan, Tsukuba

Ikebe N, Ishida S, Chiji M (1971) An occurrence of Stegodon molar from Mami hills, Nara Prefecture, central Japan. Prof. Heiichi Takehara Mem Vol, pp 163–172

Inoue N, Kitada N, Takemura K, Fukuda K, Emura T (2012) Three-dimensional subsurface structure model of Kansai International Airport by integration of borehole data and seismic profiles. Geotech Geol Eng. https://doi.org/10.1007/s10706-012-9568-4

Itihara M, Ichikawa K, Yamada N (1986) Geology of the Kishiwada district, Quadrangle series, scale 1:50,000. Geol Surv Japan, Tsukuba

Itoh Y (2015) Gunchu Formation—an indicator of active tectonics on an oblique convergent margin. Lap Lambert Academic Publishing, Saarbrücken

Itoh Y (2016) Subsurface structure of Osaka sedimentary basin and its tectonic evolution. In: Itoh Y (ed) Research frontiers of sedimentary basin interiors—a case study and methodological review on an oblique convergent margin. Nova Science Publishers Inc., NY, pp 27–70

Itoh Y, Iwata T (2017) Structural features along the Median Tectonic Line in southwest Japan: an example of multiphase deformation on an arc-bisecting fault. In: Itoh Y (ed) Evolutionary models of convergent margins—origin of their diversity. InTech, Croatia, pp 143–156. http://dx.doi.org/10.5772/67669

Itoh Y, Nagasaki Y (1996) Crustal shortening of Southwest Japan in the Late Miocene. The Island Arc 5:337–353

Itoh Y, Takemura K (2016) Subsurface structure of the Osaka Plain—its perspective based on geophysical data and future problems. News Osaka Micropaleontol 17:1–74

Itoh Y, Takemura K, Kawabata D, Tanaka Y, Nakaseko K (2001) Quaternary tectonic warping and strata formation in the southern Osaka basin inferred from reflection seismic interpretation and borehole sequences. J Asian Earth Sci 20:45–58

Itoh Y, Kusumoto S, Takemura K (2013) Characteristic basin formation at terminations of a large transcurrent fault—basin configuration based on gravity and geomagnetic data. In: Itoh Y (ed) Mechanism of sedimentary basin formation—multidisciplinary approach on active plate margins. InTech, Croatia, pp 255–272. http://dx.doi.org/10.5772/56702

Itoh Y, Kusumoto S, Takemura K (2015) Tectonically controlled asymmetric basin formation and evolution: an example from an active plate margin. In: Veress B, Szigethy J (eds) Horizons in Earth science research, vol 14. Nova Science Publishers Inc., NY, pp 123–141

Itoh Y, Green PF, Takemura K, Iwata T (2017a) Fission track thermochronology of Late Cretaceous sandstones of the Izumi Group adjacent to the Median Tectonic Line active fault system in southwest Japan. In: Itoh Y (ed) Evolutionary models of convergent margins—origin of their diversity. InTech, Croatia, pp 97–116. http://dx.doi.org/10.5772/67962

Itoh Y, Iwata T, Takemura K (2017b) Three-dimensional architecture of the Median Tectonic Line in southwest Japan based on detailed reflection seismic and drilling surveys. In: Itoh Y (ed) Evolutionary models of convergent margins—origin of their diversity. InTech, Croatia, pp 55–75. http://dx.doi.org/10.5772/67434

Iwabuchi Y, Nishikawa H, Noda N, Yukimatsu T, Taga M, Miyano M, Sakai K, Fukazawa M (2000) Basement and active structures revealed by the seismic reflection survey in Osaka Bay. Rep Hydrogr Res 36:1–23

Kondo H, Sugito N, Yoshioka T, Tsutsumi H, Kimura H (2015) Revisited spatial distribution of the Uemachi fault zone, Osaka, revealed by digital elevation models. Active Fault Res 42:1–34

Kusumoto S (2016) Estimations of subsurface structures by gravity anomaly and gravity gradient tensor. In: Itoh Y (ed) Research frontiers of sedimentary basin interiors—a case study and methodological review on an oblique convergent margin. Nova Science Publishers Inc., NY, pp 9–26

Kusumoto S, Fukuda Y, Takemura K, Takemoto S (2001) Forming mechanism of the sedimentary basin at the termination of the right-lateral left-stepping faults and tectonics around Osaka Bay. J Geogr 110:32–43

Mitamura M (1992) Stratigraphy and geological structure of the Osaka Group (Pliocene and Pleistocene) in Keihanna hills, Kinki district, Japan. Quat Res Jpn 31:159–177

Mitsuhashi A, Kadosawa H, Yoshikawa S, Iwasaki Y, Huzita K (2000) Marine geological structure and active faults in Kii strait and off the southern coast of Kii Peninsula. J Jpn Soc Mar Surv Tech 12:11–29

Nakamura K, Renard V, Angelier J, Azema J, Bourgois J, Deplus C, Fujioka K, Hamano Y, Huchon P, Kinoshita H, Labaume P, Ogawa Y, Seno T, Takeuchi A, Tanahashi M, Uchiyama A, Vigneresse JL (1987) Oblique and near collision subduction, Sagami and Suruga Troughs—preliminary results of the French-Japanese 1984 Kaiko cruise, Leg 2. Earth Planet Sci Lett 83:229–242

Oka Y (1978) The formation of the Izumi range and the Osaka Group. Quat Res Jpn 16:201–210

Oka Y, Sangawa A (1981) The formation of the sedimentary basin in the east of Inland Sea and the uplift of the Awaji Island, Japan. J Geogr 90:393–409

Okada A, Togo M (2000) Active faults in Kinki. University of Tokyo Press, Tokyo

Research Committee on Ground in Kansai (2007) Shin-Kansai jiban (Ground of Kansai)—from Osaka Plain to bay area, rev edn. Association of Research on Geotechnical Information in Kansai, Osaka

Research Group for Active Faults (1991) The active faults in Japan: sheet maps and inventories, rev edn. University of Tokyo Press, Tokyo

Takano O, Nishimura M, Fujii T, Saeki T (2009) Sequence stratigraphic distribution analysis of methane-hydrate-bearing submarine-fan turbidite sandstones in the eastern Nankai trough area: relationship between turbidite facies distributions and BSR occurrence. J Geogr 118:776–792

Yokokura T, Kano N, Yamaguchi K, Miyazaki T, Ikawa T, Ohta Y, Kawanaka T (1996) On fault systems and basement structures in and around the epicentral region of the 1995 Hyogo-ken Nanbu earthquake: a brief report. Butsuri-Tansa 49:435–451

Yokokura T, Kano N, Yamaguchi K, Miyazaki T, Ikawa T, Ohta Y, Kawanaka T, Abe S (1998) Seismic profiling of deep geological structure in the Osaka Bay area. Bull Geol Surv Jpn 49:571–590

Yokokura T, Yamaguchi K, Kano N, Miyazaki T, Ikawa T, Ohta Y, Kawanaka T, Abe S (1999) Seismic profiling of deep geological structure in the Kobe and Ashiya areas. Bull Geol Surv Jpn 50:245–267

Yokota H, Ikawa T, Sano M, Takemura K (1997) Chapter 2: seismic reflection profiles across the northern part of Osaka Bay and Rokko Mountain foothill. In: Museum of Nature and Human Activities, Hyogo (ed) The great Hanshin-Awaji earthquake disaster and Rokko movements—report on the research of active tectonics around the damaged area by the 1995 Hyogoken-Nanbu earthquake. Kobe Civil Engineering Office, Kobe, pp 57–89

Yoshikawa S, Kadosawa H, Mitsuhashi A, Iwasaki Y (1996) Geological structure of the Median Tectonic Line in Tomogashima strait area. J Jpn Soc Mar Surv Tech 8:1–10